Title
Regulation and Genetic Manipulation of Ligands for the Immunoreceptor NKG2D

Author
Gowen, Benjamin Gregory

Publication Date
2015

Peer reviewed|Thesis/dissertation

Regulation and Genetic Manipulation of Ligands for the Immunoreceptor NKG2D

by

Benjamin Gregory Gowen

A dissertation submitted in partial satisfaction of the

requirements for the degree of

Doctor of Philosophy

in

Molecular and Cell Biology

in the

Graduate Division

of the

University of California, Berkeley

Committee in charge:
Professor David H. Raulet, Chair
Professor Gregory M. Barton
Professor Michael Rape
Professor Karsten Gronert

Spring 2015

Abstract

Regulation and Genetic Manipulation of Ligands for the Immunoreceptor NKG2D

by

Benjamin Gregory Gowen

Doctor of Philosophy in Molecular and Cell Biology

University of California, Berkeley

Professor David H. Raulet, Chair

NKG2D is an important activating receptor expressed by natural killer (NK) cells and some subsets of T cells. NKG2D recognizes a family of cell surface protein ligands that are typically not expressed by healthy cells, but become upregulated by cellular stress associated with transformation or infection. Engagement of NKG2D by its ligands displayed on a target cell membrane leads to NK cell activation, cytokine secretion, and lysis of the target cell. Despite the importance of NKG2D for controlling tumors, the molecular mechanisms driving NKG2D ligand expression on tumor cells are not well defined.

The work described in this dissertation was centered on the identification of novel regulators of ULBP1, one of the human NKG2D ligands. Using a forward genetic screen of a tumor-derived human cell line, we identified several novel factors supporting ULBP1 expression, and used the CRISPR/Cas9 system to further investigate these hits. Our results showed stepwise contributions of independent pathways working at multiple stages of ULBP1 biogenesis, including transcription of the *ULBP1* gene, splicing of the *ULBP1* mRNA, and additional co-translational or post-translational regulation of the ULBP1 protein.

One of the novel regulators of ULBP1 we identified was ATF4, a stress-induced transcription factor. ATF4 drives the constitutive expression of *ULBP*1 on some cancer cell lines and causes further upregulation of *ULBP1* in response to stresses such as amino acid starvation or activation of the unfolded protein response. We found that ATF4 drives *ULBP1* transcription by binding directly to the *ULBP1* locus.

The screen also identified the RNA-binding protein RBM4 as a driver of ULBP1 expression. Analysis of RBM4-deficient cells revealed that RBM4 suppresses a novel alternative splicing event in the *ULBP1* transcript. The alternative isoform of *ULBP1* mRNA is unlikely to encode a functional protein. As such, RBM4 supports ULBP1 expression by promoting the splicing of the functional mRNA isoform.

This dissertation also describes the use of the CRISPR/Cas9 methodology to generate mice lacking two key NKG2D ligands, RAE-1ε and RAE-1δ. These mice are being used by other lab members to test hypotheses concerning regulation of NK cell activation imparted by RAE-1 expression on host cells within tumors. Additionally, these mice will soon be used to generate mice lacking all known NKG2D ligands.

The findings presented here highlight diverse mechanisms for the control of NKG2D ligand expression, and offer insight into the stress pathways that alert the immune system to danger. Furthermore, this work demonstrates the power of forward genetic screens and the CRISPR/Cas9 system for both discovery- and hypothesis-driven research.

Table of Contents

List of Figures and Tables

Acknowledgements

I could not have made it this far without the support of countless wonderful people. I'm only able to acknowledge a small fraction of them here, as properly thanking everyone who got me to this point would likely double the length of my thesis.

I will always be grateful to Dr. Jeff Fieberg, who offered me my first taste of research while I was an undergraduate at Centre College. Dr. Fieberg approaches everything with incredible energy, and his excitement kept the research moving even when the experiments wouldn't cooperate. When Dr. Fieberg uses ten exclamation points in a two-sentence email, he means every single one of them. Dr. Fieberg regularly sets all sorts of things on fire, and my passion for science was one of them. I must also thank Centre's Biochemistry and Molecular Biology professors for setting me on the path to my Ph.D. Dr. Peggy Richey was a fantastic advisor, and Dr. Steve Asmus taught me invaluable presentation skills. Finally, Dr. Stephanie Dew taught the class that sparked my interest in immunology.

When I was a wayward grad student, David Raulet took me into his lab. David guided me to projects that fit my interests and gave me the mentorship I needed to make them successful. Whenever I went to David's office with a problem (new or old), I was likely to leave with a good idea for how to tackle it, along with a fun story from David's years in science. When we hit obstacles that we couldn't clear on our own, David always knew the right person to call for advice or collaboration. I couldn't have asked for a better Ph.D. mentor.

In addition to David, Greg Barton, Michael Rape, and Karsten Gronert completed the roster of a stellar thesis committee. Each year this team gave me excellent guidance on the scientific questions at hand, where to focus my efforts, and how to pursue my career goals. I'm very lucky to have been guided by these people.

Other members of the Raulet lab have been very helpful, and also made the journey a lot more enjoyable. Kathleen Pestal bailed me out several times when I got in over my head on an experiment, and I will always value her friendship. All the members of the Raulet lab have given me experimental help along the way, but special thanks go to Alex Iannello, Michele Ardolino, Troy Trevino, and Lily Zhang. My two baymates, Lucas Horan and Thornton Thompson, were great for bouncing ideas around and spending lots of lab time together—they're both great people to share a bay or a beer with. Thornton is also a great softball and kickball teammate. I've also had the privilege of working with three talented undergraduates—Teal Russell, Jeanmarie Gonzalez, and Peter Dietzen—whose hard work was an enormous help to my research.

This work was the result of several very successful collaborations. My project began with the ULBP1 screen, done in collaboration with Jan Carette and Caleb Marceau. Jan was always very helpful whenever I had questions. Jan deserves special thanks for giving me a key piece of advice when my project was stalling. Jan told me that CRISPR had worked for his lab and suggested that I give it a shot myself. That idea worked out, to say the least. The late Chulho Kang performed the delicate injections needed to generate the *Raet1* KO mice, and his untimely death shocked and saddened us all. Near the end of my graduate work, two more collaborations gave me critical help when it was needed the most. Charles Sentman graciously provided chNKG2D T cells and detailed responses to my many, many emails about how to use them. Finally, I must give enormous credit to Stefan Muljo, Bryan Chim, Patrick Burr, and Chrysi Kanellopoulou for making the RNA-Seq and ChIP-Seq experiments possible. Stefan was always quick to offer advice on the science, the manuscript, and even do follow-up experiments. Bryan turned the mountain of sequencing data into usable information, and he has a knack for

explaining his analysis methods in exactly the right level of detail. I have had the kind of collaborations that some people only get to dream of.

Now for the emotional stuff. I grew up surrounded by the love and support of my parents and grandparents, who always encouraged my curiosity and creativity. My family has always supported my education, whether it was driving me to academic team meets, paying college tuition, or helping me move across the country for grad school. I don't have the words to properly thank my family for everything they've given me. I'll try to put my education to good use and hope that says "Thank you" in its own way.

Grad school has had its ups and down. Throughout it all, I've had Molly to help me celebrate the good times and help me survive the bad. The call of the lab kept us apart all too often, but late nights at the bench were bearable knowing that I had the most amazing wife to come home to. Molly, this thesis and its author are dedicated to you.

Benjamin Gowen
May 2015

Chapter 1
Introduction

Introduction to the immune system

A broad view

So far in my life, I have encountered influenza, norovirus, streptococcus, and myriad other microbes that viewed my body as a great place to replicate for a while. These weren't exactly pleasant meetings, but I survived. Most mammals are latently infected with one herpesvirus or another, and about a fifth of the U.S. population has been infected with the parasite *Toxoplasma gondii*, but most of us don't show any symptoms of these infections. In the average human, human cells are outnumbered by bacteria by about ten to one. Our exquisitely evolved immune system keeps these infections at bay.

Life isn't an all-out war between host and microbe, however. Many of the bacteria living in the human gut are harmless, and some perform beneficial functions. The immune system must limit the growth of pathogens while allowing the harmless microorganisms to flourish. If the immune system reacts overzealously or against inappropriate targets, autoimmune and inflammatory diseases develop. The immune system must be precisely regulated, reacting just the right amount to keep us healthy. How are immune cells activated against the right targets? This is a broad and important topic being investigated by scientists across the planet. This thesis addresses this question in one specific context.

Innate and adaptive immunity

The mammalian immune system consists of two branches: innate and adaptive. The adaptive immune system, led by T and B cells, can generate potent and incredibly specific responses and is often essential for clearing an infection. Adaptive immunity also retains immunological memory, mounting faster and more effective responses the second time an antigen is encountered. The adaptive immune system is great, but it needs help to effectively protect the host.

The innate immune system acts quickly—days before a protective adaptive response can be mounted. The innate immune system recognizes tissue damage if the skin or other barrier is broken, pathogen-associated molecular patterns (PAMPs), such as components of the bacterial cell wall, or activities associated with pathogenesis, such as invasion of the host cell cytosol. Innate immunity provides the first line of defense against an invading pathogen to keep the initial infection in check. Signals from innate immune cells then help activate and shape the adaptive immune response. This thesis focuses on the activation of natural killer (NK) cells, which are an important component of the innate immune system.

Cancer and the immune system

Although the immune system is most often thought of in the context of host defense against microbes, it also plays an important role in preventing or controlling the growth of cancer. Mutations or the re-expression of developmental genes can cause cancer cells to display "foreign" antigens, and in some cases normal proteins are overexpressed in cancer. In all these cases, the corresponding antigens can potentially be recognized by T and B cells. Tumor cells are also recognized by the innate immune system. As will be discussed below, stress pathways active in tumor cells cause the upregulation of cell surface proteins that sensitize tumors to elimination by the immune system, especially NK cells. Tumor cells are under selective pressure to escape

elimination by cell-intrinsic tumor suppressors (e.g., loss of p53 function) as well as elimination by the immune system. Late-stage tumors may make poor targets for immune cells, since an advanced tumor will be composed of descendants of cells that evolved to evade immune recognition.

Natural killer cells

Natural killer (NK) cells are lymphocytes of the innate immune system. Initially, two groups reported a subset of lymphocytes with the ability to lyse certain tumor cells in vitro (Herberman, Nunn et al. 1975, Kiessling, Klein et al. 1975). Unlike T and B cell responses, this cytotoxic activity did not require priming against the target, and the effectors were dubbed "natural killer cells." Since these initial reports, NK cells have been much more precisely defined, and our understanding of their function has grown immensely (Lanier, Phillips et al. 1986, Vivier, Tomasello et al. 2008, Vivier, Raulet et al. 2011).

NK cells are important in the early control of bacterial and viral infections, and also play an important role in cancer immunosurveillance (Ashkar, Reid et al. 2009, Jost and Altfeld 2013, Marcus, Gowen et al. 2014). NK cells recognize potential target cells using germline-encoded stimulatory and inhibitory receptors, and the activation of NK cells is controlled by the balance of signals received from these receptors. Upon activation, NK cells lyse their target cells and release pro-inflammatory cytokines, such as IFN-γ.

Inhibitory receptors

NK cells express several inhibitory receptors that bind to MHC class I (MHC I) molecules (Shifrin, Raulet et al. 2014). Classical MHC I molecules are recognized by the killer cell immunoglobulin-like receptors (KIRs) in humans and the Ly49 receptors in mice. The CD94/NKG2A receptor recognizes a non-classical MHC I molecule (HLA-E in humans, Qa-1b in mice) which presents peptides derived from MHC I leader sequences. Together these receptors allow an NK cell to "perceive" the expression of MHC I by potential target cells. CD8+ cytotoxic T cells recognize foreign antigens presented on MHC I, and many viruses interfere with MHC I expression whereas tumor cells commonly decrease or extinguish expression of MHC I molecules to evade T cell recognition. These "sneaky" cells pay a price for evading T cells. NK cells encountering a target with decreased MHC Class I expression receive less inhibitory signal, become activated, and lyse the target, a process known as "missing self recognition" (Karre, Ljunggren et al. 1986). In addition to their role in missing self recognition, NK inhibitory receptors help tune NK cell responsiveness (Shifrin, Raulet et al. 2014).

NK cells also express inhibitory receptors that recognize ligands other than MHC Class I (Vivier, Tomasello et al. 2008). The receptor KLRG1 recognizes cadherins. In humans, NKR-P1A binds the ligand LLT-1. In mice, the receptors NKRP1-B and NKRP1-D recognize the ligand Clr-b. Some viruses exploit inhibitory receptor:ligand interactions to evade NK-mediated lysis of infected cells. Human cytomegalovirus (HCMV) encodes a peptide that is presented by HLA-E, creating an HLA-E/peptide complex that engages the inhibitory CD94/NKG2A receptor (Tomasec, Braud et al. 2000, Ulbrecht, Martinozzi et al. 2000). HCMV also encodes proteins that downregulate classical MHC I molecules, so the inhibitory HLA-E/peptide complex may substitute for MHC I, with the overall effect being that HCMV-infected cells evade detection by both NK cells and T cells.

Activating receptors

NK cell activating receptors frequently recognize stress-induced ligands expressed by infected or transformed cells, allowing dangerous cells to be recognized and eliminated. Furthermore, the absence of signals from inhibitory receptors is not sufficient for NK cell activation—signals from stimulatory receptors must also be provided. NKG2D is the best-studied NK cell activating receptors and will be discussed in detail below. Other activating receptors include the "natural cytotoxicity receptors" (NCRs), SLAM family receptors, and DNAM-1 (Marcus, Gowen et al. 2014).

NKG2D and its ligands

The receptor NKG2D

NKG2D is a homodimeric receptor initially identified in a screen of cDNAs expressed by NK cells (Raulet 2003). NKG2D is expressed by virtually all NK cells in both humans and mice. NKG2D is also expressed on some subsets of conventional T cells, γδ T cells, and NKT cells, but expression can vary depending on activation state and tissue localization. The subsets of T cells expressing NKG2D also vary between mouse and human. Whereas NKG2D provides a potent activating signal to NK cells, signaling through NKG2D generally provides co-stimulatory signals to T cells. NKG2D uses the signaling adapters DAP10 (in humans and mice) and DAP12 (in mice only) (Diefenbach, Tomasello et al. 2002). Cross-linking of NKG2D results in NK cell activation, the release of the cytokine IFN-γ, and target cell lysis (Jamieson, Diefenbach et al. 2002).

NKG2D ligands

The ligands for NKG2D are cell surface glycoproteins with structural similarity to MHC Class I. To date, eight NKG2D ligands have been identified in humans (ULBP1-6, MICA, MICB), and nine have been found in mice (RAE-1α-ε, H60a-c, and MULT1). NKG2D ligands can be transmembrane or GPI-anchored, and their affinities for NKG2D (K_D) range from 10^{-6} to $6x10^{-9}$ M. A summary of NKG2D ligand structure, affinity, and chromosomal location is shown in Figure 1-1. This figure was originally published as part of the review article "Regulation of Ligands for the NKG2D Activating Receptor" (Raulet, Gasser et al. 2013).

a

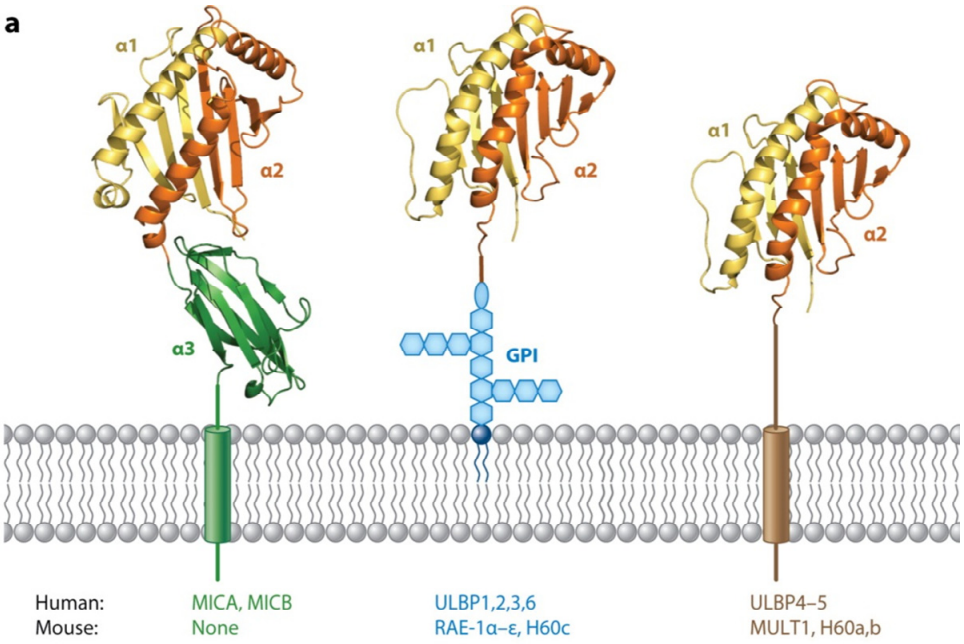

b

Human NKG2D ligands				
Ligand	**Receptor type**	**Affinity, K_D (M)**	**Chromosomal location**	**Alternate name**
MICA	TM	$0.9–1 \times 10^{-6}$	6p21.33	PERB11.1
MICB	TM	8×10^{-7}	6p21.33	PERB11.2
ULBP1	GPI	1.1×10^{-6}	6q25.1	RAET1I
ULBP2	GPI	ND	6q25.1	RAET1H
ULBP3	GPI	ND	6q25.1	RAET1N
ULBP4	TM	ND	6q25.1	RAET1E
ULBP5	TM	ND	6q25.1	RAET1G
ULBP6	GPI	ND	6q25.1	RAET1L

Mouse NKG2D ligands				
Ligand	**Receptor type**	**Affinity, K_D (M)**	**Chromosomal location**	**Alternate name**
RAE-1α	GPI	7×10^{-7}	10qA3	RAE-1a
RAE-1β	GPI	$3–19 \times 10^{-7}$	10qA3	RAE-1b
RAE-1γ	GPI	$5–6 \times 10^{-7}$	10qA3	RAE-1c
RAE-1δ	GPI	$7–8 \times 10^{-7}$	10qA3	RAE-1d
RAE-1ε	GPI	3×10^{-8}	10qA3	RAE-1e
H60a	TM	$2–3 \times 10^{-8}$	10qA3	
H60b	TM	3×10^{-7}	10qA3	
H60c	GPI	9×10^{-6}	10qA1	
MULT1	TM	6×10^{-9}	10qA1	

Figure1-1: NKG2D ligands in humans and mice

A. Diagrams of NKG2D ligands based on the structure of MICB (left) and RAE1β (middle and right). Ribbon diagrams were kindly provided by Dr. Roland Strong. **B.** Properties of the NKG2D ligands and genes. This figure was originally published in Raulet, et. al, *Annual Review of Immunology*, 2013.

All NKG2D ligands engage NKG2D and lead to NK cell activation similarly. It is possible that the ligands' differing affinities or localization within membrane microdomains could lead to stronger or weaker signaling, but evidence of this has not yet been found. The large number of NKG2D ligands is somewhat surprising in light of this functional similarity, but multiple non-mutually exclusive explanations exist. Pathogens such as MCMV encode proteins that downregulate certain NKG2D ligands; expansion of multiple distinct NKG2D ligands may be part of the evolutionary arms race between host and pathogen (Lodoen, Ogasawara et al. 2003). Alternatively, numerous NKG2D ligands may have evolved to provide protection from a wider range of unhealthy conditions, assuming that different ligands are to some extent regulated by distinct stress pathways. The presence of many NKG2D ligands with non-redundant regulatory modules increases the number of stress conditions that can be sensed by NKG2D.

Expression and regulation of NKG2D ligands

Expression of NKG2D ligands is absent or very low in most healthy tissues, which is important for preventing inappropriate NK cell activation and autoimmunity. Exceptions include the thymus and murine fetal brain, but these tissues may be protected from NK cell immunosurveillance, either because of tissue barriers or because NK cells differentiate later in embryonic development (Nice, Coscoy et al. 2009, Jung, Hsiung et al. 2012). The regulation of NKG2D ligands has been comprehensively reviewed in Raulet, Gasser, et al., 2013. A few key examples of different modes of regulation are discussed below.

Transcriptional regulation

Jung and colleagues demonstrated transcriptional control of certain NKG2D ligands in response to proliferative signals (Jung, Hsiung et al. 2012). Cultured mouse fibroblasts upregulated RAE-1ε at the surface and mRNA level. RAE-1ε decreased in response to a variety of treatments that inhibit proliferation, such as serum starvation or the cell cycle inhibitor roscovitine. Re-addition of serum to starved cultures, or removal of roscovitine, caused cells to begin proliferating again, and RAE-1ε expression was restored. The effect of proliferation on RAE-1ε expression was traced to E2F family transcription factors, which regulate cell cycle entry. E2F binding sites were identified in the *Raet1e* promoter, and chromatin immunoprecipitation (ChIP) showed binding of E2F1, E2F2, and E2F3 to the *Raet1e* promoter that decreased in response to serum starvation. This mode of regulation may be conserved in humans. The colorectal carcinoma cell line HCT-116 downregulated expression of ULBP2/5/6 and MICA/B in response to serum starvation or treatment with the cell cycle inhibitor roscovitine.

Regulation of mRNA splicing

The *Raet1e* gene (encoding the RAE-1ε protein) contains 6 annotated non-coding exons upstream of the coding sequence. Ben Hsiung, while a graduate student in the Raulet lab, identified multiple isoforms of the *Raet1e* mRNA with different patterns of exon inclusion (Hsiung 2008, Jung, Hsiung et al. 2012). A similar pattern of exon inclusion and exclusion was observed for *Raet1α*, which is highly similar to *Raet1e*. Most cell lines tested expressed multiple isoforms, and the pattern of isoform expression varied between cell lines. The mechanisms by

which alternative splicing of *Raet1* mRNA is regulated remain unclear, and the consequences of differential splicing on RAE-1ε protein expression have not been investigated. However, since the mRNA 5′ UTR's often encode regulatory elements, it is tempting to speculate that alternative splicing of *Raet1* mRNA may regulate RAE-1 expression.

Post-translational regulation

Post-translational regulation of MULT1 was shown by Nice and colleagues (Nice, Coscoy et al. 2009, Nice, Deng et al. 2010). *MULT1* mRNA is expressed in several cell lines and normal tissues that do not express MULT1 protein at the cell surface. It was found that under normal conditions, MULT1 is degraded due to ubiquitination of several lysines of its cytoplasmic tail. This process was blocked by proteasome inhibition, inhibition of lysosomal acidification, or mutation of the ubiquitinated lysines. The E3 ubiquitin ligases MARCH4 and MARCH9 constitutively associated with MULT1 and mediated MULT1 ubiquitination although additional MULT1 E3 ligases probably also participate in this regulation. Heat shock and UV irradiation increased MULT1 half-life and cell surface expression. Heat shock caused MULT1 and MARCH4/9 to dissociate, reducing ubiquitination and increasing surface expression.

Regulation by the DNA damage response

This section comes from the 2013 review article "Recognition of tumors by the innate immune system and natural killer cells" (Marcus, Gowen et al. 2014). I was a principle author of the DNA damage response subsection of that article.

Replication stress (the result of stalled replication forks) and DNA double-strand breaks activate the DNA damage response (DDR) in tumor cells and precancerous lesions (Bartkova, Horejsi et al. 2005, Gorgoulis, Vassiliou et al. 2005). DNA damage and replication stress activate the protein kinases ATR and/or ATM, which initiate the DDR kinase cascade (Cimprich and Cortez 2008, Shiloh and Ziv 2013) by phosphorylating the checkpoint kinases CHK1 and CHK2, respectively, in addition to many other target proteins. Activation of the DDR arrests cell cycle progression, and induces DNA repair functions. If DNA damage is extensive or irreparable, the DDR activates the p53 tumor suppressor, which can induce apoptosis or senescence depending on the cellular context. The DDR is often activated in developing tumors, but is also induced by many common cancer therapies, including irradiation and many chemotherapeutic drugs (Lord and Ashworth 2012).

In response to DNA damage, the mouse NKG2D ligands RAE-1 and MULT1 (Gasser, Orsulic et al. 2005, Gasser and Raulet 2006) and the human NKG2D ligands ULBP1-3 and MICA/B (Gasser, Orsulic et al. 2005, Soriani, Zingoni et al. 2009) are upregulated, although which ligand(s) and the degree of upregulation varies between different cell types and patient samples. Expression of DNAM-1 ligands also increases in response to DDR activation (Soriani, Zingoni et al. 2009, Ardolino, Zingoni et al. 2011). In the studies cited above, upregulation of ligands for both NKG2D and DNAM-1 in response to DNA damage occurred in an ATR/ATM- and CHK1/CHK2-dependent manner. The in vivo relevance of these findings is suggested by recent evidence that spontaneous tumor regression in the *Eμ-Myc* transgenic model of lymphoma/leukemia is partially ATM and DNAM-1 dependent (Croxford, Tang et al. 2013).

Although NKG2D ligand mRNA levels increase in response to DNA damage, the rate of transcription of these genes did not increase in nuclear run-on experiments, whereas the rate of

degradation of the *Raet1* mRNA was decreased, suggesting that the DDR drives stabilization of NKG2D ligand mRNAs rather than transcription of the ligand genes (B. Hsiung and D.H. Raulet, unpublished data). The mechanism of transcript stabilization remains unclear. DDR-mediated increases in DNAM-1 ligand expression also occur at the mRNA level, but the specific mechanism has not been investigated to date. It is also unknown whether NKG2D and DNAM-1 ligands are controlled by the same or different DDR effectors.

Activation of the tumor suppressor p53 is a major downstream effect of the DDR, but NKG2D ligand upregulation in response to DNA damage was p53-independent in the mouse studies performed to date (Gasser, Orsulic et al. 2005, Iannello, Thompson et al. 2013). In human cells, however, two different studies suggested that p53 stimulates transcription of certain NKG2D ligands. It was reported that preventing proteasomal degradation of p53 by the MDM2 inhibitors RITA and Nutlin allows p53 to bind the promoter region of the *ULBP1* and *ULBP2* genes, resulting in enhanced *ULBP1* expression (Li, Lakshmikanth et al. 2011, Textor, Fiegler et al. 2011). Surprisingly, another study concluded that p53 activation negatively regulates human NKG2D ligand expression (Heinemann, Zhao et al. 2012). Notably, neither of these effects of p53 were studied in the context of the DNA damage response.

Summary

The examples above illustrate the diverse stimuli leading to NKG2D ligand expression and the different modes of regulation that are used. However, our understanding of NKG2D ligand expression is patchwork. The post-translational regulation of MULT1 identified by Nice, *et al*. cannot be engaged if the MULT1 gene is not transcribed in the first place, and the signals driving MULT1 transcription are unknown (Nice, Coscoy et al. 2009). Furthermore, the regulation of human ligands for NKG2D (especially the ULBP family) have been less well-studied than the ligands found in mice. This motivated our study of ULBP1 with an unbiased approach that could, in principle, identify regulators working at any stage of ULBP1 biogenesis.

Cell stress pathways and ATF4

Definition of cell stress

"Cell stress" is a vague term any may carry different meaning in different contexts. For the purpose of this thesis, "cell stress" refers to any condition that requires a cell to adapt in order to survive or carry out its functions. For example, plasma cells must secrete large amounts of antibody. B cells differentiating into plasma cells are under stress, because the endoplasmic reticulum (ER) protein-folding capacity of the B cell is insufficient for the amount of antibody demanded (Shaffer, Shapiro-Shelef et al. 2004, Schroder and Kaufman 2005). Failure to adapt to ER stress leads to apoptosis. Plasma cells adapt to this stress by upregulating chaperone proteins and eventually building more endoplasmic reticulum, so the resulting plasma cell would not be considered "stressed".

An organism could certainly benefit from the elimination of stressed cells by the immune system. A cell that cannot meet its protein-folding burden is at best inefficient. At worst, the accumulation of unfolded proteins could lead to the formation of toxic aggregates. Most interestingly from the perspective of this thesis is that activation or such stress pathways may be

hallmarks of cancer or infection, and could therefore be coupled to the elimination of dangerous cells.

The transcription factor ATF4 is a central player in the present work, and the remainder of this chapter will discuss stress pathways that drive ATF4 expression.

The integrated stress response

Multiple forms of cellular stress, including amino acid starvation, the unfolded protein response, oxidative stress, and the presence of dsRNA converge on the phosphorylation of the translation initiation factor eIF2α (Rutkowski and Kaufman 2003, Suragani, Zachariah et al. 2012). The downstream effects of eIF2α phosphorylation are known as the "integrated stress response" or "ISR" (Harding, Novoa et al. 2000, Harding, Zhang et al. 2003, Ron and Walter 2007). Some of the stress conditions that activate the integrated stress response are discussed in more detail below, but first we will discuss the general logic and outcomes of ISR activation.

Canonical translation initiation requires the scanning ribosome and the initiating Met-tRNA to bind to the AUG start codon (Sonenberg and Hinnebusch 2009). Translational initiation generally requires that eIF2 is in the active, GTP-bound state. eIF2α phosphorylation prevents proper recycling of inactive, GDP-bound eIF2 into the active, GTP-bound state. The activation of eIF2α kinases thus decreases the pool of active eIF2. This causes a global reduction in the initiation of translation of the vast majority of proteins. A decrease in protein synthesis is beneficial to cells undergoing all forms of stress that lead to the ISR. Cells undergoing starvation, ER stress, or oxidative stress have a more limited capacity for protein synthesis than healthy cells. Inhibiting the translation of most proteins allows scarce resources to be devoted synthesizing a select group of stress-mitigating proteins, discussed below. Furthermore, some cells with active integrated stress responses risk translating proteins that are harmful to the host cell or organism. Cells undergoing ER stress can produce toxic protein aggregates, and viral infection (sensed by the dsRNA-activated eIF2α kinase PKR) can turn cells into viral replication factories. In both cases, the organism benefits from decreased protein synthesis that occurs as part of the integrated stress response.

In contrast, eIF2 inactivation favors the translation of a minority of proteins, including ATF4. *ATF4* mRNA is constitutively transcribed but contains 3 upstream open reading frames (uORFs) prior to the protein coding sequence (Lu, Harding et al. 2004, Vattem and Wek 2004). Under normal conditions, scanning ribosomes initiate at one of the uORFs, "soaking up" most of the available ribosomes before they can initiate at the protein coding ORF. Lack of active eIF2 causes ribosomes to skip some of the AUG's they encounter (Sonenberg and Hinnebusch 2009). Thus the translation of ATF4 is increased by eIF2α phosphorylation, even though global translation is decreased. The transcriptional targets of ATF4 include genes that help mitigate ISR-inducing stresses. Individual target genes are discussed below, alongside the particular stresses they address. It should be noted, however, that pathway analysis of RNA-Seq data from mouse embryonic fibroblasts (MEFs) did not identify genes involved in the immune response to be a major family of ATF4 target genes (Han, Back et al. 2013).

The targets of ATF4 target are not limited to genes that promote stress mitigation and cell survival. ATF4 drives expression of the transcription factor CHOP, and prolonged expression of ATF4 and CHOP drives apoptosis (Han, Back et al. 2013). How ATF4 and CHOP drive apoptosis is the subject of ongoing research. For perspective on ATF4 and CHOP-induced apoptosis, we recommend reviews by Tabas and Ron (Tabas and Ron 2011) and Claudio Hetz

(Hetz 2012), as well as experiments recently published by Han, Kaufman, and colleagues (Han, Back et al. 2013). Regardless of the mechanism(s) by which apoptosis is induced, it makes sense that the integrated stress response would comprise both pathways for repair and survival *and* pathways promoting apoptosis. If the offending stress cannot be resolved in a timely fashion, or if the integrated stress response is active in a tumor or virally infected cells, apoptosis or elimination of the stressed cell is the most beneficial outcome for the organism.

ER stress and the unfolded protein response

ER stress occurs when the burden of proteins in the secretory pathway exceeds the protein folding capacity of the ER (Schroder and Kaufman 2005). ER stress activates a cellular program known as the unfolded protein response (UPR). The stress mitigation mechanisms engaged by the UPR are 1) Global inhibition of protein synthesis to decrease the ER protein folding burden; 2) degradation of misfolded proteins in the ER; 3) transcriptional and translational upregulation of protein chaperones; 4) biosynthesis of additional ER; and 5) apoptosis, which may occur if mitigation mechanisms ultimately fail. Three molecular arms of the UPR achieve these effects: 1) Activation of the kinase/RNase IRE-1, leading to complete splicing and translation of transcripts encoding the transcription factor XBP1; 2) Cleavage of the transcription factor ATF6 into its active form; and 3) Activation of the eIF2α kinase PERK, which engages the integrated stress response and translation of ATF4. ATF4, along with the ATF6 arm of the UPR, upregulates transcription of *Hspa5*, which encodes the ER-resident chaperone protein BiP/GRP78 (Luo, Baumeister et al. 2003). ATF4 also drives expression of *Ero1l*, which encodes an ER-resident protein that promotes protein disulfide bond formation (Cabibbo, Pagani et al. 2000, Schroder and Kaufman 2005, Han, Back et al. 2013). Raising the level of BiP and Ero1-L increases the folding capacity of the ER.

ER stress and the UPR are common features of cancer and neurodegenerative diseases (Ma and Hendershot 2004, Kim, Bhattacharya et al. 2015). Overexpression of UPR components such as ATF6, XBP-1, and BiP/GRP78 has been found in primary tumors and cell lines derived from breast cancers(Fernandez, Tabbara et al. 2000, Fujimoto, Onda et al. 2003), hepatocellular carcinomas (Shuda, Kondoh et al. 2003), and multiple myeloma (Reimold, Ponath et al. 1996, Munshi, Hideshima et al. 2004). The mechanism by which the UPR becomes active is likely to vary between different types of cancer. Multiple myeloma arises from plasma cells, which secrete large amounts of antibody. Antibody secretion by multiple myeloma cells may place sufficient burden on the secretory pathway to activate the UPR. In mice, XBP-1-deficient B cells have impaired antibody secretion and plasma cell differentiation (Reimold, Iwakoshi et al. 2001). Hyperactive mTOR signaling, which is active in many types of cancer (Zoncu, Efeyan et al. 2011), can also contribute to UPR activation in tumor cells. Increased protein synthesis driven by mTOR signaling can cause UPR activation directly (Ozcan, Ozcan et al. 2008), or through crosstalk between mTOR and UPR signaling pathways (Appenzeller-Herzog and Hall 2012). Hypoxia, a common feature of the tumor microenvironment, can also activate the UPR, although the molecular mechanism for UPR activation by hypoxia is unclear (Wouters and Koritzinsky 2008).

Starvation

Tumors often experience nutrient and oxygen deprivation due to poor vascularization. Amino acid starvation is sensed by the eIF2α kinase GCN2, which is activated by uncharged

tRNAs (Dong, Qiu et al. 2000, Harding, Novoa et al. 2000). Similar to the case of ER stress, amino acid starvation is mitigated by inhibiting protein translation and the upregulation of ATF4. To cope with amino acid starvation, ATF4 induces transcription of numerous amino acid transporters and synthetases (Han, Back et al. 2013). Glucose deprivation also activates ATF4, via the UPR, but the specific underlying mechanism of this is unclear (Schroder and Kaufman 2005).

Hypoxia

Hypoxia can cause the upregulation of ATF4 by activating the unfolded protein response and PERK (Koumenis, Naczki et al. 2002). Hypoxia can also increase ATF4 protein expression by inhibiting negative regulators of ATF4 protein stability (Koditz, Nesper et al. 2007). Notably, both mechanisms of ATF4 upregulation are independent of the hypoxia inducible factors (HIFs). However, reports conflict on the severity of hypoxia (ranging from 1% to 0.01% O_2) and duration of treatment required for maximal ATF4 induction (Koumenis, Naczki et al. 2002, Ameri, Lewis et al. 2004, Blais, Filipenko et al. 2004, Bi, Naczki et al. 2005, Koditz, Nesper et al. 2007). This may be partially explained by the inexactness of the definition of "hypoxia". The concentration of oxygen naturally available in different tissues is known to vary dramatically (Carreau, El Hafny-Rahbi et al. 2011). Oxygen concentrations that cause hypoxic stress in some cell types may be perfectly tolerated by others that are adapted to low-oxygen environments. Upregulation of ATF4 in some tumors is coincident with hypoxic areas of the tumor (Ameri, Lewis et al. 2004, Bi, Naczki et al. 2005). Transcription of *VEGFA*, which promotes vascularization and thus increased oxygen supply, is a key target of ATF4 in response to hypoxia (Roybal, Hunsaker et al. 2005, Pan, Chen et al. 2007). It should be noted, however, that *VEGFA* was not found to be a direct transcriptional target of ATF4 in some analyses (Han, Back et al. 2013).

Oxidative stress

Oxidative stress occurs when homeostasis between reactive oxygen species (ROS) and antioxidant molecules is disrupted. Oxidative stress upregulates ATF4, which in turn activates transcription of antioxidant response genes, such as those involved in glutathione synthesis (Harding, Zhang et al. 2003, Lange, Chavez et al. 2008, Han, Back et al. 2013). In the case of oxidative stress induced by treatment with heavy metals, ATF4 is upregulated by activation of the eIF2α kinase HRI (Matts, Schatz et al. 1991, McEwen, Kedersha et al. 2005). Other oxidative stress agents may also act through HRI, but a role for other eIF2α kinases has not been ruled out.

Chapter 2
Methodology

Cell culture

Cell culture was performed at 37 °C in humidified atmosphere containing 5% CO_2. HAP1 cells were cultured in complete IMDM, consisting of IMDM (Life Technologies), 10% fetal calf serum (FCS, Omega Scientific), 100 U/ml penicillin (Life Technologies), 100 µg/ml streptomycin (Life Technologies), and GlutaMAX-I (Life Technologies). K-562 and Jurkat cells were cultured in complete RPMI, consisting of consisting of RPMI (Life Technologies), 10% fetal calf serum, 1 mM Sodium Pyruvate (Life Technologies), MEM Non-Essential Amino Acids (Life Technologies), 100 U/ml penicillin, 100 µg/ml streptomycin, 0.2 mg/ml glutamine (Sigma-Aldrich, St. Louis, MO), 10 µg/ml gentamycin sulfate (Lonza), 20 mM HEPES (Thermo Fisher Scientific), and 50 µM 2-mercaptoethanol (EMD Millipore). chNKG2D T cells were cultured in complete RPMI, but with 10 mM HEPES and supplemented with 50 U/mL recombinant human IL-2 (NCI, Frederick, MD). Mouse lymphokine-activated killer (LAK) cells were cultured in RPMI supplemented with 5% fetal calf serum, 100 U/ml penicillin, 100 µg/ml streptomycin, 0.2 mg/ml glutamine, 10 µg/ml gentamycin sulfate, 20 mM HEPES, 50 µM 2- and 1000 U/mL recombinant human IL-2. Human foreskin fibroblast cells were cultured in complete DMEM, consisting of consisting of DMEM (Life Technologies), 10% fetal calf serum, 1 mM Sodium Pyruvate, MEM Non-Essential Amino Acids, 100 U/ml penicillin, 100 µg/ml streptomycin, 0.2 mg/ml glutamine, 10 µg/ml gentamycin sulfate, 20 mM HEPES, and 50 µM 2-mercaptoethanol. Unless otherwise noted, adherent cells were lifted from culture plates with gentle trypsinization. To lift cells, growth media was aspirated, cells were washed once with PBS, and a minimal amount of trypsin (0.1% trypsin, 1 mM EDTA, in PBS) was added to cover the culture plate. Cells were incubated at 37 °C for 2 minutes, which I determined was the minimum amount of time needed to reliably lift HAP1 and other cell types under these conditions. Trypsin was immediately quenched by the addition of either complete culture media or ice cold FACS buffer.

Antibodies

Unless otherwise noted, the antibodies used recognize human antigens. Antibodies against ULBP1 (Clone 170818), ULBP2/5/6 (Clone 165903), ULBP3 (Clone 166510), MICA (Clone 159227), and MICB (Clone 236511) were purchased from R&D Systems. Antibodies against HLA-A,B,C (Clone W6/32), NKG2D (Clone 1D11), CD55 (Clone JS11), CD59 (Clone p282 H19), CD112 (Clone TX31), CD155 (Clone TX24), CD50 (Clone CBR-IC3/1), CD54 (Clone HCD54), CD102 (Clone CBR-IC2/2), CD11a (Clone HI111), CD261 (DJR1), and CD262 (DJR204 (7-8)) were purchased from Biolegend. In some experiments, the antibodies against HLA-A,B,C (Clone W6/32) and CD59 (OV9A2) were purchased from eBiosience. Antibodies against ATF4 used for ChIP were sc-200 (Santa Cruz Biotechnology), D4B8 (Cell Signaling Technologies), and ABE387 (EMD Millipore). The ABE387 antibody was a kind gift from Michael Kilberg.

Additional reagents

Histidinol, thapsigargin, MG132 and RNase A were purchased from Sigma-Aldrich. Proteinase K was purchased from Roche (Basel, Switzerland).

Retroviral gene-trap mutagenesis and screen

Mutagenesis of HAP1 cells was performed as previously described (Carette, Raaben et al. 2011). Selection of ULBP1^{low} cells was performed using sequential rounds of selection. First, 10^8 mutagenized HAP1 cells were labeled with ULBP1 antibody, and ULBP1^{high} cells were depleted by running the cells over two sequential MACS LD columns (Miltenyi Biotec, San Diego, CA). Depletion of ULBP1^{high} cells on this day was less efficient than we had achieved in previous experiments, so we chose to re-plate the selected cells, expand the cells for 2 days, and repeated the magnetic depletion of ULBP1^{high} cells. We speculate that a single round of magnetic depletion may have been sufficient if adequate depletion of ULBP1^{high} cells had been achieved. Magnetically selected cells were re-plated and expanded for 5 days. Expanded cells were labeled with ULBP1 and CD55 antibodies, and ULBP1^{low}CD55^{+} cells were sorted by FACS, re-plated, and expanded. Genomic DNA was isolated from $4x10^7$ cells using the QIAamp DNA Mini Kit (QIAGEN). Mapping of gene-trap insertion sites and statistical analysis was performed as previously described (Carette, Raaben et al. 2011). The ULBP2 screen was performed identically, but with an antibody against ULBP2.

Flow cytometry

Cells were stained with the specified antibodies in 50 µL of PBS supplemented with 2.5% FCS or 1% BSA (FACS buffer). FACS buffer included 0.05% sodium azide for analytical flow cytometry, but not cell sorting. Dead cells were excluded from analysis by staining with DAPI (Biolegend). Multicolor flow cytometry was performed on an LSR Fortessa cytometer (BD Biosciences), and data were analyzed with FlowJo software (Tree Star, Inc.).

CRISPR/Cas9 gene targeting in cultured cells

Mutant HAP1 cells were generated by transiently co-transfecting cells with a Cas9 expression vector (pMJ918, a gift from Jennifer Doudna), a sgRNA expression vector (Addgene plasmid # 41824, a gift from George Church), and a GFP expression vector using Lipofectamine 2000. sgRNA sequence+protospacer adjacent motif (PAM) are listed in Table 2-1. Transfected cells were sorted based on GFP expression 24-72 hours post-transfection. To enrich cells with a mutant phenotype, cells were stained for ULBP1 expression 5-7 days post-transfection, and single ULBP1^{low} cells were sorted into 96-well plates. Mutant cell clones were identified by sequencing PCR products surrounding the Cas9:sgRNA target site. Genomic target sequences surrounding Cas9:sgRNA target loci are shown in Figure 2-1, along with the mutant sequences present in relevant HAP1 clones.

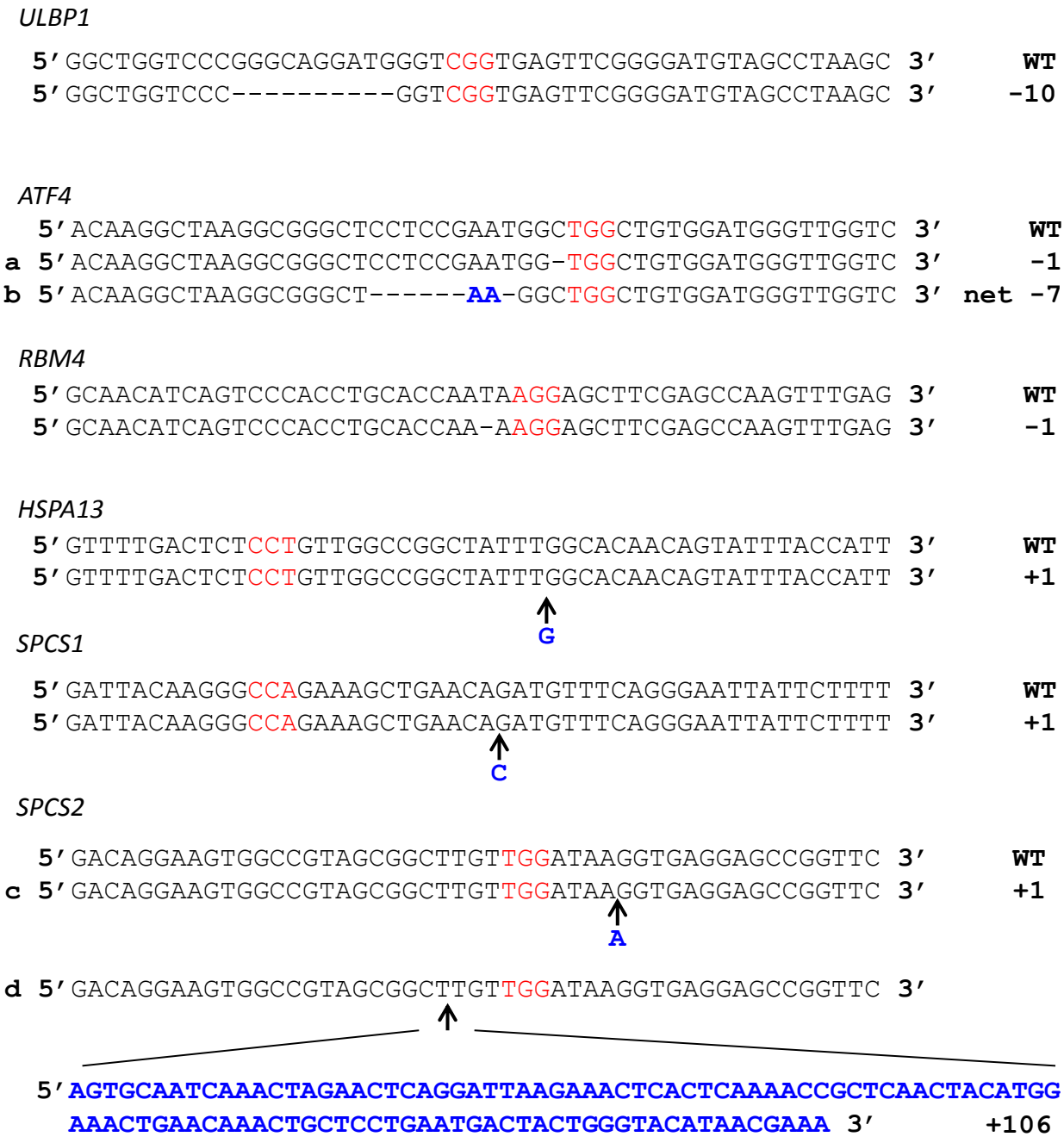

Figure 2-1: Sequences of CRISPR/Cas9 target sites in HAP1 cells
Genomic DNA sequence surrounding Cas9:sgRNA target loci as shown with protospacer-adjacent motif (PAM) in red. Inserted bases are in **bold blue** text. For *HSPA13* and *SPCS1*, the PAM was on the non-coding strand. For *ATF4*, mutation (a) was present in the *ATF4* single-KO line. Mutation (b) was present in all double- and triple-KO lines. For *SPCS2*, mutation (c) was present in the *ATF4*/*RBM4*/*SPCS2* triple-KO line. Mutation (d) was present in the *SPCS2* single-KO line.

Name	sgRNA Sequence+PAM	Used in
ULBP1 sgRNA	GGGTCCCGGGCAGGATGGGT**CGG**	HAP1
ATF4 sgRNA 1	GGCGGGCTCCTCCGAATGGC**TGG**	HAP1
ATF4 sgRNA 3	GCTCGTCACAGCTACGCCCT**GGG**	HAP1, K-562, Jurkat
ATF4 sgRNA 5	GTGGCCAACTATACGGCTCCA**GGG**	HAP1, K-562, Jurkat
RBM4 sgRNA	GAGTCCCACCTGCACCAATA**AGG**	HAP1
RBM4/RBM4b sgRNA	GCCCCGGGAGGCTACAGAGC**AGG**	HAP1, K-562
HSPA13 sgRNA	GTGCCAAATAGCCGGCCAAC**AGG**	HAP1
SPCS1 sgRNA	GCATCTGTTCAGCTAGCTTC**TGG**	HAP1
SPCS2 sgRNA	GAGTGGCCGTAGCGGCTTGT**TGG**	HAP1
SLC17A9 sgRNA	CATGAGCCAGGACTTCGGC**TGG**	HAP1
DNAJC13 sgRNA	GAACTTCTTACAGAAGCAT**TGG**	HAP1
CUL1 sgRNA	GCCTCACAATGTCGTCAACC**CGG**	HAP1
FBXW7 sgRNA	GAGAGCGGACCTCAGAACC**ATG**	HAP1
MKNK2 sgRNA	GGGTTTCCACCGTTCGTTCA**AGG**	HAP1

Table 2-1: sgRNA sequences
For each sgRNA, the protospacer adjacent motif (PAM) is indicated by **bold blue** text. Red text indicates that the 5′ G is not present in the genomic target sequence and was added to the sgRNA to allow transcription from the U6 promoter.

Mutation efficiency was not directly measured, but the fraction of HAP1 cells with loss-of-function mutations can be estimated by the fraction of ULBP1^{low} cells that appeared after mutagenesis (Figure 3-3). ULBP1^{low} cells were routinely 5-15% of the transfected population. Loss-of-function mutations were typically present in 80% of clones derived from sorted ULBP1^{low} cells.

Deletion of *ATF4* in HAP1, K-562, and Jurkat cells was performed using a pair of sgRNAs flanking the *ATF4* gene. Cells were transiently co-transfected with GFP and the Cas9/sgRNA expression plasmid px330 (Addgene plasmid #42230, a gift from Feng Zhang). Transfected cells were sorted based on GFP expression 24-72 hours post-transfection. 5-7 days post-transfection, single cells were sorted into 96-well plates without any additional selection. At least one copy of *ATF4* was deleted in 4 out of 12 total K-562 clones screened. All copies of *ATF4* were deleted in 2 of these clones (17% KO efficiency). Deletion of *ATF4* was less efficient in Jurkat cells. At least one copy of *ATF4* was deleted in only 8 out of about 90 clones screened. All copies of *ATF4* were deleted in no more than 3 of these clones, possibly only 1 (1-3% KO efficiency).

RBM4/*RBM4b* KO HAP1 and K-562 cells were generated using one sgRNA targeting a shared sequence in *RBM4* and *RBM4b*, which resulted in deletion of the intervening genomic sequence in a fraction of the clones. Cells were co-transfected with px330 for Cas9 expression (Addgene plasmid #41824), a sgRNA expression vector (Addgene plasmid #41824) and a GFP expression vector. Cells were sorted as described for the *ATF4* KO K-562 cells. In the resulting mutant cells, both *RBM4* and *RBM4b* were truncated within 50 bp of the start codon of each gene. Because *RBM4* and *RBM4b* are convergently transcribed, only the 5' end of each gene remained. At least one copy of *RBM4* was deleted in 6-10 out of 26 total K-562 clones screened. All copies of *RBM4* were deleted in 2 of these clones (8% KO efficiency).

Table 2-2: PCR primers used to detect mutations

Target	Primer direction	Primer Sequence	Amplicon Size (bp)
ULBP1 sgRNA target locus	Forward	ATAAACAGCCGTGGTGTGAG	401
	Reverse	TGTCTGGGGAGATCACGATG	
ATF4 sgRNA 1 target locus	Forward	CATTCCTCGATTCCAGCAAAGC	345
	Reverse	TGAGTGATGGGGCCAAGTGAG	
Deletion of ATF4 with sgRNAs 2 and 3	Forward	CGTCCTCGGCCTTCACAATA	442
	Reverse	TCTTCAGGATGAGGCTTCTGC	
RBM4 sgRNA target locus	Forward	TGCACATAGAAGACAAGACGGC	332
	Reverse	CCTTGTGTTCAGCCCTCTACCC	
Deletion of RBM4/RBM4b	Forward	AGCAGGCCTTAGTTCACTCCC	339
	Reverse	CGAAAATGCTGCAGTGCACCG	
HSPA13 sgRNA target locus	Forward	TGCTGTCTGAGAGGAGTGCT	476
	Reverse	CCTCCAACTCTTCTGCGGTA	
SPCS1 sgRNA target locus	Forward	ATTTAATATCTTGCCCAGGCCC	394
	Reverse	ACCCACAAATTTCTTACCAAACAT	
SPCS2 sgRNA target locus	Forward	AACCTCAAGTCCCAGCAAGC	466
	Reverse	CGGGTCCAGGTTTGAAGTGT	
DNAJC13 sgRNA target locus	Forward	TTAAGTGGCCTTATGGAGACATTT	400
	Reverse	TAAACATACAATGCTTTCTCCTGC	

Lentiviral transduction of doxycycline-inducible constructs

For doxycycline-inducible gene expression, constructs encoding *GFP, ATF4*, *RBM4*, *HSPA13*, *SPCS1*, and *SPCS2* were cloned into the lentiviral vector pFG12-TRE-UbC-rtTA-Thy1.1 (hereafter pFG12), or the pFG12-derived vector pFG42-TRE-UbC-rtTA-GFP (hereafter pFG42). The pFG12 vector was a gift from the Schlissel lab. The *ATF4* construct was a gift from Yihong Ye (Addgene plasmid #26114). The *RBM4* construct was a gift from Lan Ko, Georgia Health Sciences University. The *HSPA13* construct was a gift from Kyungpyo Park, Seoul National University. The *SPCS1* construct was a gift from Tetsuro Suzuki, Hamamatsu University School of Medicine. The *HSPA13* construct was a gift from Kyungpyo Park, Seoul National University. *SPCS2* was cloned from HAP1 cDNA.

Lentiviral supernatants were generated by cotransfecting 293T cells with pFG12/pFG42 vector, the VSV-G plasmid pMD2.G, and the packaging plasmid psPAX2 using Lipofectamine 2000 (Life Technologies), and media was changed 24 hours post-transfection. Supernatants were harvested 48 hours post-transfection, filtered with a 0.45 μM PES syringe filter, and added to target cell cultures with 4 μg/mL polybrene. Transduced cells were sorted based on Thy1.1 or GFP expression. To induce gene expression, cells were cultured in complete medium with doxycycline at the concentrations noted in the figure legends.

Quantitative Reverse-transcriptase PCR (RT-qPCR)

Total RNA was isolated from cells using the RNeasy Mini Kit and on-column DNase digestion using the RNase-free DNase Set (QIAGEN). Reverse transcription was performed with iScript Reverse Transcription Supermix (Bio-Rad). Quantitative real-time PCR (qPCR) was performed on a CFX96 thermocycler using SsoFast EvaGreen Supermix (Biorad) with the following cycling program: Initial denaturation at 98 °C, 2′, followed by 40 cycles of 98 °C, 2″, 55 °C, 5″. Data were analyzed with Bio-Rad CFX Manager Software version 3.1 Gene expression was normalized to the reference genes *ACTB*, *GAPDH*, and *HPRT1*, normalizing the gene of interest to the geometric mean of the three reference genes (Vandesompele, De Preter et al. 2002). Primer sequences are listed in Table 2-3.

Table 2-3: Primers used for qPCR

Target	Primer direction	Primer sequence	Amplicon Size (bp)
ACTB	Forward	TTGGCAATGAGCGGTTCC	92
	Reverse	GTTGAAGGTAGTTTCGTGGATG	
GAPDH	Forward	CAACAGCGACACCCACTCCT	115
	Reverse	CACCCTGTTGCTGTAGCCAAA	
HPRT1	Forward	AGGATTTGGAAAGGGTGTTTATTC	109
	Reverse	CAGAGGGCTACAATGTGATGG	
Total *ULBP1* (Exon 3-Exon 3)	Forward	GCCAGGATGTCTTGTGAGCATGAA	134
	Reverse	TTCTTGGCTCCAGGATGAAGTGCT	
ULBP1 Canonical isoform (Exon 1-Exon 2)	Forward	ATCAGCGCCTCCTGTCCAC	136
	Reverse	AAAGACAGTGTGTGTCGACCCAT	
ULBP1 Alternative isoform (Extended Exon 1-Exon 2)	Forward	GGAATTGCAGGAGGGTGGAG	183
	Reverse	CAAAGGCTTTGGCCTTGTGGTTAA	
ULBP1 Spliced transcript (Exon 2-Exon 3)	Forward	TAAGTCCAGACCTGAACCACA	477
	Reverse	CCATTGAAGAGGAACTGCCAAG	
ULBP1 Alternative isoform and primary transcript (Exon 1-Extended Exon 1)	Forward	CCGGGCAGGATGGGTCG	263
	Reverse	TGTCTGGGGAGATCACGATG	
ULBP1 Unspliced transcript (Intron 1-Exon 2)	Forward	CCCTCAGAGGCCTTCACTTG	195
	Reverse	AAGGCCTTTCATCCACCAGG	
ULBP2	Forward	GCCGCTACCAAGATCCTTCT	161
	Reverse	TCATCCACCTGGCCTTGAAC	
ULBP3	Forward	CTCGCGATTCTTCCGTACCT	127
	Reverse	TCTGGACCTCACACCACTGT	
MICA	Forward	ATGTCCTGCCTGATGGGAATGGAA	189
	Reverse	CAGCAGCAACAGCAGAAACATGGA	
MICB	Forward	TGGATCTGTGCAGTCAGGGTTTCT	176
	Reverse	TGAGGTCTTGCCCATTCTCTGTCA	
ULBP1 Promoter ChIP	Forward	GCTGTCAGATGACGAGCCC	80
	Reverse	ATACACTGGGCGGGATCCTA	
ASNS Promoter ChIP	Forward	TGGTTGGTCCTCGCAGGCAT	66
	Reverse	CGCTTATACCGACCTGGCTCCT	
ASNS Exon 7 ChIP	Forward	GCAGCTGAAAGAAGCCCAAGT	62
	Reverse	TGTCTTCCATGCCAATTGCA	

Chromatin Immunoprecipitation (ChIP)

Cells were re-plated in fresh media 12-24 hours prior to treatment. Media was then replaced with fresh media or fresh media containing 2 mM histidinol, and cells were incubated for 24 hours. Chromatin complexes were cross-linked by adding formaldehyde to culture media to final concentration of 1%, and cells were incubated at room temperature for 10 minutes.

Cross-linking was quenched by adding glycine to a final concentration of 0.125 M. Cells were washed 2 times with ice cold PBS, and cell pellets were flash-frozen in a slurry of dry ice and ethanol.

Cells were resuspended in ChIP Lysis Buffer #1 and incubated for 10' at 4 °C with rotation, and centrifuged for 8' at 800 x *g* at 4 °C. Pellets were resuspended in ChIP Lysis Buffer #2 and incubated for 10′ at 4 °C with rotation, and centrifuged for 8′ at 800 x *g* at 4 °C. Pellets were resuspended in 3 volumes (~200 µL) of ChIP Lysis Buffer #3. Chromatin was sheared to an average fragment size of 200 bp using a Covaris S2 Sonifier. Sheared chromatin was diluted in additional ChIP Lysis Buffer #3, followed by addition Triton X-100 (final concentration 1%) and NaCl (final concentration 150 mM) and divided into 1 mL aliquots for immunoprecipitation. Antibody was added to chromatin samples, followed by overnight incubation at 4 °C, with rotation. Antibody-chromatin complexes were captured with Protein G Dynabeads (Life Technologies) at 4 °C for 2 hours, with rotation. Beads were washed 2x with Low Salt Wash Buffer, 1x with High Salt Wash Buffer, 1x with LiCl Wash Buffer, and 2x with TE. Beads were resuspended in ChIP Elution Buffer, and chromatin was eluted by incubating samples at 65 °C for 15'. Supernatant containing eluted chromatin was removed from the beads and reverse cross-linked by incubating samples overnight at 65 °C.

RNase A was added to samples to a final concentration of 0.2 mg/mL, followed by incubation at 37 °C for 1 hour. Proteinase K was then added to a final concentration of 0.4 mg/mL, followed by incubation at 56 °C for 1 hour. DNA was then isolated using the QIAGEN MinElute Kit, followed by qPCR as described above or Illumina Library prep.

ChIP-Seq libraries were prepared using the NEBNext Ultra DNA Library Prep Kit for Illumina (New England Biolabs), including optional size selection of adapter-ligated DNA and 13 cycles of PCR amplification. Final libraries were analyzed with a Qubit fluorometer (Life Technologies) and Bioanalyzer 2100 (Agilent) to assess quantity and quality. Libraries were clustered at a density of 6.5 pM with a cluster station and sequenced on a GAIIx Genome Analyzer (Illumina).

ChIP Buffer compositions and antibody concentrations

ChIP Lysis Buffer #1: 50 mM HEPES pH7.5, 140 mM NaCl, 1 mM EDTA, 10% Glycerol, 0.5% NP-40, 0.25% Triton X-100, Protease Inhibitors*

ChIP Lysis Buffer #2: 10 mM Tris pH 8.0, 200 mM NaCl, 1 mM EDTA, 0.5 mM EGTA, Protease Inhibitors*.

ChIP Lysis Buffer #3: 10 mM Tris pH 8.0, 100 mM NaCl, 1 mM EDTA, 0.5 mM EGTA, 0.1% Sodium Deoxycholate, 0.5% N-lauroylsarcosine, Protease Inhibitors*.

Low Salt Wash Buffer: 20 mM Tris pH8.1, 150 mM NaCl, 2 mM EDTA, 0.1% SDS, 1% Triton X-100.

High Salt Wash Buffer: 20 mM Tris pH8.1, 500 mM NaCl, 2 mM EDTA, 0.1% SDS, 1% Triton X-100.

LiCl Salt Wash Buffer: 20 mM Tris pH8.1, 0.25 M LiCl, 1 mM EDTA, 1% NP-40, 1% Sodium Deoxycholate

TE: 10 mM Tris pH 8.0, 1 mM EDTA

Elution Buffer: 10 mM Tris pH 8.0, 300 mM NaCl, 1 mM EDTA, 1% SDS

*Complete Mini EDTA-free Protease Inhibitor Cocktail (Roche)

Antibody amounts per 1 mL IP: Anti-ATF4 (sc-200): 5 µg, Anti-ATF4 (D4B8): 1.06 µg, Anti-ATF4 (ABE387): 20 µg, Rabbit IgG control: 5 µg

RNA-Seq

Total RNA was purified with RNAzol RT (Sigma-Aldrich) according to the manufacturer's instructions. For *RBM4* KO samples, equal amounts of total RNA were pooled from 4 independent *RBM4* KO cell clones (1B2, 1B6, 1B7, and 1B9). For *ATF4* KO samples, equal amounts of total RNA were pooled from 4 independent *ATF4* KO cell clones (2A9, 2A10, and 2A11). RNA-Seq libraries were prepared using the NEBNext Ultra Directional RNA Library Prep Kit (New England BioLabs), including poly(A) selection using the NEBNext Poly(A) mRNA Magnetic Isolation module. Library quality assessment and clustering were performed as described for ChIP-Seq. Paired-end sequencing was performed using a GAIIx Genome Analyzer (Illumina).

RNA-Seq reads were aligned using Tophat version 2.0.11 (Kim, Pertea et al. 2013) using the reference human genome hg19 and the reference transcriptome CRCh37.59 using the following options:

--library-type fr-firststrand --no-coverage-search --mate-inner-dist 300

Guided transcriptome reconstruction was done with Cufflinks Version 2.2.1 . Cufflinks was run on the Tophat output file "accepted_hits.bam" for each sample, using the hg19 reference genome and transcript annotation files and the options

-b hg19_ucsc.fa -M hg19.rRNA.gtf -g hg19_ucsc.refGene.gtf -u --min-frags-per-transfrag

After assembly was complete for each sample, the assembled transcripts were merged together using **Cuffmerge** with the command template:

cuffmerge -o combined/ --min-isoform-fraction 0 -s hg19 assembly_list.txt

The merged transcriptome was compared against the reference transcriptome using **Cuffcompare**:

cuffcompare -r hg19_ucsc.refGene.gtf -s hg19 -R -M merged.gtf

This produced comparative statistics and, most importantly for this pipeline, a **".tmap**" file that lists the most closely matching reference transcript for each of the assembled transcripts from **merged.gtf**. The merged transcriptome was converted to **genePred format (.gp)** using the UCSC binary utility, **gtfToGenePred** using the command:

gtfToGenePred merged.gtf merged.gp

The file **merged.gp** was joined to the .**tmap** file produced by **Cuffcompare** above, to obtain a transcriptome file that is annotated with transcript IDs, exonic coordinates, gene IDs and short-names of the most closely matching reference transcripts. The Tophat output files **"accepted_hits.bam"** for each sample were sorted and converted to **BED** format using the BEDTools-2.17.0 utility **bamToBed** with the command:

bamToBed -split -i accepted_hits.bam | sort -k1,1 -k2,2n -k3,3n > accepted_hits.bed

An executable (written by the Muljo Lab, NIH) called kcGEXM was used to obtain normalized read counts and calculate reads per kilobase per million (RPKM) for transcripts. kcGEXM uses the genePred and BED files as input:

kcGEXM -f gp -r merged.tmap.gp accepted_hits.bed > sample_name.cnt

where -f precedes the format of the reference annotation file and -r precedes the reference annotation file.

RNA-Seq read densities were normalized to the total number of aligned reads in a sample using Bedtools version 2.17.0 (Quinlan and Hall 2010) and data were visualized with IGV version 2.3.47 (Robinson, Thorvaldsdottir et al. 2011). Sashimi plots were generated using MISO version 0.5.2 (Katz, Wang et al. 2010) with Python version 2.7.

Cytotoxicity assay

Splenocytes from *Rag2*$^{-/-}$ mice were cultured for 6 days in 1000 U/mL recombinant human IL-2 to generate activated NK cells (LAK cells). Target cells were plated at $5x10^6$ cells/dish in 10 cm tissue culture dishes 24 hours prior to harvest for the cytotoxicity assay. LAK cells were co-cultured with ^{51}Cr-labeled target in a standard 3 hour chromium-release assay. Each effector:target condition was performed in triplicate wells in a 96-well plate. 10^4 target cells were used per well.

Chimeric Antigen Receptor (CAR) T cell stimulation assay

Human T cells expressing a chimeric NKG2D (chNKG2D) receptor and DAP10 were prepared by the Sentman lab as previously described (Zhang, Barber et al. 2006). Frozen vials of chNKG2D T cells were thawed, plated at 10^6 viable cells/mL, and cultured overnight. Target cells were plated at $5x10^6$ cells/dish in 10 cm tissue culture dishes 24 hours prior to harvest for the stimulation assay.

Prior to NKG2D blockade on chNKG2D T cells, NKG2D antibody (Clone 1D11) and isotype control antibody (PK136) were centrifuged for 1 hour at 16,000 x *g* at 4 °C to remove any antibody aggregates that may have been present. chNKG2D T cells were harvested and co-incubated with 30 µg/mL NKG2D or isotype control antibody at room temperature for 1 hour. HAP1 target cells were harvested by gentle trypsinization (0.1% trypsin, 1 mM EDTA in PBS for 2 minutes at 37 °C) and trypsin was immediately quenched by adding 5 volumes of complete media containing 10% FCS. Target cells and chNKG2D T cells (10^5 cells each) were added to the wells of a 96-well V-bottom tissue culture plate and incubated for 24 hours at 37 °C. The addition of target cells reduced the concentration of antibody to 22.5 µg/mL.

Following co-culture, cells were pelleted at 750 x *g* for 5 minutes. Cell-free supernatants were harvested, and the concentration of secreted IFN-γ was measured with a Human IFN-gamma DuoSet ELISA Kit (R&D Systems, Cat. No. DY285-05) according to the manufacturer's instructions. ELISAs were performed using supernatants diluted 3x in ELISA Reagent Diluent (20 mM Tris pH 7.2, 0.1% BSA, 0.05% Tween-20, 150 mM NaCl).

Hypoxia and anoxia

Hypoxic and anoxic cell culture conditions were created using modular incubation chambers. Cell culture plates were placed in the modular incubation chambers along with an open dish of water to help maintain high humidity. For hypoxia, the chamber was flushed with hypoxic air (1% O2, 5% CO2, balance nitrogen) for 5 minutes at a flow rate of 20 L/minute. After flushing, the chamber tubing was clamped, the chamber was disconnected from the air supply, and the chamber was placed in a 37 °C incubator. Cells were analyzed 24 hours later.

Anoxia culture conditions (<0.1% O2) were produced using a BD GasPak EZ Anaerobe Container System (BD REF #260678). A single GasPak was placed in the modular incubation chamber, and the chamber was placed in a 37 °C incubator. Cells were analyzed 24 hours later. It should be noted that the oxygen-scavenging reaction produces CO2, and CO2 levels can exceed 13% if 2 GasPaks are used. This system is intended for culturing anaerobic bacteria and may or may not be ideal anoxia experiments with mammalian cells.

Generation of Raet1 *KO mice*

Raet1 mutant mice were generated using the CRISPR/Cas9 system. We chose a shared Cas9 target site present in the second coding exon of the highly related *Raet1d* and *Raet1e* genes. *Cas9* mRNA and the *Raet1* sgRNA were *in vitro* transcribed and injected into single-cell embryos as described (Wang, Yang et al. 2013). F_0 mice carrying frame-shift mutations in both *Raet1d* and *Raet1e* genes were identified by PCR and were back-crossed to C57BL/6 mice, and the resulting *Raet1* heterozygous F_1 mice were intercrossed to produce homozygous mutants.

Raet1 genomic target sequence with protospacer-adjacent motif (PAM, underlined):
5'-TAGGTGCAACTTGACCATCAAGG-3'.

Oligonucleotides used to clone the *Raet1* sgRNA:
Fwd: 5'-CACCGGTAGGTGCAACTTGACCATCA-3',
Rev: 5'-AAACTGATGGTCAAGTTGCACCTACC-3'.
The underlined GG dinucleotide in the forward primer, which is not present in the genomic target sequences, was added to the 5' end of the sgRNA sequence to allow for better transcription from the T7 promoter.

Table 2-4: *Raet1* genotyping PCR primers

Primer Name	Primer Sequence	Direction	Target
Raet1 Genotyping E	GAAGATCAAGTGACCATAGGTG	Forward	*Raet1e*
Raet1 Genotyping G	CAGAGGTTGTGTCAAACATTTG	Reverse	*Raet1e*
Raet1 Genotyping H	GAGGGGTTCTACTAACCAGAG	Forward	*Raet1d*
Raet1 Genotyping I	CAGAGGTTGTGTTAAACATTCC	Reverse	*Raet1d*

Chapter 3
Identification of novel regulators of ULBP1

A genetic screen to identify regulators of human NKG2D ligand expression

Outline of genetic screening of haploid human cells

Unbiased screens of all sorts are incredible tools for discovery. A well-executed screen can uncover pathways that you might never have tested in a purely hypothesis-driven approach. Genome-wide mutagenesis screens have been applied to model organisms and pathogens with great success. Random mutagenesis works great when only one copy of each gene is present in the target cell, as is the case with bacteria, or yeast in the haploid phase of their life cycle. Random mutagenesis in a diploid organism is trickier. The odds of creating loss-of-function mutations in both alleles of given gene within a single cell are incredibly low. This is generally considered to be a good thing from a "fitness of the species" perspective, but it can make life more difficult for researchers. Nonetheless, mice and other model organisms with point mutations can be bred to homozygosity, and this has been the basis for many successful ENU mutagenesis screens.

A different approach is required for the study of human cells. Random mutagenesis is even more problematic, since many cell lines are severely aneuploid. Lacking the ability to create homozygous loss-of-function mutants in human cells, many researchers have turned to RNAi-based screens to knock-down gene expression across the genome. Unfortunately, "knock-down" is not equivalent to "knock-out," and the decrease in gene expression achieved with an shRNA (when they even work at all) may not be sufficient to observe a phenotype.

In 1987, a near-haploid cell line (named KBM7) originating from a patient with chronic myelogenous leukemia was reported (Andersson, Beran et al. 1987). A human cell line with a single copy of most genes could allow for random mutagenesis screens, and in 2009, Carette and colleagues reported a genome-wide screen of KBM7 cells to identify host genes exploited by several pathogens (Carette, Guimaraes et al. 2009). The authors mutagenized KBM7 cells with a retroviral gene-trap vector, which ablates (or severely reduces) gene expression when the virus integrates into a gene. Following phenotypic selection and isolation of selected cell clones, the mutations present in pathogen-resistant cells were identified.

After their first report, Carette and colleagues improved their screen. First, the authors employed high-throughput DNA sequencing to identify mutations (Carette, Guimaraes et al. 2011). Rather than mapping gene-trap insertion sites from individual cell clones, DNA was isolated from the bulk population of mutant cells before and after selection, and sequencing libraries were prepared from genomic DNA surrounding gene-trap insertion sites. Mutations enriched by phenotypic selection could be identified by counting the number of independent gene-trap insertions found in a given gene before and after selection. The improved screen does not require a pure population of cells with the desired phenotype, only that the desired cells be highlight *enriched*. For example, if an interesting mutant cell is present in the selected population at a frequency of 1 in 1,000 cells, you might never find or appreciate the mutant if screening individual cell clones. However, if the interesting mutation found at only 1 in 1,000,000 in the initial pool of cells and enriched up to 1 in 1,000, this thousand-fold enrichment would be much easier to appreciate.

The other improvement to the screen was more of a happy accident. Carette and colleagues set out to create an induced pluripotent stem cell (iPSC) line from KBM7 cells, which could be useful in numerous ways. Notably, a haploid iPSC line would open the door for similar genetic screens in iPSC's and all of the cell types that can be derived from them. The authors

were unable to isolate a population of pluripotent cells that was stably haploid, but they did obtain a non-pluripotent, adherent cell line dubbed HAP1 (Carette, Raaben et al. 2011). As an experimental workhorse, HAP1 cells have certain advantages over KBM7. HAP1 cells are haploid for all chromosomes, whereas KBM7 cells retain two copies of chromosome 8. HAP1 cells are also easier to transfect and transduce. However, defining the "cell type" of HAP1 is not meaningful. HAP1 cells are no longer a CML line, and they certainly are not iPSC's. According to Jan Carette, based on transcriptome analysis, the cells look more like a neural progenitor cell than anything else. But HAP1 cells are not proper neural progenitor cells either. To my mind, the truest categorization of HAP1 cells is "really, really useful." If HAP1 cells have the phenotype you want to study, don't worry too much about categories. Just be happy to have this fantastic tool of discovery!

Expression of NKG2D ligands on HAP1 cells

We set out to use HAP1 cells to study regulation of NKG2D ligands. An important first step was to determine if unstimulated HAP1 cells express NKG2D ligands, which ones, and to what degree. Figure 3-1 shows the cell surface expression of NKG2D ligands on HAP1 cells. Like many primary tumors and cancer cell lines, HAP1 cells express multiple NKG2D ligands. ULBP2, ULBP5, and ULBP6 have a high degree of amino acid similarity, and the antibody used for staining cross-reacts with all three ligands. In unstimulated HAP1 cells, the staining is due to ULBP2 alone, as RNA-Seq analysis showed expression of *ULBP2* mRNA, but little to no expression of the mRNAs encoding *ULBP5* or *ULBP6*. HAP1 cells also stained with a ULBP4 monoclonal antibody (not shown), but it was later discovered that the antibody used cross-reacts with ULBP2. *ULBP4* mRNA could not be detected by RT-qPCR or RNA-Seq.

Screening for drivers of ULBP1 and ULBP2 expression

Many cancer cells express NKG2D ligands, but the pathways driving NKG2D ligand expression on those cells is unknown in many cases. HAP1 cells offered the opportunity to identify novel factors supporting the expression of NKG2D ligands in a cancer-derived cell line. HAP1 cells showed the brightest staining for ULBP1, making it particularly amenable to a loss-of-expression screen. The choice to screen for drivers of ULBP1 was purely technical. Our understanding of all the NKG2D ligands is incomplete, and I would happily screen for drivers of ULBP3 or MICA. Since the staining of ULBP1 was the brightest of all the NKG2D ligands, it seemed the most practical option for our first attempt at screening HAP1 cells. After our first ULBP1 screen showed promising results, we performed another screen for drivers of ULBP2 expression.

Figure 3-2 shows the workflow of the ULBP1 screen. Following mutagenesis, we selected for mutants with decreased expression of ULBP1, but intact expression of the unrelated GPI-anchored protein CD55. In the first round of selection, we depleted $ULBP1^{high}$ cells from the mutant cell population using magnetic bead-based depletion of cells labeled with a ULBP1 antibody. After briefly expanding the selected cells, we used flow cytometry to further select for $ULBP1^{low}CD55^{+}$ cells. Selection of $CD55^{+}$ cells was used to reduce the fraction of selected cells that had lost ULBP1 expression for trivial reasons such as mutations in the GPI synthesis and anchoring pathways or mutations that impact cell membrane proteins generally. A similar workflow was used to screen for drivers of ULBP2 expression.

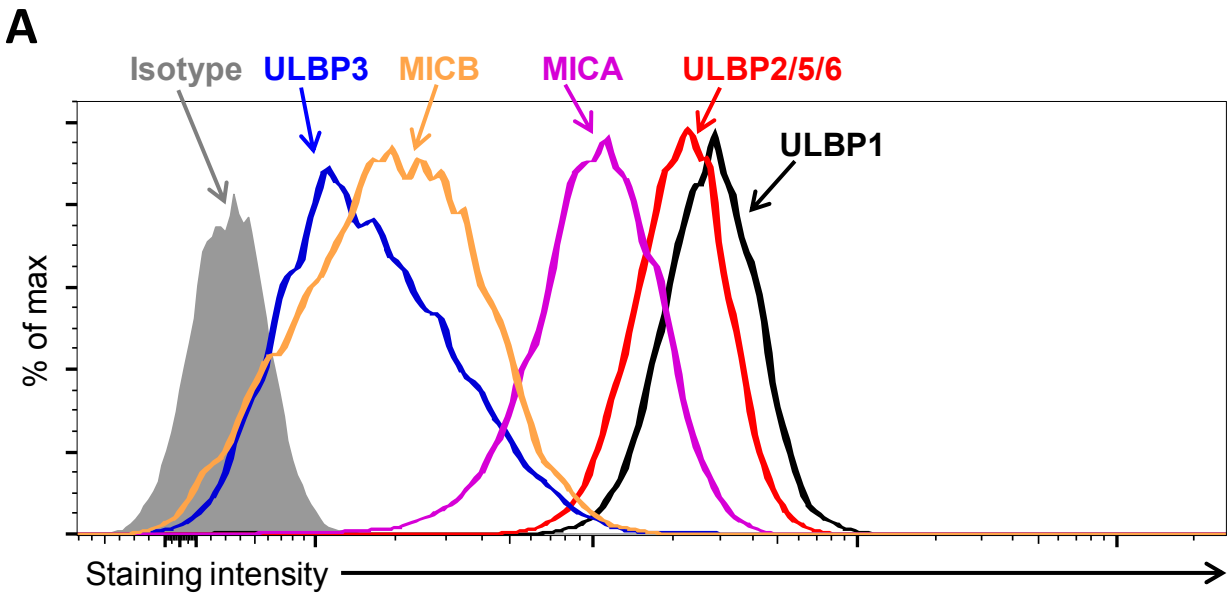

Figure 3-1: Expression of NKG2D ligands on HAP1 cells
A. HAP1 cells were stained with antibodies against NKG2D ligands and analyzed by flow cytometry. Isotype control staining is shown by the shaded gray histogram. The data shown are representative of at least three independent experiments.

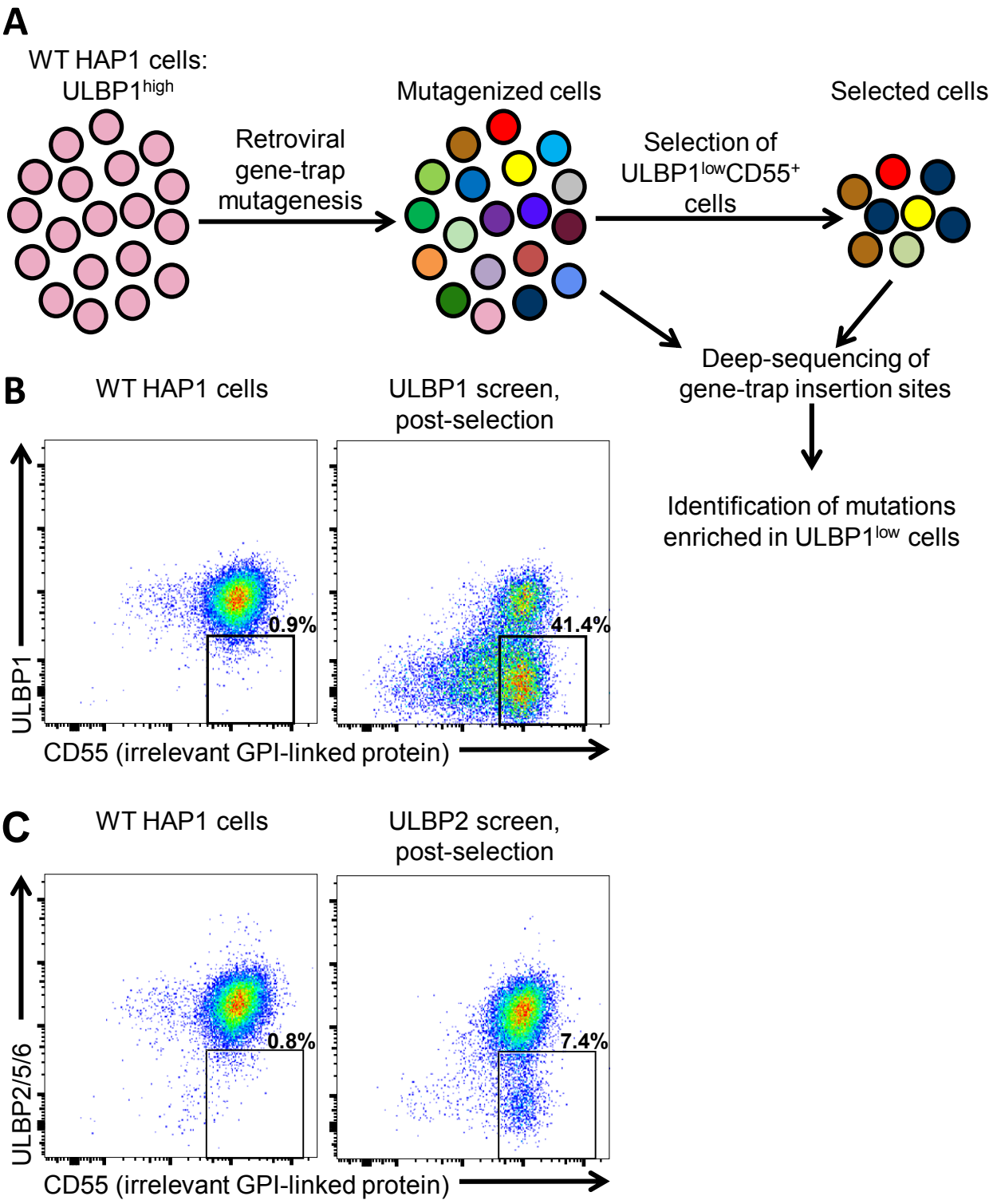

Figure 3-2: Genetic screens for drivers of ULBP1 and ULBP2 expression
A. Outline of the genetic screen used for ULBP1. **B**. Flow cytometric analysis of ULBP1 and CD55 expression on WT HAP1 cells and selected cells from the ULBP1 screen. **C**. Flow cytometric analysis of ULBP2/5/6 and CD55 expression on WT HAP1 cells and selected cells from the ULBP2 screen.

At each step of screen, the selection of ULBP1^{low} cells was more stringent than the selection of ULBP2^{low} cells. Magnetic depletion of cells in the ULBP1 screen reduced the total cell number by 100-fold, while magnetic depletion in the ULBP2 screen only achieved a 20-fold reduction. Upon sorting by FACS, a clear population of ULBP1^{low}CD55^{+} cells was present for selection. ULBP2^{low}CD55^{+} cells were rare, and a more liberal selection gate had to be used to ensure the relevant cells were captured. Figure 3-2 shows the staining of WT and selected HAP1 cells after selection and expansion.

Deep-sequencing was employed to quantify the frequencies of insertion sites of the retroviral gene-trap in selected cells, for comparison with the sites in unselected cells. Table 3-1 shows a selected "hit-list" of genes that were targeted significantly more frequently in selected ULBP1^{low}CD55^{+} cells than in unselected cells. A validation of the approach was that the *ULBP1* gene itself was a highly significant hit in the ULBP1 screen. Many genes encoding enzymes involved in GPI synthesis were also represented despite the selection for CD55 expression. We chose hits for validation and follow-up experiments based on their statistical ranking and expectations that the corresponding proteins play roles in stress responses, protein biogenesis or gene/mRNA regulation.

Table 3-2 shows the "hit-list" for the ULBP2 screen. The results of the screen were rather disappointing compared to the ULBP1 screen. One third of the hits came from known "bad actors" that have appear on numerous unrelated screens in the Carette lab. Mutation of these genes may have broad phenotypes or confer a proliferative advantage to mutant cells, rather than affecting ULBP2 in a specific way. *ULBP2* itself was significantly enriched in the screen ($p=0.012$), but much less so than ULBP1 on the corresponding screen ($p<10^{-75}$). All in all, the ULBP2 screen appeared less successful than the ULBP1 screen, and we had difficulty confirming any of the hits we followed up on. The one exception is ATF4, which was a hit on both the ULBP1 and ULBP2 screens, and is explored in Chapter 4. The sections below will focus on hits from the ULBP1 screen. Possibilities for improving the ULBP2 screen in the future are discussed at the end of this chapter.

Gene symbol	Function/Process	P-value
PIGW	GPI synthesis/anchoring	1.12E-196
PIGQ	GPI synthesis/anchoring	3.26E-155
PIGB	GPI synthesis/anchoring	2.38E-103
ULBP1	NKG2D ligand	2.65E-76
PIGO	GPI synthesis/anchoring	1.49E-65
PIGU	GPI synthesis/anchoring	9.44E-64
PGAP2	GPI synthesis/anchoring	5.89E-54
MPDU1	GPI synthesis/anchoring	4.19E-53
PIGP	GPI synthesis/anchoring	1.64E-50
PIGL	GPI synthesis/anchoring	6.83E-48
PIGH	GPI synthesis/anchoring	3.84E-36
PIGC	GPI synthesis/anchoring	4.50E-31
PIGX	GPI synthesis/anchoring	1.12E-26
RBM4	RNA-binding protein	1.29E-24
PIGV	GPI synthesis/anchoring	4.43E-23
PIGK	GPI synthesis/anchoring	5.26E-18
DPM3	GPI synthesis/anchoring	2.28E-17
PIGN	GPI synthesis/anchoring	3.98E-16
SPCS1	Non-catalytic subunit of signal peptidase complex	1.25E-15
PIGM	GPI synthesis/anchoring	6.06E-14
C1GALT1C1	Protein O-linked glycosylation	2.22E-13
PIGT	GPI synthesis/anchoring	1.77E-12
PIGF	GPI synthesis/anchoring	1.77E-12
SLC35A1	Golgi-localized CMP-sialic acid transporter	1.77E-12
PIGA	GPI synthesis/anchoring	3.03E-12
PIGS	GPI synthesis/anchoring	3.88E-12
GPAA1	GPI synthesis/anchoring	1.19E-11
ST3GAL2	Sialyltransferase	1.64E-11
SPCS2	Non-catalytic subunit of signal peptidase complex	6.20E-09
HSPA13	Microsome-associated protein with ATPase activity	1.24E-05
FLJ37453	Non-coding RNA	0.00115
SLC17A9*	Vesicular nucleotide transporter	0.00715
RPS25	Ribosomal protein	0.00715
ATF4	Stress-induced transcription factor	0.0206
PMM2	Oligosaccharide synthesis, protein glycosylation	0.0234
NCRNA00167	Non-coding RNA	0.0363
CRNKL1*	Pre-mRNA splicing	0.0363
ICK	Intestinal cell kinase, MAPK-related	0.0363
TBC1D19	TBC domain-containing protein	0.0416
ZNF236	Zinc-finger protein	0.0496

Table 3-1: List of genes enriched for gene-trap insertions in the ULBP1 screen

The gene symbols of hits ($p<0.05$) are shown with a brief description of known or predicted gene functions. A p-value of enrichment was determined using Fisher's exact test, followed by correction for the false discovery rate. The list was manually curated to remove known false-positives that have appeared on several unrelated screens. Yellow shading indicates genes followed up on in this study. Light blue shading indicates genes involved in GPI biosynthesis and anchoring. Light orange shading genes involved in protein glycosylation. Asterisks indicate that ULBP1^{low} cells did not arise when *SLC17A9* or *CRNKL1* were targeted with CRISPR/Cas9.

Gene symbol	Function/Process	P-value
PIGO	GPI synthesis/anchoring	7.26E-21
PGAP2	GPI synthesis/anchoring	1.62E-19
PIGB	GPI synthesis/anchoring	1.22E-15
MPDU1	GPI synthesis/anchoring	1.43E-15
EP300	Histone acetyltransferase	7.46E-15
PIGW	GPI synthesis/anchoring	3.75E-13
PIGQ	GPI synthesis/anchoring	1.15E-12
ASXL1	Polycomb group chromatin binding protein	3.66E-11
PIGL	GPI synthesis/anchoring	4.22E-09
PIGF	GPI synthesis/anchoring	3.70E-08
PIGP	GPI synthesis/anchoring	3.70E-08
DNAJC13*	Trafficking through endosomes	3.70E-08
MKNK2*	MAPK interacting kinase	0.000117
PIGM	GPI synthesis/anchoring	0.000119
LINC01465	Non-coding RNA	0.000188
OTX2-AS1	Non-coding RNA	0.000223
FBXW7*	E3 ubiquitin ligase	0.00134
PIGV	GPI synthesis/anchoring	0.00374
ULBP2	NKG2D ligand	0.0116
ILF3-AS1	Non-coding RNA	0.0119
SP2	Transcription factor	0.0143
CUL1*	Subunit of ubiquitin ligase complex	0.0145
OMG	Oligodendrocyte myelin glycoprotein	0.0145
NGFRAP1	Neurotrophin receptor-associated protein	0.0222
NR2F6	Orphan nuclear receptor	0.0233
LSR	Lipoprotein receptor	0.0327
SLFN11	Binds tRNAs, potential bad actor found in multiple screens	0.0351
TATDN2	Unknown	0.0362
KDM5C	Lysine demethylase	0.0362
ATF4	Stress-induced transcription factor	0.0411
NAGA	Lysosomal exoglycosidase	0.0464

Table 3-2: List of genes enriched for gene-trap insertions in the ULBP2 screen
The gene symbols of hits ($p<0.05$) are shown with a brief description of known or predicted gene functions. A p-value of enrichment was determined using Fisher's exact test, followed by correction for the false discovery rate. The list was manually curated to remove known false-positives that have appeared on several unrelated screens. Yellow shading indicates genes followed up on in this study. Light blue shading indicates genes involved in GPI biosynthesis and anchoring. Asterisks indicate that ULBP2^{low} cells did not arise when *DNAJC13*, *MKNK2*, *FBXW7*, or *CUL1* were targeted with CRISPR/Cas9.

Rapid validation and triage of hits with the CRISPR/Cas9 system

To confirm that the genes identified by the screen actually regulate ULBP1, and are not simply false-positives, it was necessary to isolate cells with mutations in the candidate genes. Mutant cells of can be isolated by sorting single ULBP1^{low}CD55^{+} cells into 96-well plates, expanding the clones, and screening for gene-trap insertions in the gene of interest by PCR. This is a slow, laborious process. The Carette lab reports that in practice the approach only works for the top few hits found on a screen, and my experience was similar. Luckily, fishing for a specific mutant in a complex pool of gene-trapped cells has been replaced by a much more targeted approach.

Using the CRISPR/Cas9 system, we could specifically target genes identified by our screen. We designed guide RNAs (also called single guide RNAs, or sgRNAs) targeting sites in the 5' coding regions of each candidate gene in HAP1 cells. The *ULBP1* gene was targeted for comparison. In vivo, cleaved DNA is frequently re-joined with the introduction of (typically small) insertions or deletions at the cleavage site (Mali, Yang et al. 2013). After HAP1 cells were transiently transfected with plasmids encoding Cas9 and a sgRNA for each candidate gene, a population of ULBP1^{low} cells appeared that was absent in control transfected cells (Figure 3-3); in each case, individual ULBP1^{low} cells were sorted into 96-well plates, and expanded clones were screened for mutations by PCR and sequencing. For further analysis we selected clones with frameshift mutations in each targeted gene. Since the sites targeted were near the beginning of each coding region, and the cells are haploid, the frameshift mutations are expected to result in complete loss of function of the corresponding proteins.

One very nice advantage of confirming hits with CRISPR/Cas9 is the ability to rapidly triage hits. The appearance of ULBP1^{low} cells after targeting *ATF4* is not conclusive evidence that ATF4 drives ULBP1 expression, but the result is *highly* suggestive and motivates the hunt for mutant cell clones. On the other hand, when *SLC17A9* and *CRNKL1* were targeted, ULBP1 expression was unchanged compared to control transfected cells, despite evidence of mutations in the target loci (data not shown). This result alone does not rule out the possibility these genes regulate ULBP1, but it encouraged us to devote our efforts to other, more promising hits.

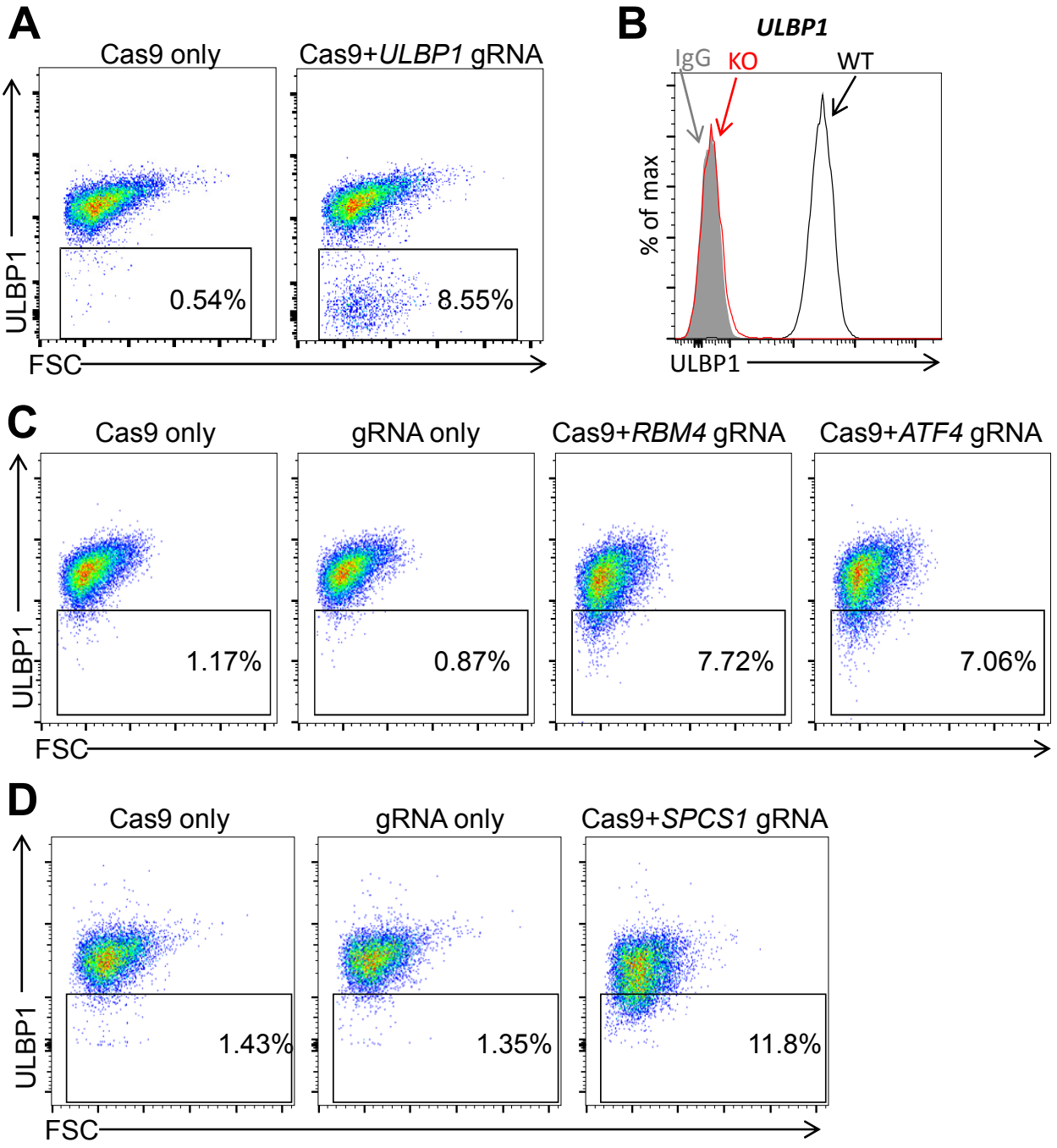

Figure 3-3: Target gene mutagenesis with the CRISPR/Cas9 system
A. HAP1 cells were co-transfected with plasmids encoding Cas9, a *ULBP1*-specific gRNA, and GFP. Successfully transfected (GFP+) cells were sorted 24-72 hours post-transfection and re-plated. 5-7 days post-transfection, cells were stained for ULBP1 expression analyzed by flow cytometry. **B**. Staining of a ULBP1 KO clone isolated from cells targedted in Panel A. **C-D**. *RBM4*, *ATF4*, and *SPCS1* were targeted and analyzed as in Panel A.

The hits that we validated were ATF4, a stress-associated transcription factor, RBM4 (an RNA-binding protein), HSPA13 (a protein chaperone), and SPCS1 and SPCS2, which are both non-catalytic subunits of the signal peptidase complex. As expected, cells with a ULBP1 mutation lacked ULBP1 staining altogether (Figure 3-3). Each of the other mutations analyzed resulted in a partial 2-3-fold decrease in cell surface expression of ULBP1 (Figure 3-4). In all cases, ULBP1 expression on mutant lines could be restored by re-expressing the gene of interest with a doxycycline-inducible lentiviral vector (Figure 3-4). Consistent with their presumptive roles in gene expression and/or splicing, *ATF4* and *RBM4* KO cells each showed decreased amounts of canonically spliced *ULBP1* mRNA, and the fold change in mRNA levels corresponded to the change in expression seen at the cell surface (Figure 3-4). Consistent with roles as chaperones and protein processing components, *HSPA13*, *SPCS1*, and *SPCS2* KO cells all showed WT amounts of *ULBP1* mRNA.

The effects of the mutations were specific to ULBP1, as we found no change in the levels of other cell surface proteins, including other NKG2D ligands, HLA Class I, the unrelated GPI-anchored protein CD59, or ligands for the NK cell receptor DNAM-1 (Figure 3-5). The finding that the mutations each affect only ULBP1 among the NKG2D ligands tested supports the hypothesis that different NKG2D ligands are subject to distinct regulatory processes, at least in part. It was surprising that *SPCS1* and *SPCS2* mutations only impacted cell surface staining of ULBP1 of the 7 membrane proteins tested, as we predicted that mutating components of the signal peptidase complex would cause a more generalized defect in cell surface protein expression. These findings established that ATF4, RBM4, HSPA13, SPCS1 and SPCS2 each contribute partially to normal steady state cell surface display of ULBP1 in HAP1 cells.

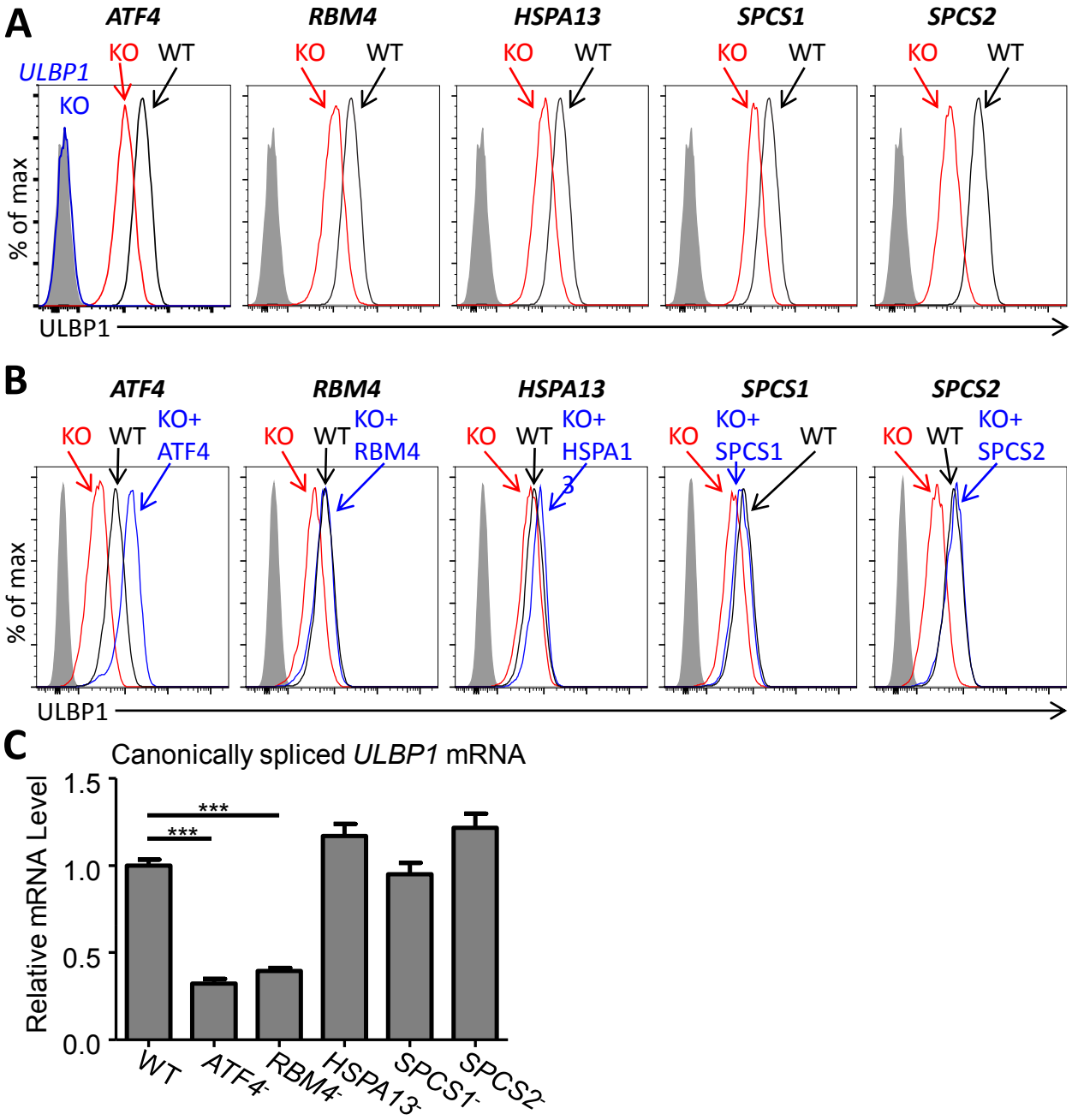

Figure 3-4: Decreased ULBP1 expression upon loss of identified drivers
A-B. Flow cytometric analysis of cell surface expression of ULBP1 on WT and mutant HAP1 cells. **B**. Mutant cell lines were transduced with a doxycycline-inducible lentiviral vector containing the gene of interest. Cells were treated for 24 hours with doxycycline (Dox) at a final concentration of 100 ng/mL for *ATF4* and 1000 ng/mL for all other genes. The shaded gray histogram represents isotype control staining. **C**. RT-qPCR analysis of *ULBP1* mRNA expression levels in WT and mutant HAP1 cells. Expression levels were normalized to *ACTB*, *GAPDH*, and *HPRT1* and are shown as mean ±SE. The data were analyzed by 1-way ANOVA with Dunnet's Multiple Comparisons Test comparing all samples to WT. Data in this figure are representative of at least 3 independent experiments.

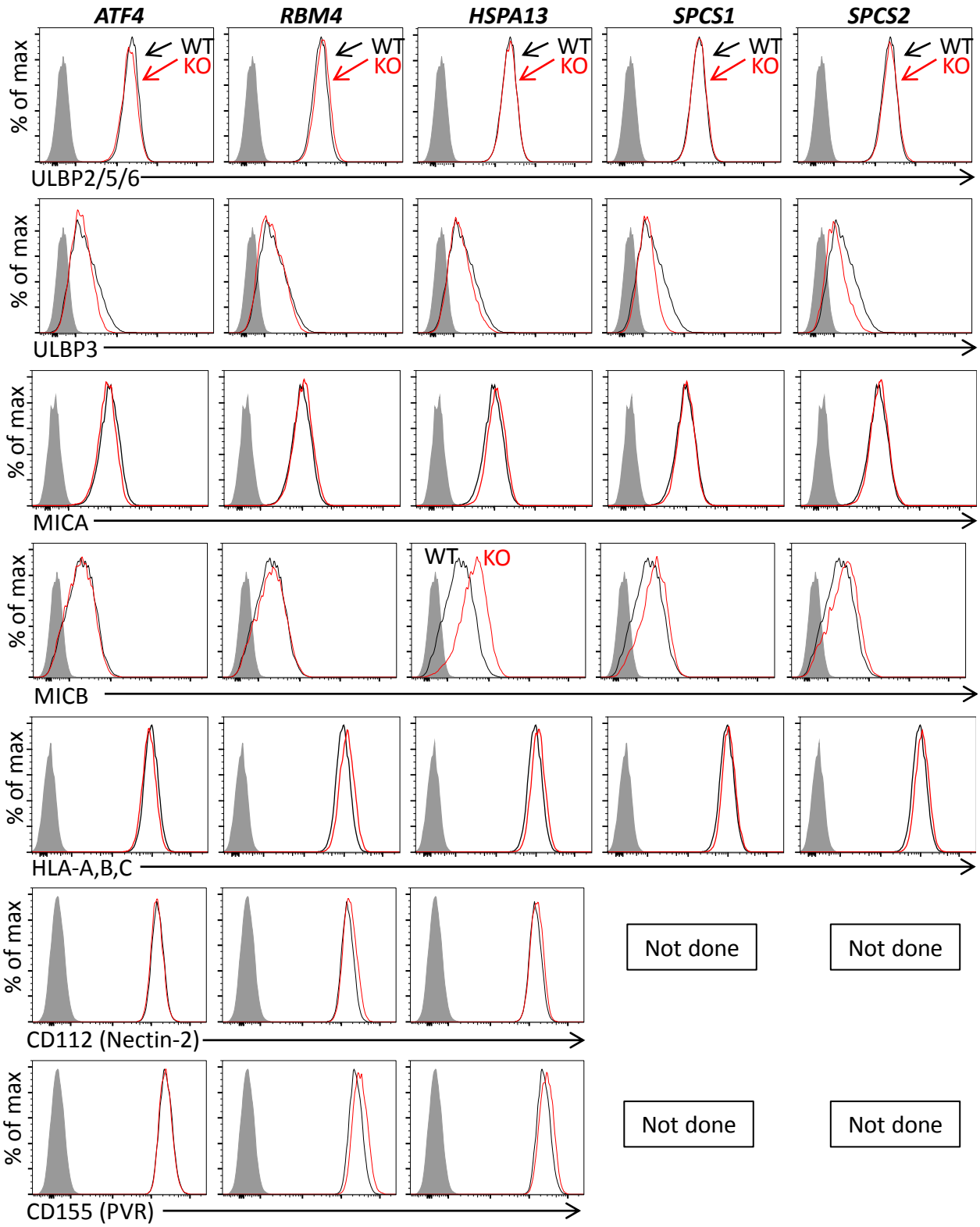

Figure 3-5: Mutations specifically affect ULBP1

WT and mutant HAP1 cells were stained for NKG2D ligands and other cell surface protein and analyzed by flow cytometery. Data in this figure are representative of at least three independent experiments.

Stepwise regulation of ULBP1 expression

To assess whether the genes implicated in ULBP1 expression work independently or in common pathways, we generated and analyzed double and triple mutant cell lines. We generated *ATF4/RBM4* double mutant cells by targeting *ATF4* in the *RBM4* KO line; we generated triple mutant cells by further targeting either *HSPA13* or *SPCS2* in the double-KO line. Notably, we observed stepwise decreases in ULBP1 expression with each additional mutation, with triple mutant cells showing up to a 20-fold reduction in ULBP1 expression compared to WT cells. These data suggested that the genes tested (with the likely exception of SPCS1 versus SPCS2) contribute largely independently to steady state ULBP1 expression in HAP1 cells (Figure 3-6). *ATF4/RBM4* double mutants showed a larger decrease in *ULBP1* mRNA than either single mutant, suggesting that ATF4 and RBM4 may act independently in regulating the amounts of *ULBP1* mRNA. There were no greater decreases in *ULBP1* mRNAs when mutations in either *HSPA13* or *SPCS2* were added to the double mutant cells (Figure 3-6).

HSPA13

HSPA13 (also known as STCH) belongs to the Hsp70 family of chaperone proteins (Otterson, Flynn et al. 1994). HSPA13 is associated with microsomes and displays ATPase activity, but little is known about its function, including whether HSPA13 participates in cellular stress responses. One report showed that HSPA13 binds to and promotes the expression of the ion transporters NBCe1 and NHE1, which help maintain intracellular pH homeostasis (Bae, Koo et al. 2013). The mechanism by which HSPA13 supports expression of ULBP1 is unclear and could be through direct or indirect effects.

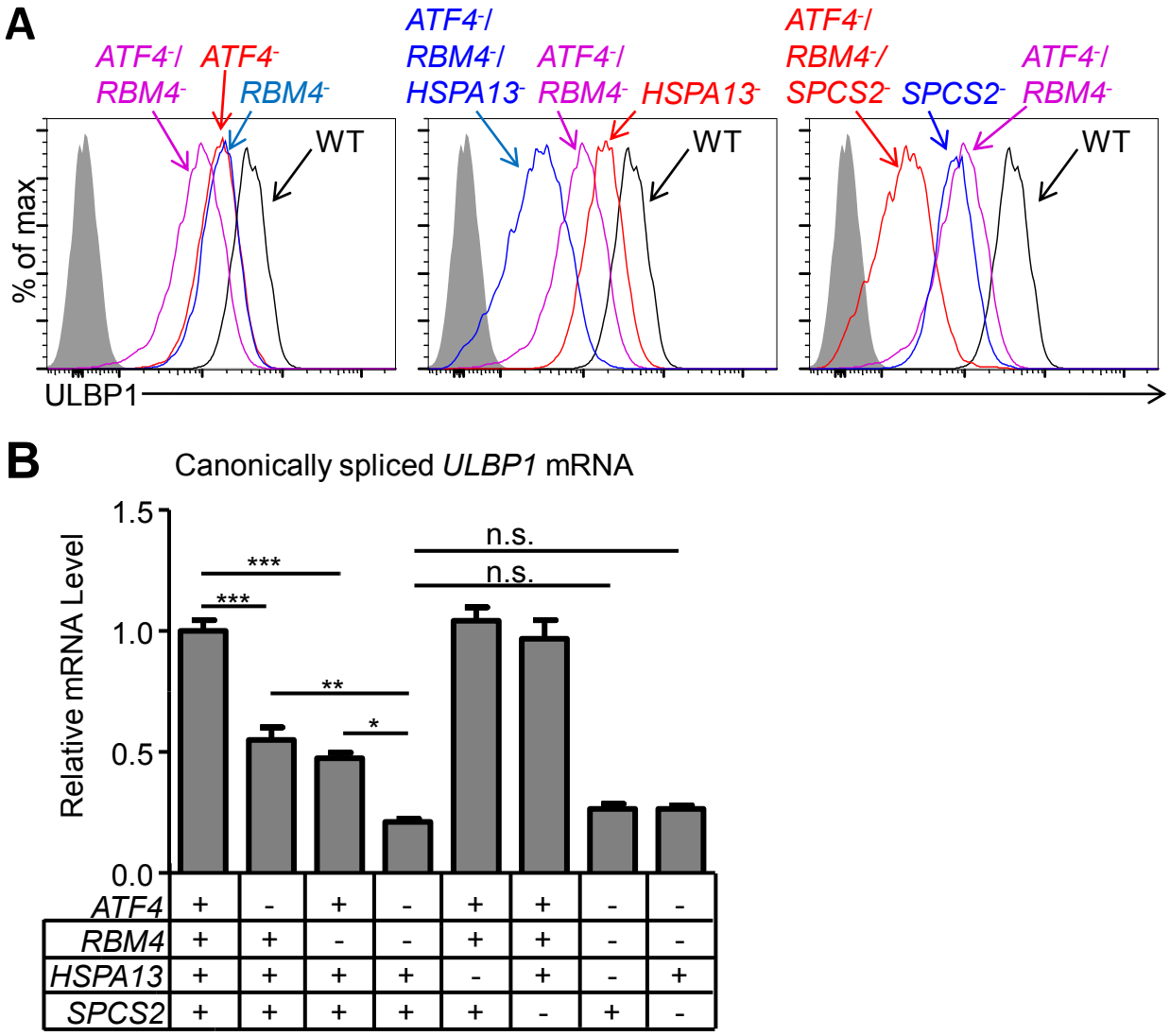

Figure 3-6: Double and triple-mutant cell lines show stepwise decrease in ULBP1 expression

A. Flow cytometric analysis of ULBP1 expression on single, double, and triple mutant HAP1 cells. *ATF4*$^{-}$/*RBM4*$^{-}$ double-mutant cells were generated by mutagenesis of *ATF4* in *RBM4*$^{-}$ cells. Triple-mutant cells were generated by targeting *HSPA13* or *SPCS2* in *ATF4*$^{-}$/*RBM4*$^{-}$ double-mutant cells. **B**. RT-qPCR analysis of *ULBP1* mRNA expression levels in the cells described in A. Expression levels were normalized to *ACTB*, *GAPDH*, and *HPRT1* and are shown as mean ±SE. The data were analyzed by 1-way ANOVA with Bonferroni's Multiple Comparisons Test. **P*<0.05, ***P*<0.01, ****P*<0.001. Data in this figure are representative of at least three independent experiments.

SPCS1 and SPCS2

SPCS1 and SPCS2 are non-catalytic subunits of the signal peptidase complex, but surprisingly little is known about their function (Mullins, Meyer et al. 1996). We were surprised that HAP1 cells lacking *SPCS1* or *SPCS2* did not have a more general defect in cell surface protein expression, as shown by the findings that of seven cell surface proteins tested, only ULBP1 expression was decreased (Figures 3-4 and 3-5). However, it should be noted that seven proteins represent a small fraction of the proteome, and we expect that a proteome-wide investigation would reveal many additional affected proteins. In yeast, SPCS1 and SPCS2 are required for maximal signal peptidase activity under certain growth conditions (Fang, Panzner et al. 1996, Mullins, Meyer et al. 1996), and in mammalian cells SPCS1 supports expression of the HCV protein NS2 (Suzuki, Matsuda et al. 2013). It will be of future interest to define the properties that determine if a given protein depends on SPCS1 and SPCS2 for maximal expression.

A double-mutant yeast strains lacking both SPCS1 and SPCS2 are viable and grow similarly to WT cells (Mullins, Meyer et al. 1996). We attempted to generate *SPCS1*/*SPCS2* double-KO HAP1 cells, but we could not isolate any clones with null mutations in both genes. WT HAP1 cells were co-transfected with plasmids encoding Cas9 and sgRNAs specific for SPCS1 and SPCS2 and single ULBP1^{low} cells were sorted. Of 27 clones genotyped by PCR and sequencing, only 2 clones retained single, mutant copies of both *SPCS1* and *SPCS2*. In both of these clones, *SPCS1* carried a frame-shift mutation, while *SPCS2* carried an in-frame mutation, potentially allowing for expression of a functional SPCS2 protein. Additional experiments will be needed to determine if loss of both SPCS1 and SPCS2 is lethal in mammalian cells.

CRNKL1

Little is known about *CRNKL1*, but it has been implicated in pre-mRNA splicing (Chung, Zhou et al. 2002). Since RBM4 regulates the alternative splicing of ULBP1, future studies of *CRNKL1* should be considered. Expectations should be tempered, though. Mutagenesis of confirmed regulators of ULBP1 in HAP1 cells caused ULBP1^{low} cells to appear, but mutagenesis of *CRNKL1* had no visible effect in the bulk population of cells. A role for *CRNKL1* cannot currently be ruled out, though, and a *CRNKL1* KO cell line was never isolated. At the time of this writing, the evidence suggests that *CRNKL1* is a false-positive identified by the screen. Nevertheless, I believe that additional evaluation of the role of CRNKL1 is justified for the following reasons:

- Strategies for gene targeting with CRISPR/Cas9 and the screening of mutant clones have improved since the first attempt at *CRNKL1* mutagenesis. The amount of hands-on time that would be needed to isolate a *CRNKL1* KO cell line (assuming the mutation isn't lethal) has decreased considerably in the past two years.
- Now that the alternatively spliced isoform of *ULBP1* mRNA has been characterized, potential effects of CRNKL1 on *ULBP1* splicing can be more easily addressed.
- Confirming that CRNKL1 regulates *ULBP1* splicing, or definitively ruling it out, may be helpful in other experiments addressing the regulation of *ULBP1* by RBM4.

Genes involved in glycosylation

Glycosylation of proteins in the secretory pathway is often required for their proper folding, sorting, and function (Helenius and Aebi 2004). Expression of MICA requires proper N-linked glycosylation (Andresen, Skovbakke et al. 2012). Four hits from the ULBP1 screen are involved in protein glycosylation: *C1GALT1C1*, *SLC35A1*, *ST3GAL2*, and *PMM2*. This result suggests that ULBP1 must be properly glycosylated for optimal cell surface expression. ULBP1 amino acid 82 is a predicted site of N-linked glycosylation, and digestion with PNGase F, which removed all N-linked glycans, increases the electrophoretic mobility of ULBP1 (Schneider and Hudson 2011). PNGase F-treated mature ULBP1 still had lower mobility than unmodified ULBP1 polypeptide, suggesting that ULBP1 may also be subject to O-linked glycosylation. In support of this hypothesis, *C1GALTC1* has been implicated in O-linked, but not N-linked glycosylation. However, it remains possible that ULBP1 expression is unchanged on cells with glycosylation defects, but the ULBP1 antibody used in the screen is unable to recognize the unglycosylated protein.

Functional assays to address whether regulator mutations impact functional stimulation of immune cells

It is well established that changes in NKG2D ligand expression on target cells affect the stimulation of NKG2D-expressing effector cells (Diefenbach, Jensen et al. 2001, Sutherland, Chalupny et al. 2002, Takada, Yoshida et al. 2008, Nice, Coscoy et al. 2009). Nevertheless, we set out to test the ability of HAP1 cells to activate NKG2D-dependent effector cells. Such experiments are complicated by the fact that NK cells express many activating and inhibitory receptors in addition to NKG2D, and the ligands for some of these receptors are unknown (Vivier, Raulet et al. 2011). Thus, the importance of signaling through NKG2D varies depending on the degeneracy of receptor:ligand interactions between target and effector cells that are necessary for target cell recognition. Furthermore, the quantitative effect of an individual NKG2D ligand will depend on the expression levels and affinities of all NKG2D ligands expressed on that target cell. As such, the precise functional consequence of down-regulating ULBP1, whether by 2-fold or 100-fold, is predicted to be highly cell- and context-dependent.

NK cell assays

We first attempted an in vitro cytotoxicity assay using mouse NK cells as effectors. Lymphokine-activated killer (LAK) cells were generated by culturing *Rag2*$^{-/-}$ mouse splenocytes for 6 days with 1000 U/mL recombinant human IL-2. LAK cell cultures are >95% NK cells when generated this way. We hoped that the use of mouse NK cells against human target cells would simplify our experiment. Mouse NKG2D can recognize human ULBP1, but this is not the case for human KIRs and may well not be the case for other activating receptors such as NKp30. HAP1 cells were excellent targets for killing by mouse LAK cells, but the killing was primarily NKG2D-independent, as shown by the finding that LAK cells generated from WT or *NKG2D* KO mice killed HAP1 cells almost equally well. The data in Figure 3-7 depicts the largest difference observed in replicate experiments. Furthermore, *ULBP1* KO HAP1 cells were killed just as well as WT HAP1 cells by WT (or *NKG2D* KO) NK cells (data not shown). Hence, there are apparently numerous redundant activating interactions between mouse NK cells and HAP1

cells, and we would not expect to observe decreased killing in this assay due to the reduced ULBP1 expression resulting from regulator mutations.

It should be noted that in some experiments, we were surprised to see a reduction in killing of *ATF4* KO vs WT HAP1 cells by LAK cells (Figure 3-8A). This result was not consistently reproducible, though, as it only occurred in two experiments out of at least four experiments performed (Figure 3-8A and B). Further experimentation will be necessary to gauge the significance of these data. Most importantly, this difference is not directly relevant to the topic of this thesis, because the effect was independent of NKG2D expression, as shown by the finding that it occurred with LAK cells from *NKG2D* KO mice (Figure 3-8A and B).

Chimeric antigen receptor T cell assays

In light of the difficulties we encountered in using mouse LAK cells to detect NKG2D-dependent differences in HAP1 cell killing, we switched to a functional assay in which cell activation depends on NKG2D alone. For this purpose, we collaborated with the laboratory of Charles Sentman and employed activated human T cells transduced with a construct encoding a chimeric NKG2D receptor and the DAP10 signaling adaptor protein (Zhang, Barber et al. 2006). In the chimeric NKG2D receptor, the NKG2D cytoplasmic domain is fused to the signaling domain of the CD3ζ chain. These cells (hereafter referred to as chNKG2D T cells) can be potently activated by target cells expressing NKG2D ligands, but do not respond to other NK-activating ligands. We stimulated chNKG2D T cells for 24 hours with WT, *ATF4* KO, *RBM4* KO, *HSPA13* KO, or *ULBP1* KO HAP1 cells and then measured secretion of the pro-inflammatory cytokine IFN-γ by chNKG2D T cells. In all cases, addition of NKG2D antibodies to the cultures blocked stimulation completely (Figure 3-9), whereas stimulation with *ULBP1* KO KO HAP1 cells resulted in a modest though significant reduction in IFN-γ production compared to stimulation with WT cells (Figure 3-9). These data suggested that although NKG2D ligands other than ULBP1 collectively play a larger role than ULBP1 does in NKG2D-dependent stimulation by HAP1 cells, the assay should provide some utility for assessing defective functional responses resulting from mutations in ULBP1 regulators.

Using this assay, we observed that *ATF4* KO and *HSPA13* KO HAP1 cells were as defective as *ULBP1* KO cells in stimulating IFN-γ production by chNKG2D T cells (Figure 3-9). These data were important as they support the conclusion that higher ULBP1 expression imparted by ATF4 and HSPA13 contributes significantly to NKG2D-mediated recognition of the cells.

Surprisingly, in the same assays we observed that *RBM4* KO HAP1 cells were similar to WT HAP1 cells in their capacity to stimulate the chNKG2D T cells, even though the expression of ULBP1 was reduced to a similar extent on *RBM4* KO HAP1 cells as on *ATF4* KO and *HSPA13* KO cells. In two out of two experiments performed, chNKG2D T cells derived from Donor 1 were stimulated to a similar degree by WT and *RBM4* KO cells (representative data shown in Figure 3-9A). In the same experiments, *RBM4* KO cells were more similar to *ATF4* KO cells in their ability to stimulate chNKG2D T cells derived from Donor 2, but the difference between WT and *RBM4* KO cells was not statistically significant (representative data shown in Figure 3-9B). We speculate that the RBM4 mutation increases the capacity of HAP1 cells to stimulate the chNKG2D T cells in a fashion that compensates for the reduction in ULBP1 expression on the cells.

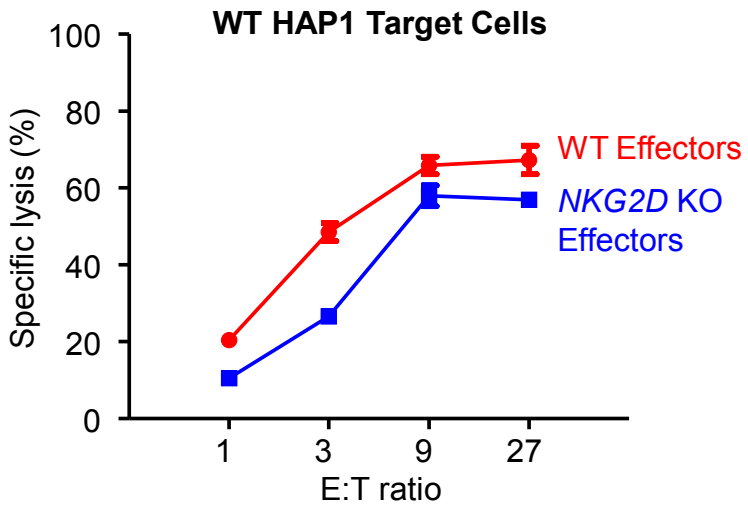

Figure 3-7: Killing of HAP1 cells by activated mouse NK cells is primarily NKG2D-independent

Splenocytes from *NKG2D* WT and KO mice on a *Rag2*$^{-/-}$ background were cultured for 6 days in 1000 U/mL recombinant human IL-2 to generate activated NK cells (LAK cells). LAK cells were mixed with WT HAP1 cells at 4 Effector:Target ratios and co-incubated for a 3 hours chromium-release assay. The difference in HAP1 cell lysis between WT and NKG2D KO LAKs was highly variable. This figure shows the largest difference ever observed.

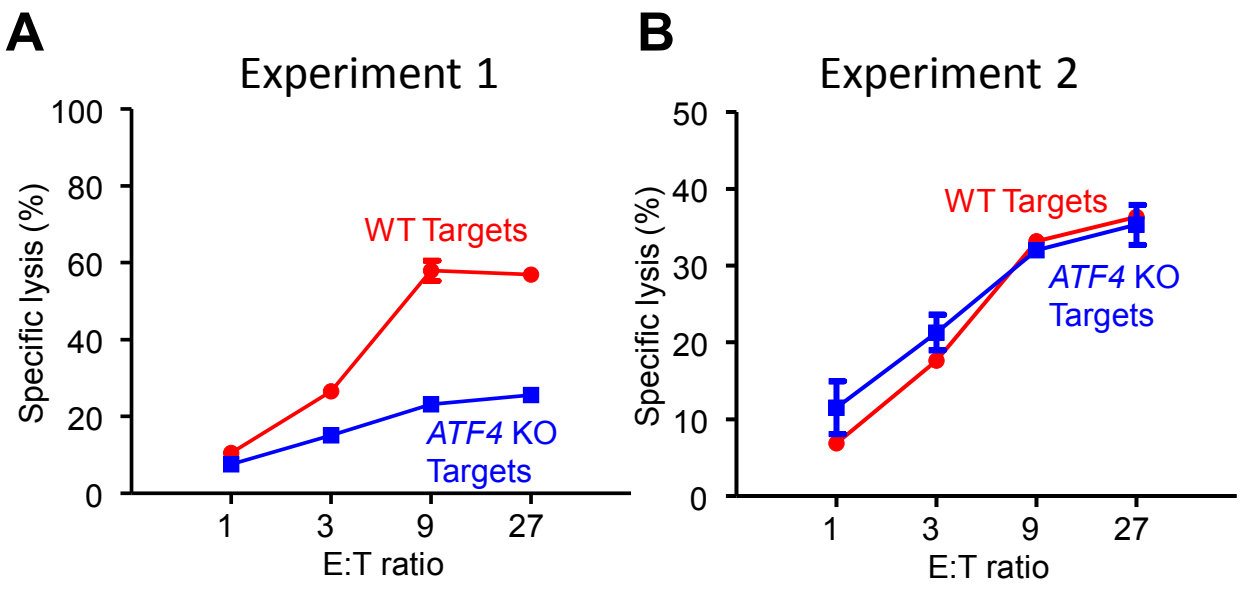

Figure 3-8: *ATF4* KO HAP1 cells may be resistant to lysis by activated mouse NK cells, but the result is poorly reproducible

Splenocytes from *NKG2D* KO mice on a *Rag2*$^{-/-}$ background were cultured for 6 days in 1000 U/mL recombinant human IL-2 to generate activated NK cells (LAK cells). LAK cells were mixed with WT or *ATF4* KO HAP1 cells at 4 Effector:Target ratios and co-incubated for a 3 hour chromium-release assay. The difference between lysis of WT vs. ATF4 KO HAP1 cells was poorly reproducible. Panel A is representative of two experiments where a difference in lysis was observed. Panel B is representative of two experiments where a difference in lysis was not observed.

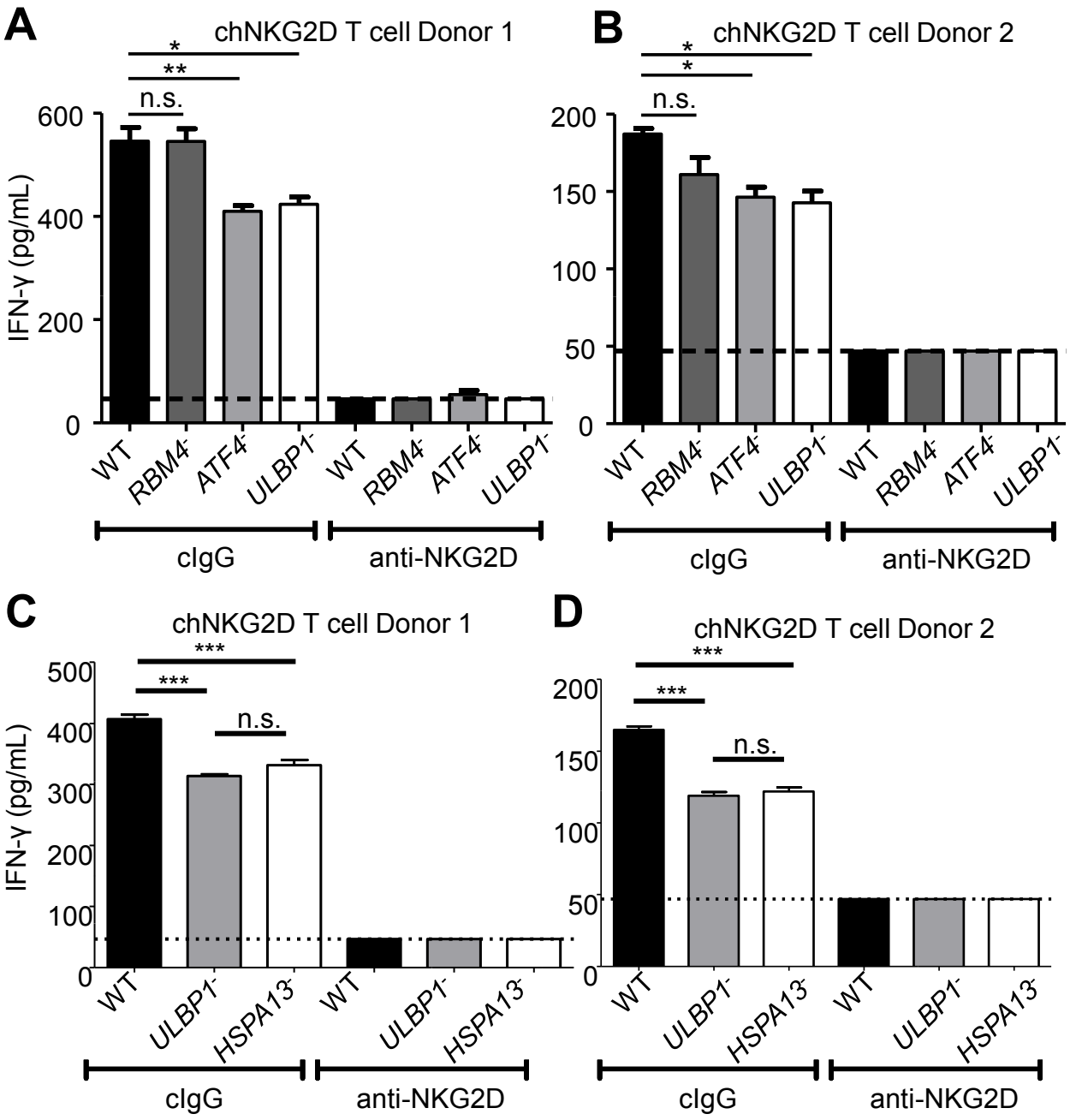

Figure 3-9: Stimulation of NKG2D-driven T cells by WT and mutant HAP1 cells
Human T cells expressing a chimeric NKG2D fusion protein (chNKG2D) were stimulated with WT and mutant HAP1 cells. T cells were pre-blocked with anti-NKG2D or control IgG (30 µg/mL) for 1 hour at room temperature. T cells and HAP1 target cells were mixed 1:1 (10^5 cells each) and co-incubated at 37 °C for 24 hours. Secreted IFN-γ was measured by ELISA. Biological triplicates were performed for each condition. The dashed line at 46.9 pg/mL represents the limit of measurement in these experiments. Data in Panels A and B are representative of 3 experiments. Data in Panels C and D are representative of two experiments. Data are plotted as mean ±SE and were analyzed by 1-way ANOVA with Bonferroni's Multiple Comparisons Test. *P<0.05, **P<0.01, ***P<0.001, n.s.: not significant.

Failure of the ULBP2 screen

As with the ULBP1 screen, we followed up on hits from the ULBP2 screen by targeting hits with CRISPR/Cas9 mutagenesis. ULBP2/5/6 staining did not change on a population of HAP1 cells after they were transfected with plasmids encoding Cas9 and sgRNAs targeting *FBXW7*, *CUL1*, or *MKNK2*. Given that ULBP1^{low} populations were readily observed in comparable targeting experiments with several hits from the ULBP1 screen, the failure to confirm these ULBP2/5/6 hits suggests that some or all of them may be spurious. However, loss-of-function mutant clones were not obtained, so an effect cannot be ruled out. A mutant clone was isolated with a 1 bp insertion in Exon 4 of *DNAJC13*, but there was essentially no change in ULBP2/5/6 staining (Figure 3-10). These results were disappointing, especially when considering the large number of validated hits arising from the ULBP1 screen. One exception was ATF4, which was identified on both the ULBP1 and ULBP2 screens. The *ATF4* mutation had a modest effect on ULBP2 expression in some experiments, as discussed in Chapter 4.

To identify drivers of ULBP2 expression, an improved screen should be done. To avoid complications from the cross-reactivity of the ULBP2 antibody, the screen could be performed in *ULBP5*/*ULBP6* KO HAP1 cells. Better enrichment of ULBP2^{low} cells could be achieved by adding a second round of sorting by FACS. It is possible that redundant factors drive ULBP2 expression in HAP1 cells, and loss of any single regulator is unlikely to cause an appreciable change in ULBP2 expression. If this is the case, genome-wide CRISPR-based screens could be applied to other ULBP2-expressing cell lines.

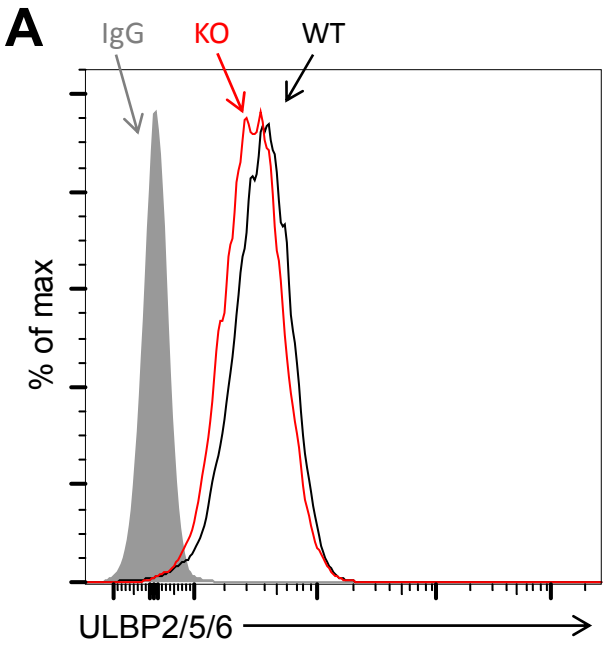

Figure 3-10: Loss of DNAJC13 has little or no effect on ULBP2/5/6 staining
A. WT and *DNAJC13* KO HAP1 cells were stained with a ULBP2/5/6 antibody and analyzed by flow cytometry. In unstimulated WT HAP1 cells, the staining is due almost exclusively to ULBP2. Data in this figure are representative of two independent experiments.

Discussion

The mutant screen identified several factors that regulate expression of ULBP1 in HAP1 cells. Loss of function mutations in each of the corresponding genes resulted in relatively modest reductions in cell surface ULBP1 when examined separately. The capacity of the screen to detect mutations that each have relatively modest effects is testimony to its remarkable power for identifying pathways that function in a partially redundant fashion. Overall, the data suggest that most of the pathways studied control different steps in the biogenesis of ULBP1, with ATF4 controlling transcription, RBM4 regulating RNA processing, and HSPA13, SCPS1 and SPCS2 regulating post-translational steps such as protein processing. Mechanistic studies of ATF4 and RBM4 are discussed in Chapters 4 and 5, respectively.

The power of the CRISPR/Cas9 method to rapidly generate double and triple mutant cell lines led to the finding that disabling multiple regulators resulted in much more striking reductions in ULBP1 expression than disabling them individually. Thus, each regulator contributes incrementally to ULBP1 expression, lending some support to the hypothesis proposed elsewhere that stress pathways might act cooperatively to quantitatively define a "threat level" confronting a cell, by acting collectively to control the amount of an NKG2D ligand displayed on the cell. Previously published evidence demonstrated that greater NK-dependent tumor elimination occurs with increasing amounts of cell surface NKG2D ligand (Diefenbach, 2001), also consistent with the "threat level" hypothesis.

When characterizing the phenotypes of our mutant HAP1 cell lines, we were surprised to find that in each case, ULBP1 was the only NKG2D ligand with substantially altered expression, the one exception being an increase in MICB expression observed on *HSPA13* KO cells. These data strongly support the conclusion that different ligands are at least partially specialized with respect to their regulatory mechanisms, providing the capacity to respond to specific classes of threats. Conversely, previous studies showed that that certain other regulatory pathways, such as the DNA damage response, regulate several NKG2D ligands similarly (Gasser, Orsulic et al. 2005). The system as a whole, therefore, encompasses both generic and specific regulators.

In functional assays, HAP1 cells were excellent targets for killing by mouse LAK cells and stimulated IFN-γ production by activated human T cells expressing a chimeric NKG2D receptor. However, partial or complete loss of ULBP1 expression on our mutant HAP1 cell lines had modest, or even zero, effects in these experiments. This result was somewhat disappointing with respect to enabling us to demonstrate robust functional effects of regulator mutations, but not at all surprising. HAP1 cells express high levels of other NKG2D ligands, as well as ligands for other activating receptors. As such, ULBP1 only contributes a fraction of the total activating signal that HAP1 cells can deliver to effector cells. It should be noted that the results of our experiments should NOT be construed as evidence that the regulators of ULBP1 we have found are of no functional importance in the immunosurveillance of stressed cells. Analyses of panels of tumor cells and tumor cell lines have shown that tumors vary considerably in the number of different NKG2D ligands expressed, and in the extent to which killing of the tumor cells by NK cells is NKG2D dependent (Jamieson, Diefenbach et al. 2002, Pende, Rivera et al. 2002, Guerra, Tan et al. 2008). HAP1 cells are especially prolific in expressing different NKG2D ligands and other NK-activating ligands, making it difficult to discern effects of regulators of only one of the ligands.

Chapter 4
Regulation of *ULBP1* transcription by ATF4

ATF4 supports ULBP1 expression on multiple tumor-derived cell lines

Having validated several hits from our screen, we decided to further investigate the roles of ATF4 and RBM4 in regulating ULBP1 expression. This chapter will address the mechanisms of ULBP1 regulation by ATF4. To address whether ATF4 regulates *ULBP1* in other cell types, we mutated *ATF4* in the K-562 chronic myelogenous leukemia cell line and the Jurkat acute T cell leukemia cell line using CRISPR/Cas9 targeting with flanking guide RNAs so as to delete the *ATF4* gene. WT K-562 cells had relatively low ULBP1 expression, and mutation of *ATF4* resulted in the complete disappearance of ULBP1 on the cell surface, which was accompanied by an 11-fold reduction in *ULBP1* mRNA in the cells (Figure 4-1). In contrast, ATF4-deficiency in Jurkat cells resulted in a modest reduction in *ULBP1* mRNA and a barely detectable reduction in ULBP1 cell surface staining. By comparison, HAP1 cells showed intermediate effects of ATF4-deficiency. The results suggested that under steady state conditions, ATF4 drives basal ULBP1 expression in multiple tumor cell lines.

ATF4 drives *ULBP1* transcription in response to cell stress

ATF4 is induced in a variety of stress conditions that arise in unhealthy, infected and transformed cells, where coupling these stress conditions to NKG2D ligand expression may enable destruction of undesirable cells. Multiple forms of cellular stress, including amino acid starvation, the unfolded protein response, oxidative stress, and the presence of dsRNA converge on the phosphorylation of the translation initiation factor eIF2α (Rutkowski and Kaufman 2003, Suragani, Zachariah et al. 2012). Phosphorylation of eIF2α globally suppresses protein translation, but selectively activates the translation of ATF4 (Harding, Novoa et al. 2000). The transcriptional targets of ATF4 include amino acid transporters and protein chaperones, which in combination with the overall reduction in protein synthesis help mitigate the cellular stress (Harding, Zhang et al. 2003). However, ATF4 expression also drives the expression the pro-apoptotic transcription factor CHOP (GADD153), suggesting that ATF4 not only drives adaptation to stress, but also promotes cell death if the stress cannot be overcome (Tabas and Ron 2011, Han, Back et al. 2013). Increased ATF4 expression was detected in some tumors (Bi, Naczki et al. 2005), providing a possible mechanism for coupling malignant transformation to expression of ULBP1, and consequently to tumor immunosurveillance.

To drive stress-induced ATF4 expression, we treated cells with the drugs histidinol (HisOH), which competitively inhibits histidine tRNA charging, thus mimicking amino acid starvation (Hansen, Vaughan et al. 1972, Thiaville, Dudenhausen et al. 2008), or thapsigargin (Tg), which induces the unfolded protein response (Oslowski and Urano 2011). Histidinol or thapsigargin treatment each significantly induced *ULBP1* mRNA in WT K-562, HAP1, and Jurkat cells, but induction was abrogated or severely blunted in *ATF4* KO cells (Figure 4-2). RNA-Seq analysis of HAP1 cells confirmed ATF4-dependent upregulation of *ULBP1* mRNA in response to histidinol treatment (Figure 4-3). Analysis of *ULBP2* by RNA-Seq and RT-qPCR showed that histidinol treatment caused an increase in *ULBP2* mRNA that was partially ATF4-dependent (Figure 4-4). Expression of *ULBP3*, *MICA*, and *MICB* all appeared to decrease in response to histidinol when analyzed by RNA-Seq, but this decrease only occured for *MICA* when the RNA levels were measured by RT-qPCR (Figures 4-5-4-7). The reason for the discrepancy between the RNA-Seq and RT-qPCR data is unclear. It should be noted that RNA-Seq was performed using pooled RNA isolated from 3 independent *ATF4* KO HAP1 clones,

whereas the RT-qPCR experiments were performed using RNA isolated from a single *ATF4* KO cell clone (clone 2A9). Loss of ATF4 did not affect any basal expression of *ULBP3*, *MICA*, or *MICB* mRNAs, nor did it affect the response to histidinol treatment. *ULBP4*, *ULBP5*, and *ULBP6* mRNAs were absent or barely detectable by RNA-Seq analysis of untreated HAP1 cells, and those genes showed no sign of induction by histidinol (data not shown). These data suggest that the ATF4-mediated stress response induces expression of *ULBP1*, and to a minor extent *ULBP2*, but not most other NKG2D ligands.

Stress-induced cell surface expression of ULBP1 protein was also examined. Although histidinol and thapsigargin induce transcription of ATF4-regulated genes, they also inhibit protein synthesis, both directly (e.g., by limiting the availability of charged histidine tRNAs) and indirectly, by causing eIF2α phosphorylation, making it difficult to predict the outcome for any specific *ATF4* regulated protein. Nevertheless, in K-562 cells, we observed a dramatic ATF4-dependent induction of cell surface ULBP1 by histidinol, compared to the low background observed in uninduced cells (Figure 4-8A). In HAP1 and Jurkat cells, in contrast, histidinol induced ULBP1 cell surface expression slightly in WT cells, but caused decreased ULBP1 expression in *ATF4*-mutant cells (Figure 4-8A), consistent with the aforementioned inhibition of protein synthesis resulting from histidinol treatments. Indeed, histidinol treatments resulted in significantly decreased cell surface expression of HLA proteins, which are not regulated by ATF4 (Figure 4-8C). As summarized by the graphs in Figure 4-8D, the overall effect of ATF4 induction resulting from histidinol treatment is to induce and/or maintain ULBP1 cell surface expression in the face of global protein synthesis inhibition associated with this stress pathway.

HAP1, K-562, and Jurkat cells are all tumor-derived cell lines, and numerous events associated with transformation may have primed these cell lines for induction of ULBP1 in response to cell stress. To address whether stress can induce ULBP1 expression in more "normal", untransformed cells, we treated early passage human foreskin fibroblasts (HFF) with histidinol or thapsigargin. ULBP1 was absent from the surface of HFF cells, and was not induced by either histidinol or thapsigargin treatment (Figure 4-9A). RT-qPCR showed that *ULBP1* mRNA was present in untreated HFF cells, but the level of expression was much lower than in HAP1 cells (between 50- and 150-fold less than HAP1 cells, depending on the reference genes used, data not shown). The effect of histidinol treatment varied in the three experiments performed (Figure 4-9B). In the first experiment, histidinol treatment histidinol caused a 20-fold induction of *ULBP1* mRNA. In the second experiment, the induction of *ULBP1* was only 5-fold, and was not statistically significant. In the third experiment, histidinol did not affect *ULBP1* expression at all. Thapsigargin treatment caused a 25- to 40-fold induction of *ULBP1* mRNA in all three experiments performed. Even after the best inductions, however, the amount of *ULBP1* mRNA detected in RT-qPCR experiments was lower than seen in untreated HAP1 cells, where cell surface ULBP1 was readily detected. More specifically, the RT-qPCR results indicated that untreated HAP1 cells expressed 45- to 150-fold more *ULBP1* mRNA than untreated HFF cells, and untreated HAP1 cells expressed 3- to 5-fold more *ULBP1* mRNA than thapsigargin-treated HFFs, depending on the reference gene(s) used for normalization (data not shown). Furthermore, we cannot conclude that the inductive effect of either drug in these cells is ATF4-dependent. Taken together, the data suggest that stress pathways known to induce ATF4 expression can drive upregulation of *ULBP1* mRNA in relatively "normal" cells, but the maximum expression level in those cells may be inadequate to result in appreciable cell surface expression. We speculate that additional stress pathways may need to be activated to adequately amplify ULBP1 expression to achieve appreciable amounts of cell surface expression.

To address whether ATF4 directly regulates *ULBP1* transcription, we used ChIP-Seq analysis to determine whether it binds to *ULBP1* regulatory elements in histidinol-treated HAP1 cells. ChIP-Seq with three independent ATF4 antibodies showed a strong peak of ATF4 binding associated with the *ULBP1* promoter, along with a smaller peak ~27 kb downstream in the intergenic region, which could function as an enhancer or play some other role. No other notable ATF4 binding was observed in the 266 kb interval shown, which includes genes encoding 5 other functional NKG2D ligands (*ULBP2-6; RAET1K* is a pseudogene), at least two of which are expressed in HAP1 cells (Figure 4-10). The *MICA* and *MICB* genes were also devoid of ATF4 binding (data not shown). HOMER Motif Analysis software identified ATF4-binding motifs in both peaks (Heinz, Benner et al. 2010). ATF4 binding at the *ULBP1* promoter was confirmed by conventional ChIP-qPCR, which also demonstrated that ATF4 binds to the ULBP1 gene in HAP1 cells under steady state conditions, and that ATF4 binding is sharply enhanced after histidinol treatment (Figure 4-11). A similar pattern of ATF4 binding was observed at the *ASNS* promoter, a known target of ATF4, but not at a negative control site in the *ASNS* gene body (Chen, Pan et al. 2004).

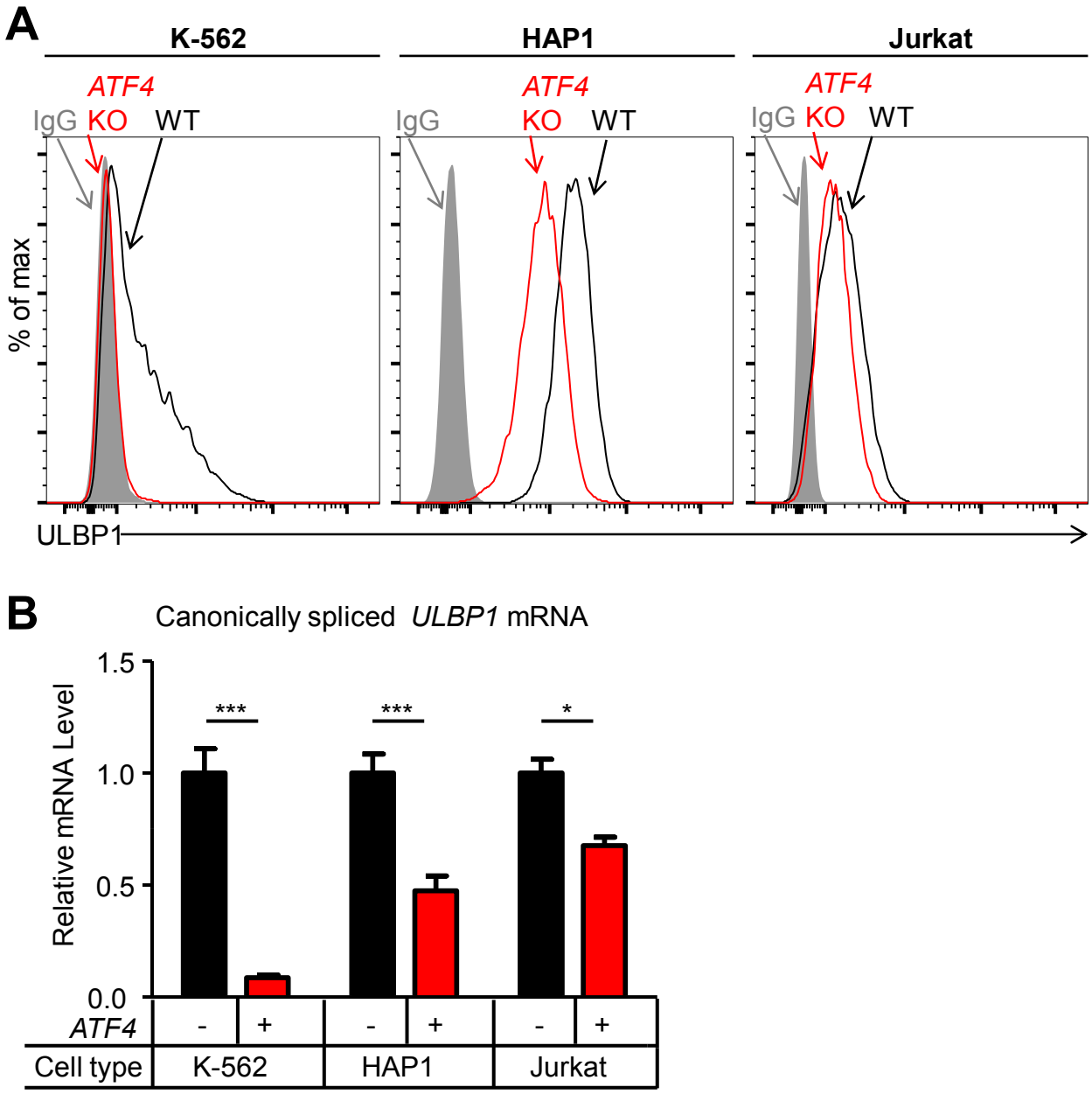

Figure 4-1: ATF4 drives basal ULBP1 expression on multiple cell lines
A. Flow cytometric analysis of ULBP1 expression on WT and *ATF4* KO K-562, HAP1, and Jurkat cells. **B**. RT-qPCR analysis of *ULBP1* mRNA expression levels in the cells described in A. Expression levels were normalized to *ACTB*, *GAPDH*, and *HPRT1* and are shown as mean ±SE. Expression in WT cells was set to "1.0" for each cell type; the different cell types are not comparable in this experiment. The data were analyzed by 2-way ANOVA with Bonferroni's Multiple Comparisons Test. **P*<0.05, ****P*<0.001. Data in this figure are representative of at least 3 independent experiments.

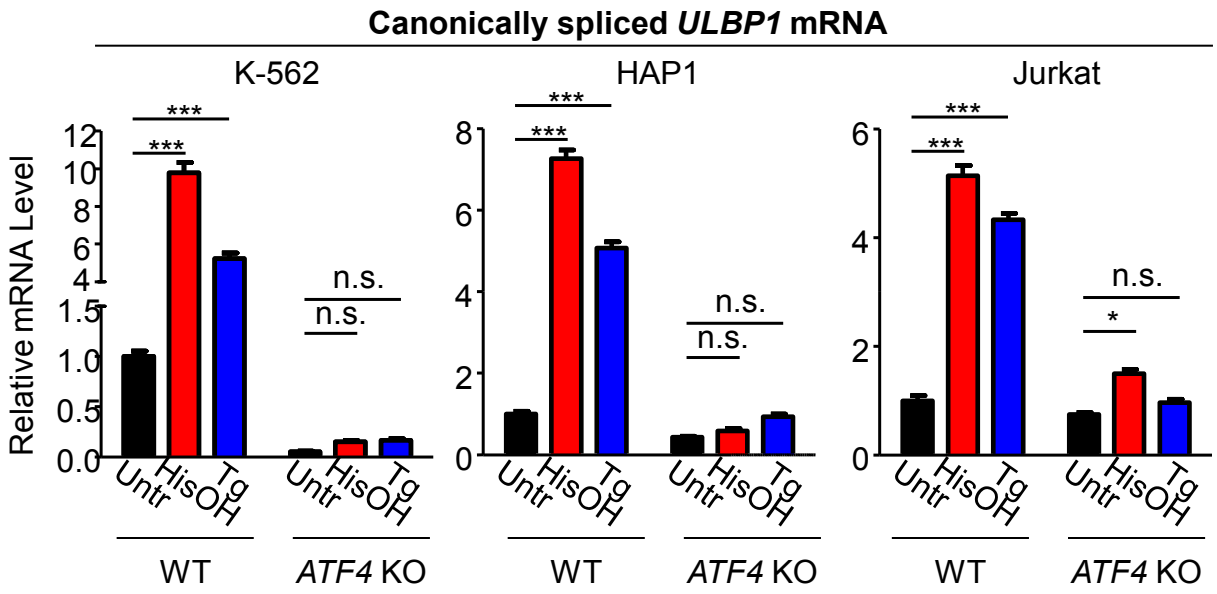

Figure 4-2: ATF4 drives increased expression of *ULBP1* mRNA in response to amino acid starvation and activation of the unfolded protein response
Cells were treated for 24 hours with 2 mM histidinol (HisOH) to mimic amino acid starvation or 300 nM thapsigargin (Tg) to induce ER stress. RNA was isolated from treated and control cells, and *ULBP1* mRNA levels were determined by RT-qPCR. Expression levels were normalized to *ACTB*, *GAPDH*, and *HPRT1* and are shown as mean ±SE. Expression in untreated WT cells was set to "1.0" for each cell type; the different cell types are not comparable in this experiment. For reference, the Cq values for *ULBP1* in untreated WT cells were 32.2 for K-562 cells, 27.9 for HAP1 cells, and 30.5 for Jurkat cells. The data were analyzed by 2-way ANOVA with Bonferroni's Multiple Comparisons Test. **P*<0.05, ****P*<0.001, n.s.: not significant. Data in this figure are representative of at least three independent experiments.

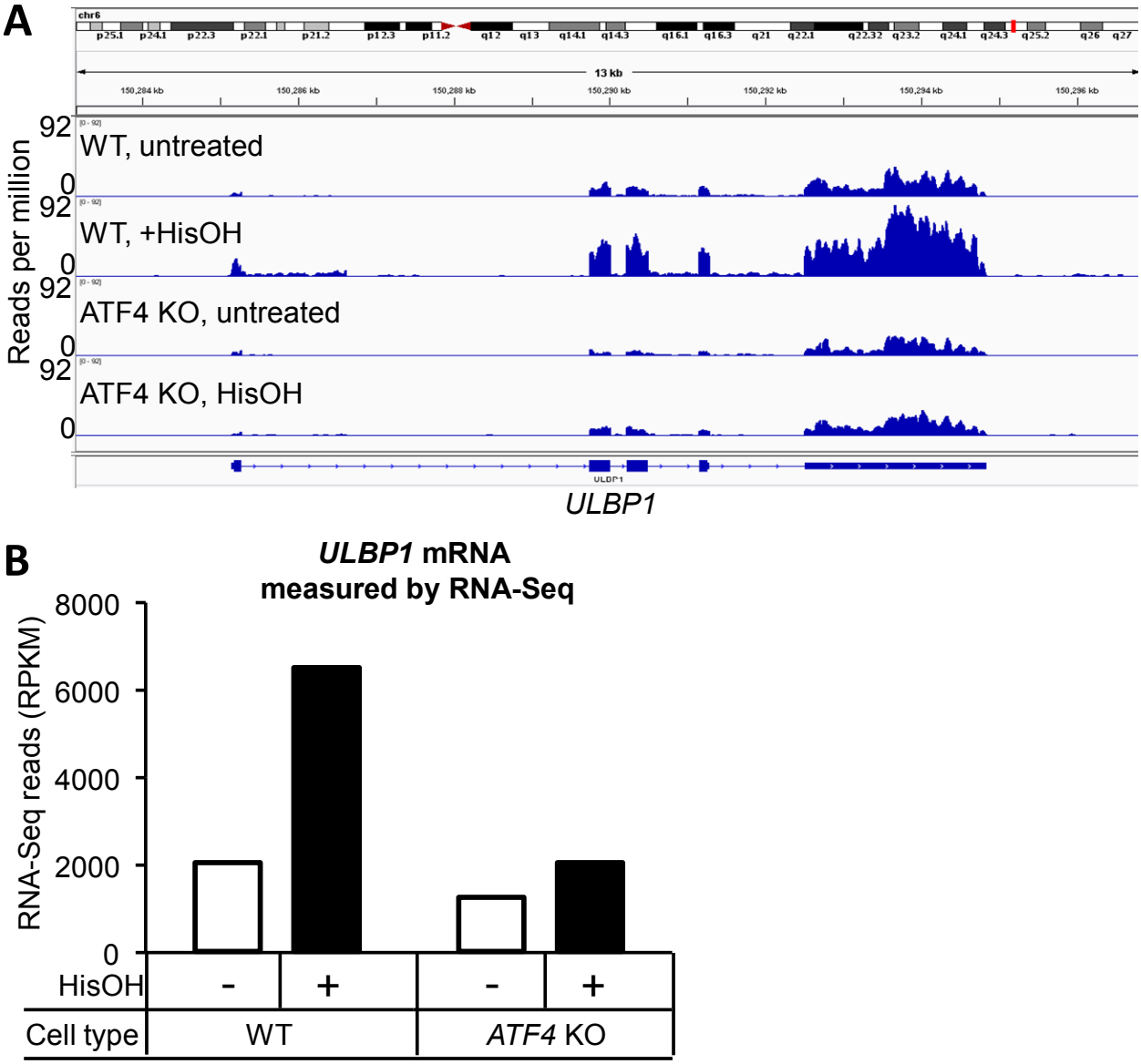

Figure 4-3: RNA-Seq analysis of *ULBP1* expression in HAP1 cells in response to histidinol

A. WT and *ATF4* KO HAP1 cells were treated for 24 hours with 2 mM histidinol (HisOH). Total RNA was isolated from histidinol treated and control cells and analyzed by RNA-Seq. RNA-Seq read densities were normalized to the total number of aligned read in each sample (reads per million) and plotted with IGV.

B. Quantification of reads aligning to *ULBP1,* presented as reads per kb per million (RPKM). Data in this figure are derived from a single RNA-Seq experiment.

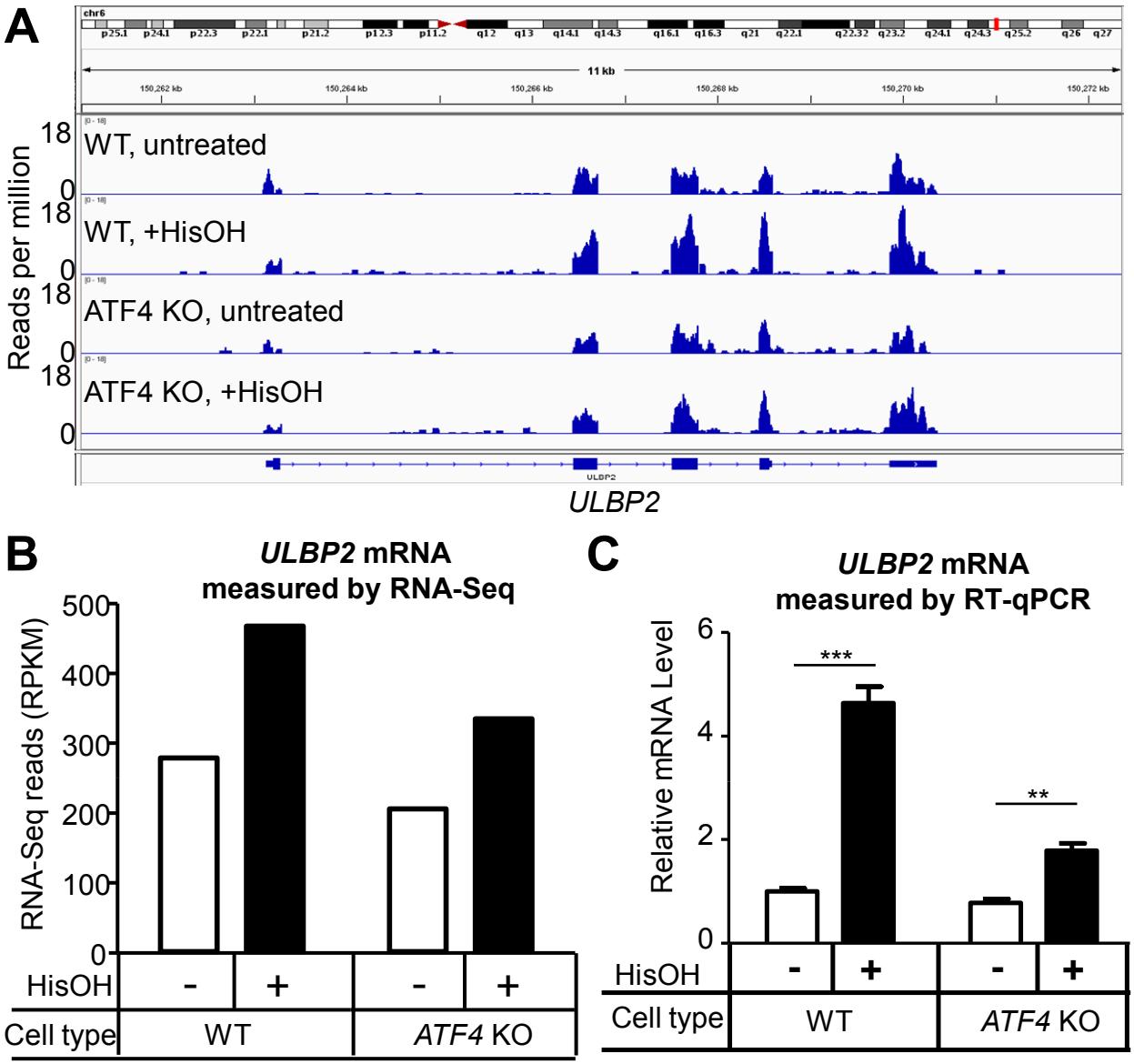

Figure 4-4: Analysis of *ULBP2* mRNA expression in HAP1 cells in response to histidinol

A. WT and *ATF4* KO HAP1 cells were treated for 24 hours with 2 mM histidinol (HisOH). Total RNA was isolated from histidinol treated and control cells and analyzed by RNA-Seq. RNA-Seq read densities were normalized to the total number of aligned read in each sample (reads per million) and plotted with IGV.

B. Quantification of reads aligning to *ULBP2* in Panel A, presented as reads per kb per million (RPKM). Data in this figure are derived from a single RNA-Seq experiment. **C.** RT-qPCR analysis of *ULBP2* mRNA expression in cells treated as in Panel A. For RT-qPCR expression levels were normalized to *ACTB*, *GAPDH*, and *HPRT1* and are shown as mean ±SE. The RT-qPCR data were analyzed by 2-way ANOVA with Bonferroni's Multiple Comparisons Test. ***P*<0.01, ****P*<0.001. Panels A and B are derived from a single RNA-Seq experiment. Data in Panel C are representative of at least three independent experiments.

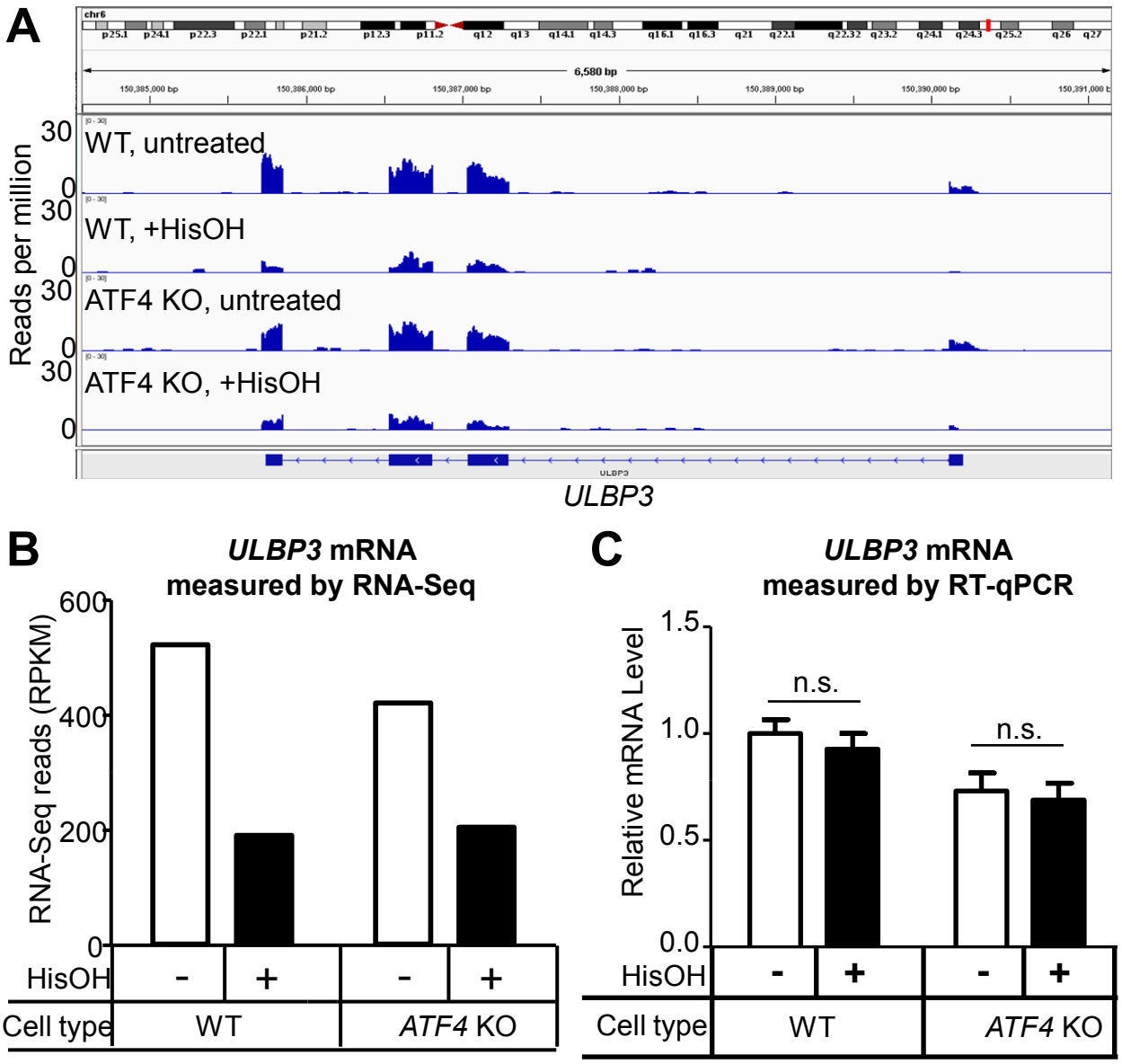

Figure 4-5: Analysis of *ULBP3* mRNA expression in HAP1 cells in response to histidinol

A. WT and *ATF4* KO HAP1 cells were treated for 24 hours with 2 mM histidinol (HisOH). Total RNA was isolated from histidinol treated and control cells and analyzed by RNA-Seq. RNA-Seq read densities were normalized to the total number of aligned read in each sample (reads per million) and plotted with IGV.

B. Quantification of reads aligning to *ULBP3* in Panel A, presented as reads per kb per million (RPKM). Data in this figure are derived from a single RNA-Seq experiment. **C.** RT-qPCR analysis of *ULBP3* mRNA expression in cells treated as in Panel A. For RT-qPCR expression levels were normalized to *ACTB*, *GAPDH*, and *HPRT1* and are shown as mean ±SE. The RT-qPCR data were analyzed by 2-way ANOVA with Bonferroni's Multiple Comparisons Test. ***P*<0.01, ****P*<0.001. Panels A and B are derived from a single RNA-Seq experiment. Data in Panel C are representative of at least three independent experiments.

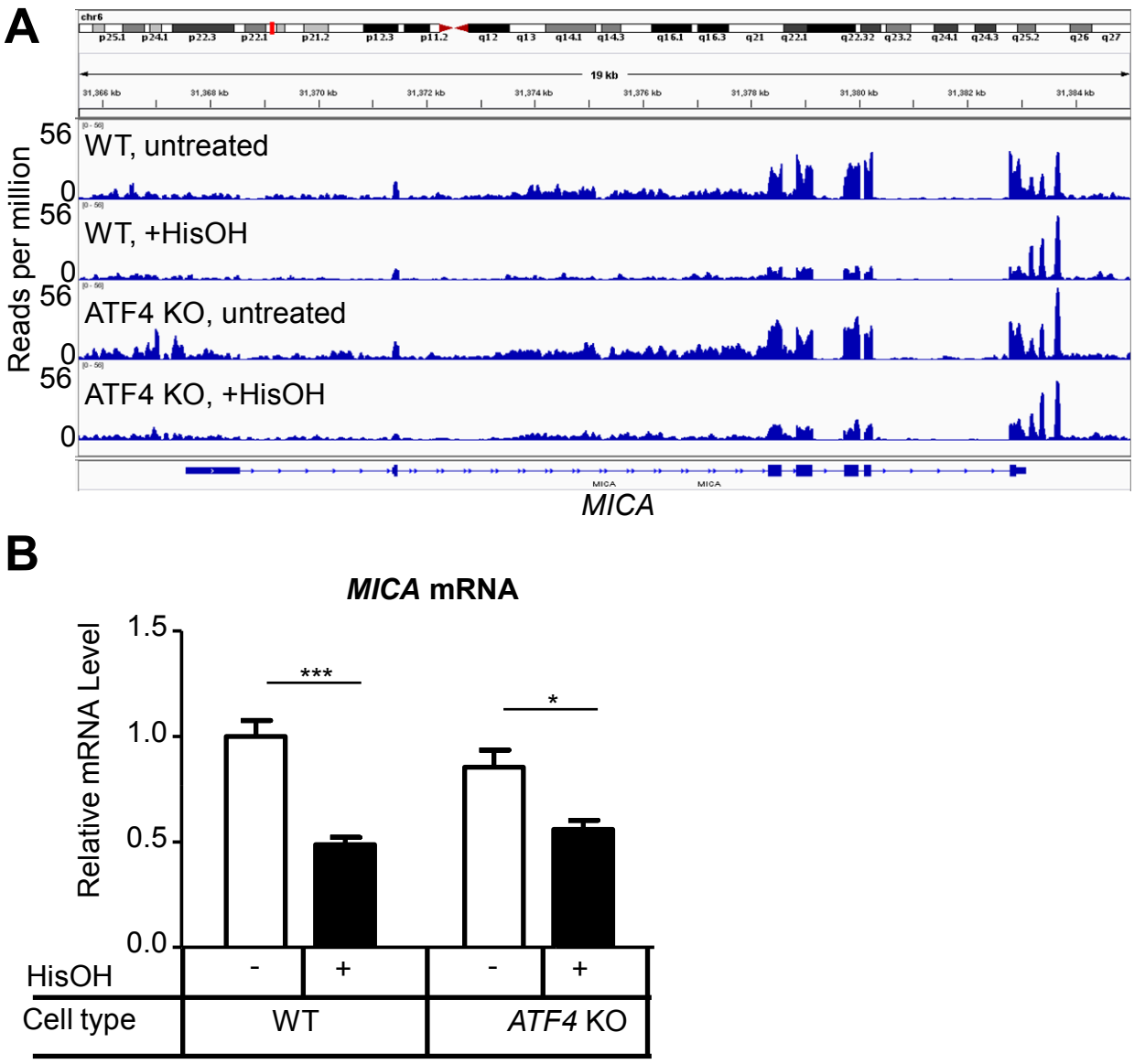

Figure 4-6: Analysis of *MICA* mRNA expression in HAP1 cells in response to histidinol

A. WT and *ATF4* KO HAP1 cells were treated for 24 hours with 2 mM histidinol (HisOH). Total RNA was isolated from histidinol treated and control cells and analyzed by RNA-Seq. RNA-Seq read densities were normalized to the total number of aligned read in each sample (reads per million) and plotted with IGV. MICA read counts could not be calculated due to complications with the RNA-Seq analysis pipeline. **B.** RT-qPCR analysis of *MICA* mRNA expression in cells treated as in Panel A. For RT-qPCR expression levels were normalized to *ACTB*, *GAPDH*, and *HPRT1* and are shown as mean ±SE. The RT-qPCR data were analyzed by 2-way ANOVA with Bonferroni's Multiple Comparisons Test. ***P*<0.01, ****P*<0.001. Panel A are derived from a single RNA-Seq experiment. Data in Panel B are representative of at least three independent experiments.

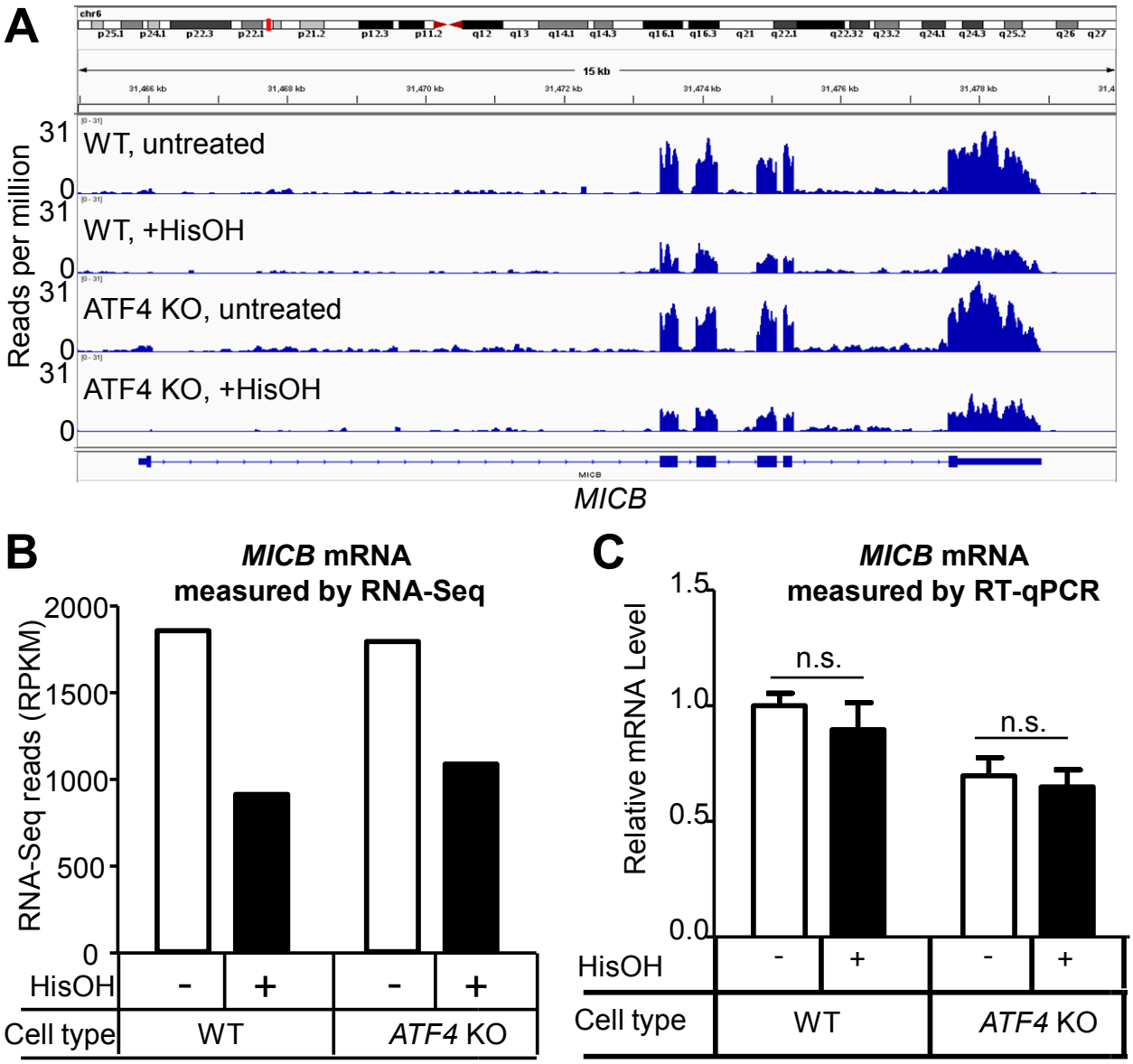

Figure 4-7: Analysis of *MICB* mRNA expression in HAP1 cells in response to histidinol

A. WT and *ATF4* KO HAP1 cells were treated for 24 hours with 2 mM histidinol (HisOH). Total RNA was isolated from histidinol treated and control cells and analyzed by RNA-Seq. RNA-Seq read densities were normalized to the total number of aligned read in each sample (reads per million) and plotted with IGV.

B. Quantification of reads aligning to *MICB* in Panel A, presented as reads per kb per million (RPKM). Data in this figure are derived from a single RNA-Seq experiment.

C. RT-qPCR analysis of *MICB* mRNA expression in cells treated as in Panel A. For RT-qPCR expression levels were normalized to *ACTB*, *GAPDH*, and *HPRT1* and are shown as mean ±SE. The RT-qPCR data were analyzed by 2-way ANOVA with Bonferroni's Multiple Comparisons Test. ***P*<0.01, ****P*<0.001. Panels A and B are derived from a single RNA-Seq experiment. Data in Panel C are representative of at least three independent experiments.

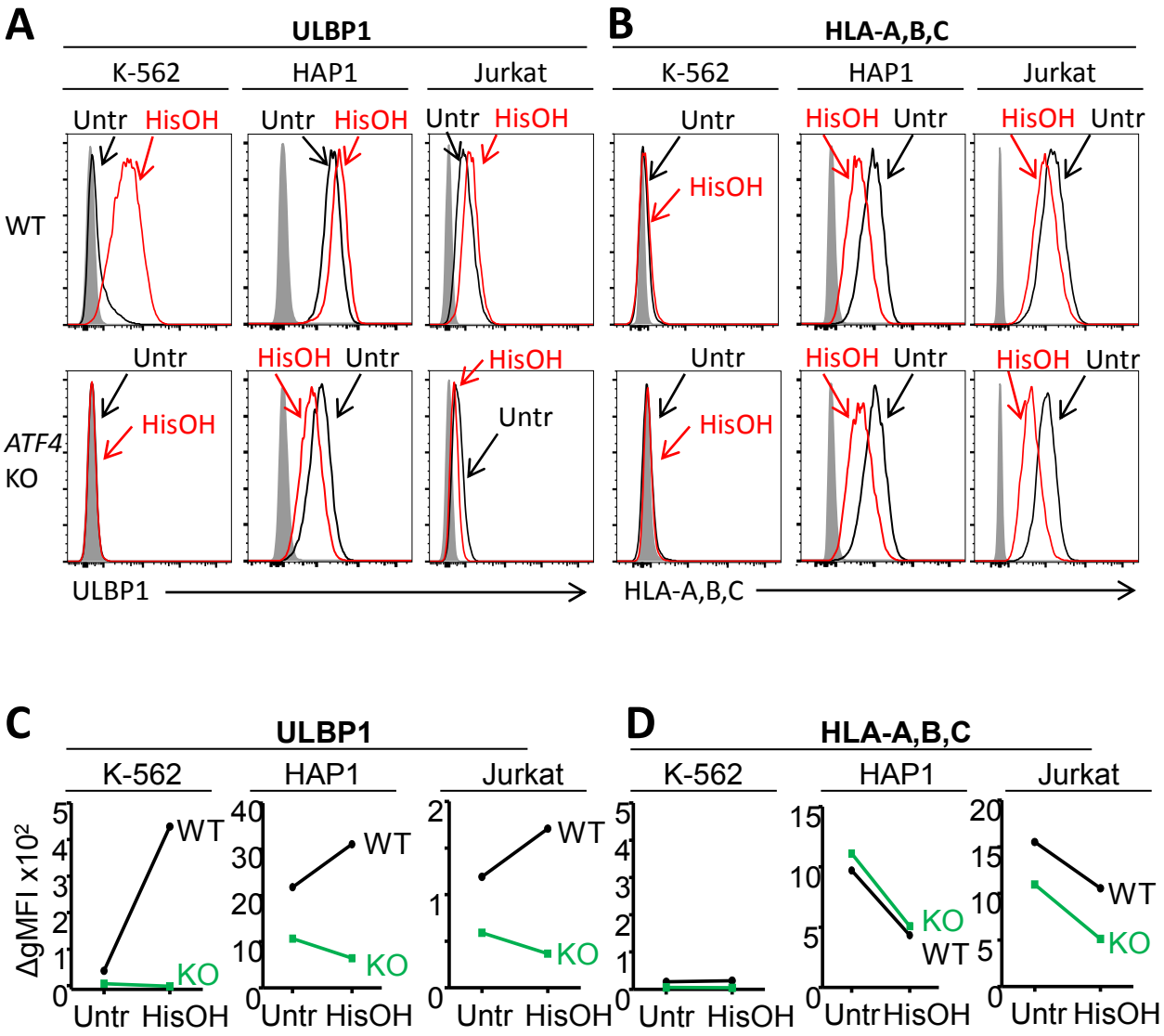

Figure 4-8: ATF4 drives increased expression of ULBP1 protein at the cell surface in response to cell stress

A-B. Cells were treated for 24 hours with 2 mM histidinol (HisOH) to mimic amino acid starvation. Surface expression of ULBP1 and HLA Class I were analyzed by flow cytometery. **C-D**. Quantification of surface staining shown in Panels A-B. Data are plotted as the geometric mean fluorescence intensity of the specific stain minus the intensity of the isotype control (ΔgMFI). Data in this figure are representative of at least three independent experiments.

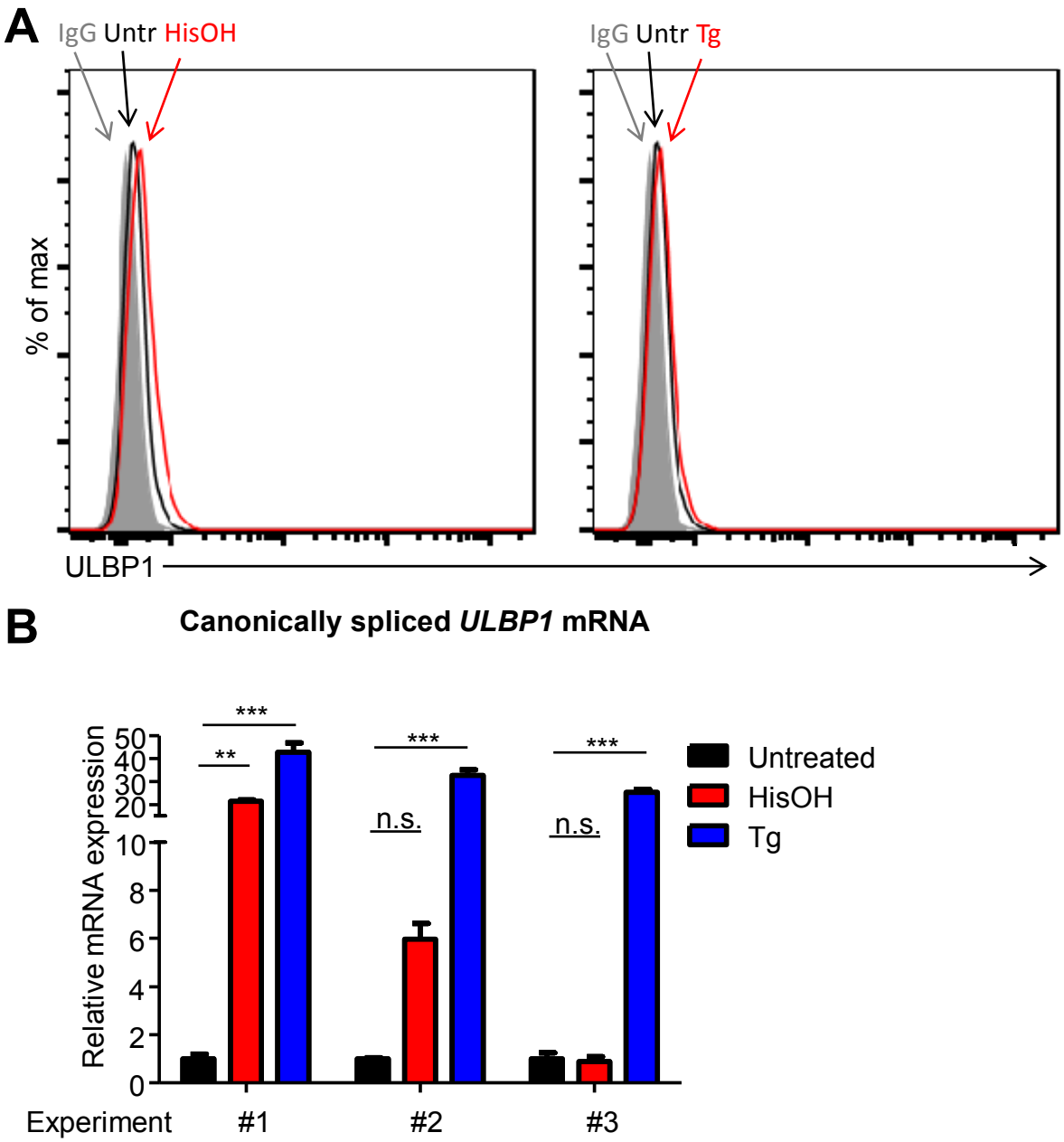

Figure 4-9: Cell stress can induce *ULBP1* mRNA, but not cell surface protein, in early passage human foreskin fibroblasts

A. Human foreskin fibroblasts were treated for 24 hours with 2 mM histidinol (HisOH) or 300 nM thapsigargin (Tg). Surface expression of ULBP1 was analyzed by flow cytometry. Data in this panel are representative of three independent experiments.

B. RNA was isolated from cells treated as in Panel A, and expression of *ULBP1* mRNA was analyzed by RT-qPCR. The results of three independent experiments are shown, and the data are plotted as mean ±SE. The Cq values for ULBP1 mRNA were 35.1, 33.0, and 33.0 in Experiments 1, 2, and 3, respectively. For each experiment, the data were analyzed by one-way ANOVA followed by Dunnet's multiple comparison test, comparing HisOH and Tg-treated cells to the untreated control sample. ***P*<0.01, ****P*<0.001, n.s.: not significant.

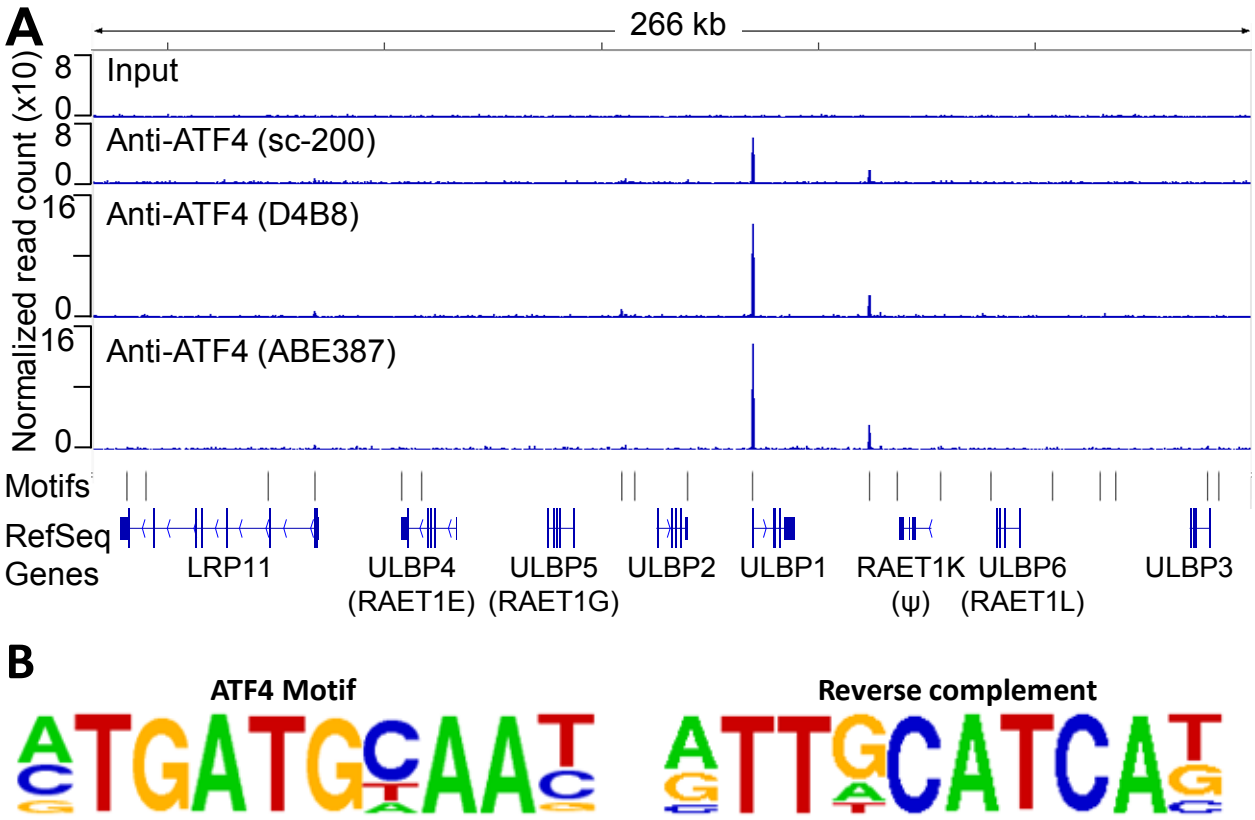

Figure 4-10: ATF4 is bound to the *ULBP1* locus

A. ATF4 ChIP-Seq: Hap-1 cells were treated with 2 mM histidinol (HisOH) for 24 hours, followed by formaldehyde cross-linking. ATF4-bound chromatin was immunoprecipitated using three independent ATF4 antibodies, and the isolated DNA was sequenced and aligned to the human genome. *RAET1K* is a pseudogene. **B.** The ATF4 motif used in Panel A.

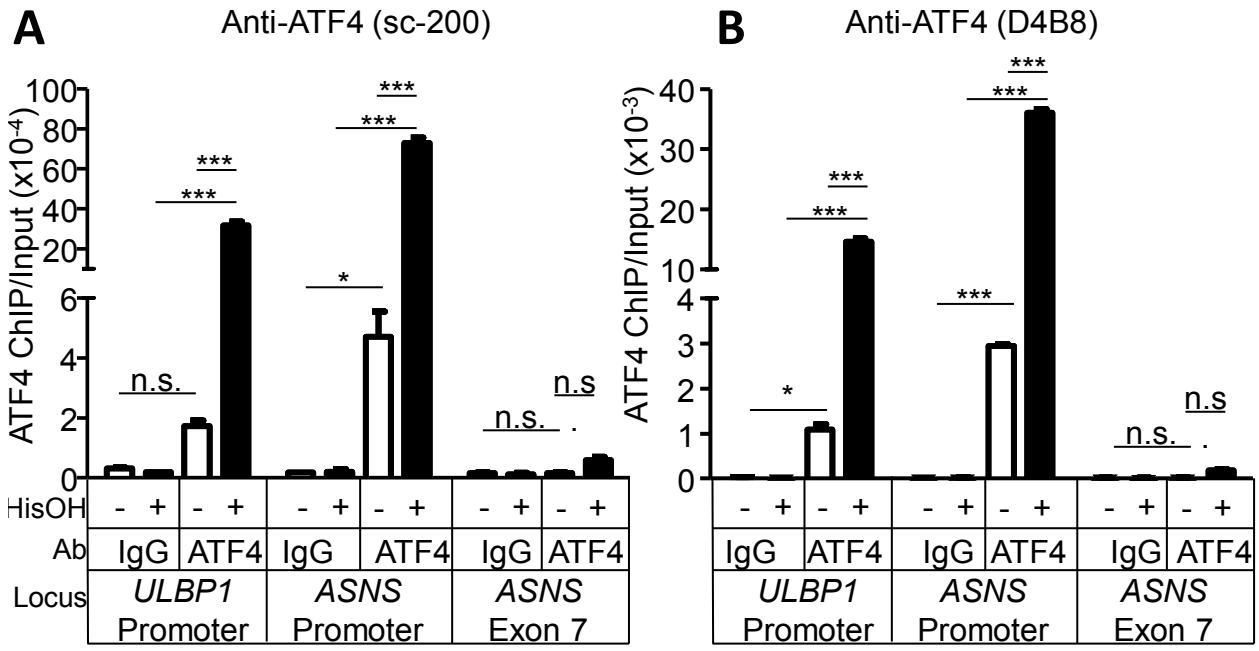

Figure 4-11: Confirmation of ATF4 ChIP-Seq result by ChIP-qPCR

A-B. ChIP-qPCR of ATF4 using the antibody sc-200 (A) or D4B8 (B). Samples were treated as in Panel A, followed by qPCR. ChIP signal was normalized to the amount of Input DNA for each sample. Data are plotted as mean ±SE and were analyzed by 2-way ANOVA with Bonferroni's Multiple Comparisons Test. Data are representative of two experiments using both untreated and HisOH-treated cells, and a third experiment using only HisOH-treated cells. **P*<0.05, ****P*<0.001, n.s.: not significant.

Additional treatments that may induce ATF4

Proteasome inhibition has been shown to upregulate *ULBP1* and the mouse NKG2D ligand *Mult1* at the RNA level (Butler, Moore et al. 2009, Nice 2009). Proteasome inhibition has pleiotropic effects, one of which is the induction of ATF4 (Koditz, Nesper et al. 2007). Treatment of WT and *ATF4* KO HAP1 cells with the proteasome inhibitor MG132 increased ULBP1 mRNA and cell surface protein (Figure 4-12). The increase in ULBP1 expression was slightly blunted in *ATF4* KO cells as compared to WT, but we conclude that the effect of proteasome inhibition on ULBP1 is primarily ATF4-independent.

Treatment of HAP1 cells with $CoCl_2$ caused upregulation of ULBP1 cell surface protein and mRNA, and the effect was abrogated in *ATF4* KO cells (Figure 4-13). However, the physiological relevance of this result is questionable. Under normoxic conditions, PHD family prolyl hydroxylases promote ubiquitination and degradation of ATF4 and the hypoxia inducible factors HIF1α and HIF2α (Koditz, Nesper et al. 2007, Mucaj, Shay et al. 2012). Hypoxia inhibits PHD-mediated degradation of ATF4 and the HIFs. $CoCl_2$ is frequently used to mimic hypoxia because it prevents prolyl hydroxylation of the HIFs and their subsequent degradation. It is possible that $CoCl_2$ treatment could similarly stabilize ATF4, although this has not been demonstrated. Furthermore, the eIF2a kinase HRI is activated by heavy metals, although activation by $CoCl_2$ has not been examined (McEwen, Kedersha et al. 2005). ATF4 expression could plausibly be induced by either mechanism. However, it is not clear that the sensing of heavy metals is a physiological function of HRI, and induction of ATF4 by hypoxia can be tested directly. Further experiments with $CoCl_2$ treatment were not pursued.

To directly test the effect of hypoxia, WT and *ATF4* KO HAP1 cells were incubated for 24 hours at 20% or 1% O_2. Hypoxia did not alter ULBP1 expression at the cell surface in either WT or *ATF4* KO cells, and cells cultured at 1% O_2 showed a slight decrease in *ULBP1* mRNA (Figure 4-14). Treatment caused a slight increase in *VEGFA* mRNA, indicating that at least some degree of hypoxia was achieved. However, the degree of oxygen deprivation and treatment time necessary to induce ATF4 varies (see Introduction), and it was not clear that ATF4 was induced in this experiment. In the future, several parameters could be adjusted for a thorough investigation of relationship between hypoxia and ULBP1. Longer treatment times or lower oxygen levels might induce higher ATF4 levels in HAP1 cells. Other cell types may be more responsive to hypoxia than HAP1.

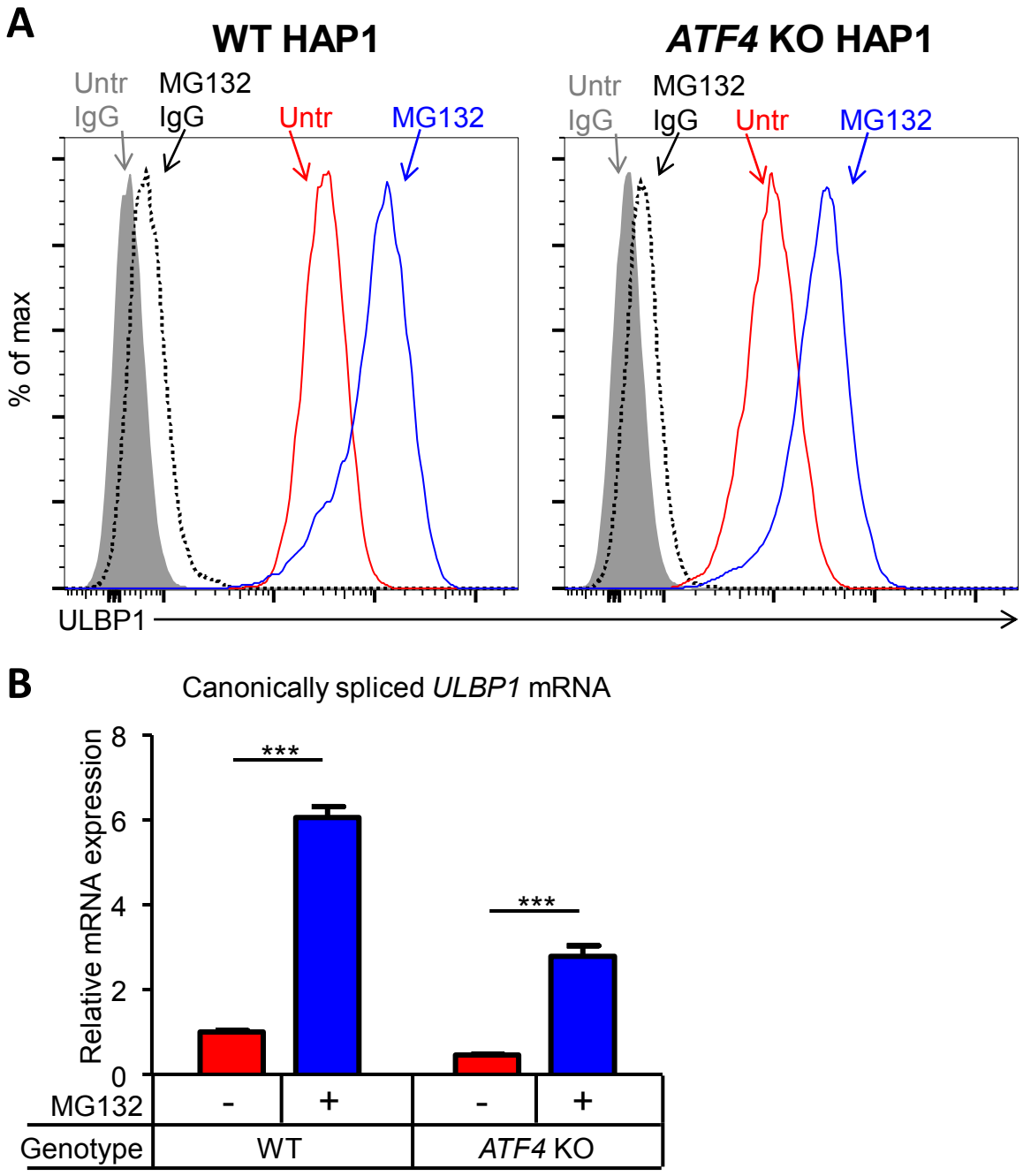

Figure 4-12: Proteasome inhibition increases ULBP1 expression independently of ATF4

A. WT and *ATF4* KO HAP1 cells were treated for 24 hours with the proteasome inhibitor MG132 (5 μM) and analyzed by flow cytometry. **B**. RT-qPCR analysis of *ULBP1* mRNA expression levels in cells treated as in Panel A. Expression levels were normalized to *ACTB*, *GAPDH*, and *HPRT1* and are shown as mean ±SE. The data were analyzed by 2-way ANOVA with Bonferroni's Multiple Comparisons Test. ***P<0.001. Panel A is representative of 3 independent experiments. Panel B is representative of 2 independent experiments.

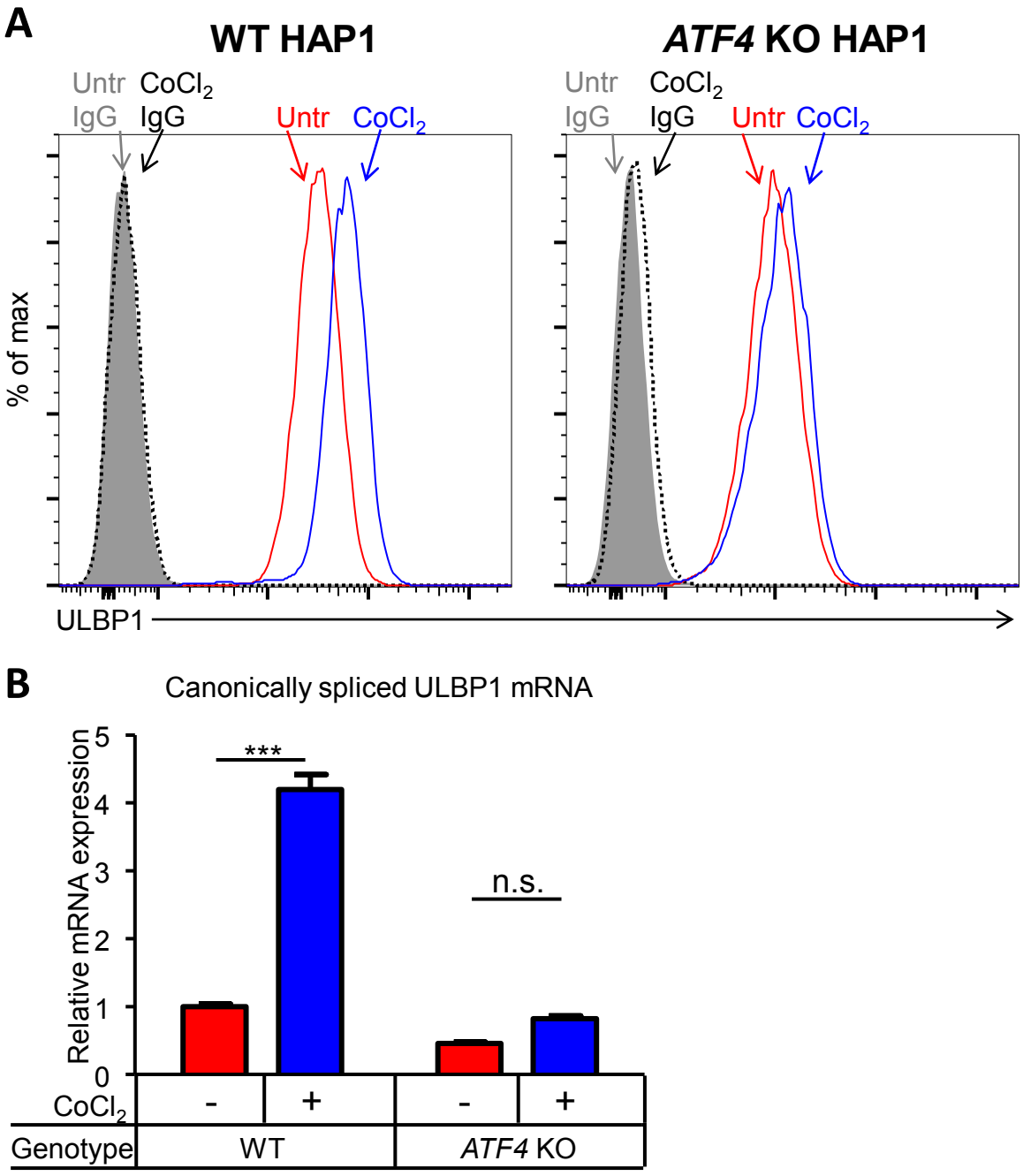

Figure 4-13: $CoCl_2$ treatment drives an ATF4-dependent increase in ULBP1 expression

A. WT and *ATF4* KO HAP1 cells were treated for 24 hours with 400 µM $CoCl_2$ and analyzed by flow cytometry. **B**. RT-qPCR analysis of *ULBP1* mRNA expression levels in cells treated as in Panel A. Expression levels were normalized to *ACTB*, *GAPDH*, and *HPRT1* and are shown as mean ±SE. The data were analyzed by 2-way ANOVA with Bonferroni's Multiple Comparisons Test. ****P*<0.001, n.s.: not significant. Panel A is representative of 2 independent experiments. Panel B is representative of 3 independent experiments

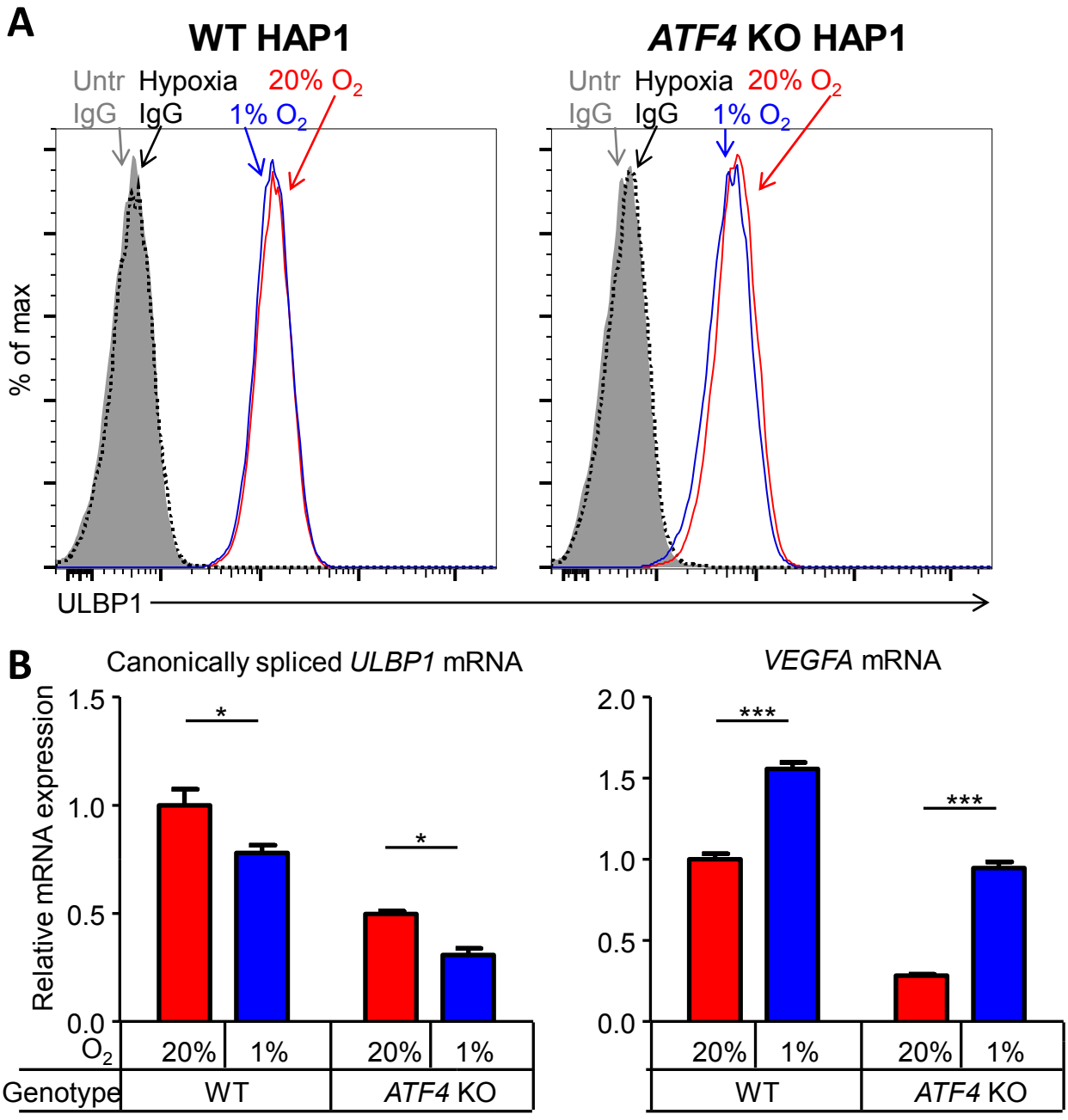

Figure 4-14: Hypoxia does not increase ULBP1 expression on HAP1 cells
A. WT and *ATF4* KO HAP1 cells were cultured for 24 hours in 20% or 1% O_2 and analyzed by flow cytometry. **B**. RT-qPCR analysis of *ULBP1* and VEGFA mRNA expression levels in cells treated as in Panel A. Expression levels were normalized to *ACTB*, *GAPDH*, and *HPRT1* and are shown as mean ±SE. The data were analyzed by 2-way ANOVA with Bonferroni's Multiple Comparisons Test. **P*<0.05 ,****P*<0.001. Data in this figure are from a single experiment.

Discussion

A key finding of this thesis was that ATF4, a mediator of several stress responses, transcriptionally activates *ULBP1*. We had previously considered the possibility that those stress responses regulate NKG2D ligands, but saw no effect because we focused on the wrong NKG2D ligands. The data show that ATF4 binds to two locations at the *ULBP1* locus and drives *ULBP1* transcription. No additional ATF4 binding or transcriptional induction was detected for most other NKG2D ligand genes, although *ULBP2* was modestly upregulated by histidinol treatment in a manner partially dependent on ATF4. Since ATF4 was not bound to the *ULBP2* promoter, we speculate that *ULBP2* transcription is regulated by a transcription factor that is induced by ATF4, or that ATF4 binding to the sites in the *ULBP1* gene modestly activates the neighboring *ULBP2* gene.

Disruption of ATF4 resulted in reduced ULBP1 expression under steady state conditions in all three of the tumor cell lines we studied. These data suggest that steady state activity of ATF4 in tumor cell lines, i.e. without purposeful infliction of stress, contributes to constitutive ULBP1 expression. Overexpression of unfolded protein response (UPR) components has been found in primary tumors and cell lines derived from breast cancers (Fernandez, Tabbara et al. 2000, Fujimoto, Onda et al. 2003), hepatocellular carcinomas (Shuda, Kondoh et al. 2003), and multiple myeloma (Reimold, Ponath et al. 1996, Munshi, Hideshima et al. 2004), a possible explanation for the steady state activity of ATF4 in cultured cell lines. In vivo, inadequate vascularization can cause tumors to become hypoxic and nutrient-starved, two conditions known to induce ATF4 expression. Previous studies have shown that ATF4 expression is frequently induced in primary tumors and tumor cell lines (Fernandez, Tabbara et al. 2000, Shuda, Kondoh et al. 2003, Ma and Hendershot 2004), and is highest in hypoxic regions of the tumor (Ameri, Lewis et al. 2004, Bi, Naczki et al. 2005). ATF4 could promote tumor cell survival in these cases by driving transcription of the angiogenic factor *VEGFA* and amino acid transporters (Jain 2005, Roybal, Hunsaker et al. 2005, Han, Back et al. 2013). However, ATF4 expression may therefore also serve as one of the danger signals used to alert the host to malignancy. By inducing *ULBP1* transcription, as well as apoptosis by intrinsic mechanisms (Tabas and Ron 2011), this stress pathway may also limit tumorigenesis.

The three tumor cell lines we examined illustrate the different ways that ATF4 can support steady-state ULBP1 expression in different contexts. In some cases, expression of ULBP1 may be entirely dependent on ATF4. This is the case in unstimulated K-562 cells, in which basal ULBP1 expression was detected (though weakly) in WT cells but was absent from the surface of *ATF4* KO cells. In other cases, exemplified by HAP1 and Jurkat cells, numerous factors contribute to ULBP1 expression, with ATF4 being only one of them. Those cells had higher basal ULBP1 expression than K562 cells and showed a modest decrease in ULBP1 expression when *ATF4* was mutated.

The impact of ATF4 on *ULBP1* transcription was most notable when additional stressors were applied that induce ATF4 expression. Outcomes at the level of protein expression are difficult to predict a priori, because these stressors induce transcription of ATF4 target genes, but also cause global suppression of translation as a result of eIF2α phosphorylation. We observed a range of outcomes in different cell lines. Amino acid starvation of K-562 cells, imparted by histidinol treatment, caused a substantial increase in *ULBP1* mRNA and surface protein, and the response was ablated in *ATF4* KO cells. In this case, the increase in *ULBP1* transcription overwhelmed the global decrease in translation. In contrast, in HAP1 and Jurkat cells, amino

acid starvation of WT cells caused a five- to seven-fold increase in *ULBP1* mRNA, but a much smaller increase in ULBP1 protein at the cell surface. Nevertheless, the impact of ATF4 was made apparent by the observation that ULBP1 protein levels *decreased* on the surface of similarly stressed *ATF4* KO cells. In these cell lines, therefore, the induction of *ULBP1* transcription by ATF4 serves to *maintain* (and slightly increase) expression of ULBP1 protein in the face of cellular stress. Maintaining ULBP1 expression that is induced by distinct regulatory pathways is important in cells where translational inhibition is likely to occur, such as in hypoxic tumors.

Although not explored in this study, induction of ULBP1 by ATF4 may also play a role in antiviral immunity. As mentioned above, ATF4 expression is induced by phosphorylation of eIF2α, and viral infection can activate PERK and PKR, which phosphorylate eIF2α and therefore induce ATF4 expression (Mohr and Sonenberg 2012, Jheng, Ho et al. 2014). Indeed, ATF4 upregulation has been observed when cultured cells are infected with infectious bronchitis virus (IBV) or human cytomegalovirus (HCMV) (Xuan, Qian et al. 2009, Liao, Fung et al. 2013). Certain viruses have evolved mechanisms to inhibit or reverse eIF2α phosphorylation, suggesting that viruses are under strong selective pressure to avoid activating this pathway (Mohr and Sonenberg 2012). The global inhibition of protein translation caused by eIF2α phosphorylation limits the synthesis of viral proteins, thus limiting viral replication, but increased ULBP1 expression (via ATF4) may serve as an additional host-defense mechanism by enabling immune cells to eliminate cells that support viral replication.

Regulation of *ULBP1* expression by ATF4 fits the existing paradigm for ATF4 target genes. ATF4 is induced by amino acid starvation, oxidative stress, hypoxia, and the unfolded protein response. ATF4 target genes include amino acid transporters, anti-oxidant response genes, angiogenic factors, and protein chaperones, and thus ATF4 initially promotes cell survival against these insults. However, the pro-apoptotic targets of ATF4, such as *CHOP*, provide an important safety mechanism for the host. Without a pro-apoptotic component, the transcriptional targets of ATF4 would be ripe for exploitation by an expanding, poorly vascularized, hypoxic, and starved tumor. Upregulation of ULBP1 by ATF4 provides an additional layer of host defense, marking potentially dangerous cells for elimination by the immune system.

Chapter 5
Regulation of *ULBP1* mRNA splicing by RBM4

Results

RBM4 is an RNA-binding protein that has been implicated in several steps of gene regulation, but has been most studied for its regulation of RNA splicing (Markus and Morris 2009). We compared WT and *RBM4* KO HAP1 cells by RNA-Seq to determine a potential role of RBM4 in splicing of *ULBP1* transcripts. As a result, we discovered a novel isoform of *ULBP1* that to our knowledge has not been previously reported (Figure 5-1). Analysis of sequence reads that aligned to splice junctions revealed that most transcripts in WT cells exhibited the expected splicing pattern to encode the normal ULBP1 protein (Figure 5-1). In *RBM4* KO cells, in contrast, approximately 60% of transcripts had undergone an alternative splicing event of the first and second exons, in which the 5′ splice site at the 3′ border of the first exon was ignored in favor of a 5′ splice site located 1.3 kb downstream within the first intron (Figure 5-1). Splicing of the downstream exons of *ULBP1* appeared normal in *RBM4* KO cells. The alternatively spliced transcripts in *RBM4* KO cells encode a premature stop codon shortly after the predicted ER signal peptide, and are unlikely to encode a functional protein fragment. We did not observe differential splicing of the other NKG2D ligands expressed by HAP1 cells (*ULBP2*, *ULBP3*, *MICA*, and *MICB;* Figures 5-2 and 5-3).

The alternative splicing of *ULBP1* transcripts in RBM4 KO cells was confirmed by RT-qPCR analysis (Figure 5-4). Canonically spliced *ULBP1* transcripts were less abundant in *RBM4* KO cells, while the alternatively spliced transcripts were more abundant; the overall abundance of *ULBP1* transcripts was unchanged as a result of RBM4-deficiency. The reduction in canonically spliced transcripts was commensurate with the reduction in cell surface ULBP1 protein, suggesting that RBM4 impacts cell surface expression of *ULBP1* primarily by facilitating the correct splicing of the first two exons of *ULBP1* transcripts.

RBM4 shares high amino acid similarity with a homolog, RBM4b (Lai, Kuo et al. 2003). The *RBM4* and *RBM4b* genes are adjacent to one another on chromosome 11 and are convergently transcribed, but expression of RBM4b protein is much more restricted than the ubiquitously expressed RBM4 (Pfuhl, Mamiani et al. 2008). We generated HAP1 cells lacking both *RBM4* and *RBM4b* using a sgRNA targeting a shared sequence in the coding region of both genes, resulting in a deletion of the 37 kb between the two target sites. *RBM4*/*RBM4b* double-KO cells showed identical ULBP1 expression as cells lacking *RBM4* alone, suggesting that RBM4b does not influence *ULBP1* RNA splicing in HAP1 cells (Figure 5-5). The absence of a role for RBM4b may reflect limited or no expression of RBM4b protein in HAP1 cells.

We extended our investigation of RBM4 function to a second cell line by simultaneously targeting the *RBM4* and *RBM4b* genes in K-562 cells. Interestingly, one *RBM4/RBM4b* KO clone showed an increase in ULBP1 staining compared to WT cells, while another KO clone was similar to WT (Figure 5-6). RT-qPCR showed no significant change in the expression of the canonical isoform of ULBP1, although the alternative isoform and total transcript were upregulated in both KO clones (Figure 5-6).

It is presently unclear why cell surface expression of ULBP1 was decreased upon RBM4 mutation in HAP1 cells, but no such change (or even an increase) occurred in K-562 cells. We speculate on possible reasons for this discrepancy at the end of this chapter. Importantly, our key finding—suppression of *ULBP1* alternative splicing by RBM4—was observed in both cell lines.

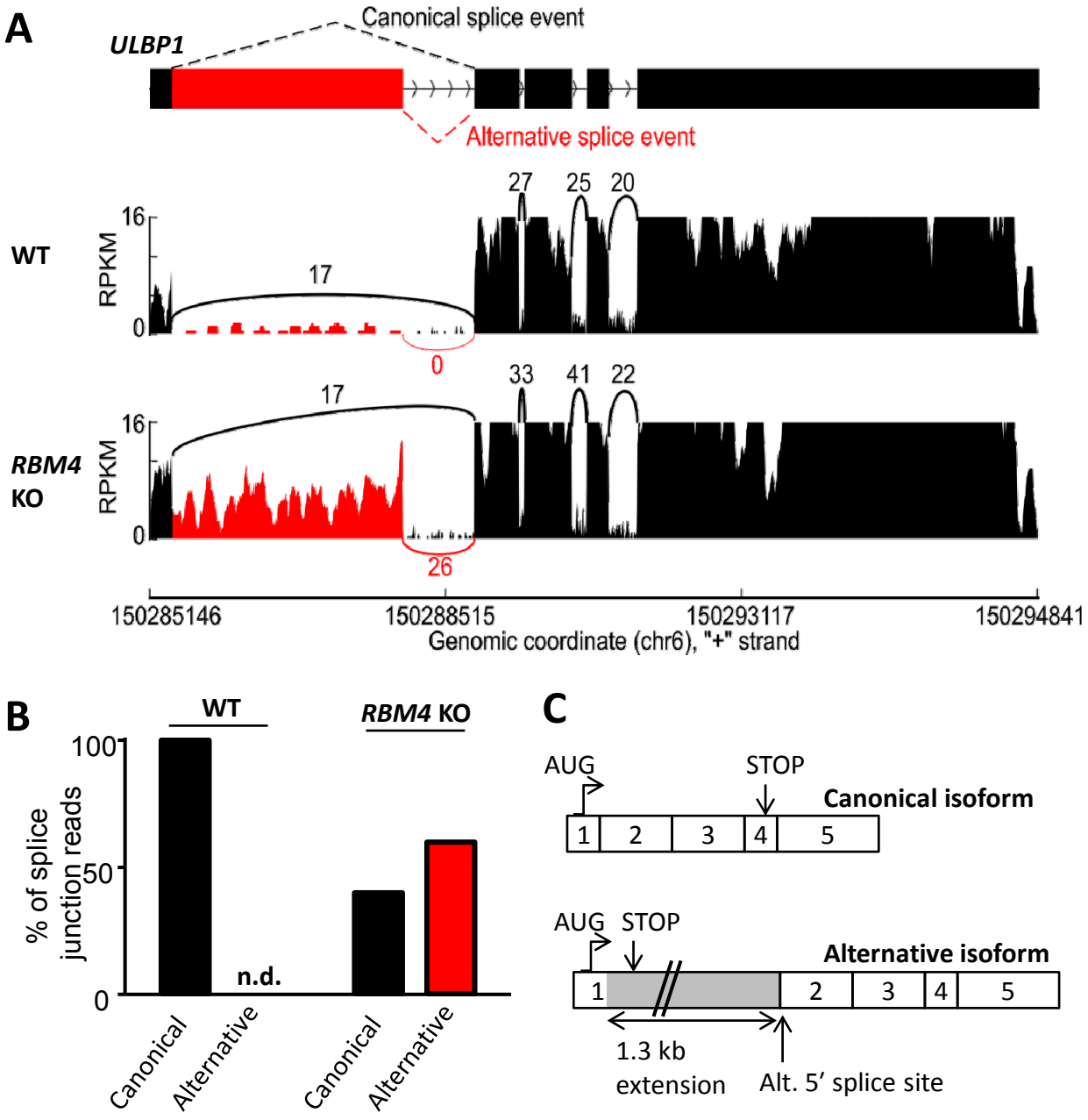

Figure 5-1: RNA-Seq reveals alternative splicing of *ULBP1* in *RBM4* KO HAP1 cells

A. RNA was isolated from WT and *RBM4* KO HAP1 cells and analyzed by RNA-Seq. Sashimi plots of reads mapping to *ULBP1* were generated with MISO. **B.** Quantification of splice junction-spanning reads mapping to canonical or alternatively spliced ULBP1 mRNA. Reads spanning the canonical or alternative splice junction are expressed as a percent of the total number of junction-spanning reads (canonical + alternative). n.d.: not detected. **C.** Diagram of the canonical and alternative isoforms of *ULBP1* mRNA.

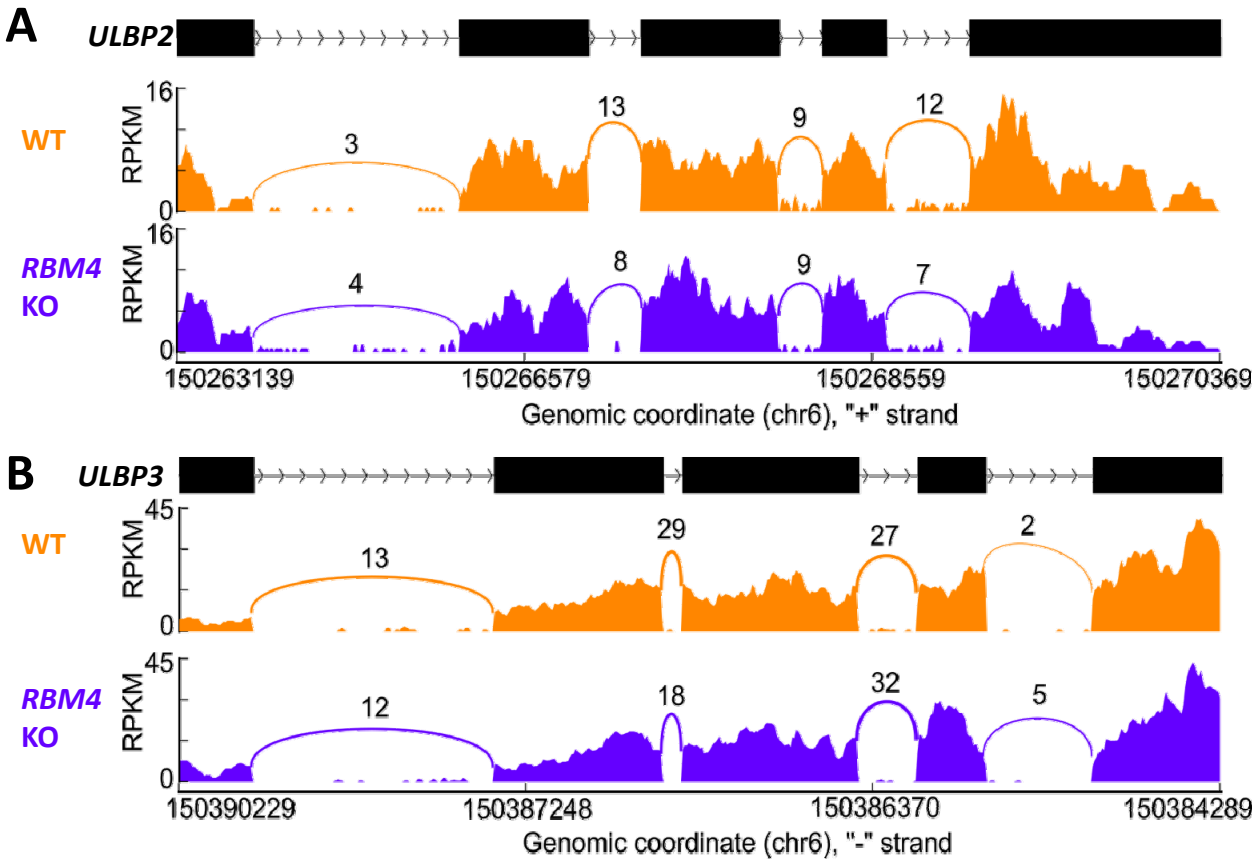

Figure 5-2: The splicing of mRNAs encoding *ULBP2* and *ULBP3* is unchanged in *RBM4* KO HAP1 cells

A,B. RNA was isolated from WT and *RBM4* KO HAP1 cells and analyzed by RNA-Seq. MISO was used to generate Sashimi plots of reads mapping to *ULBP2* (**A**) and *ULBP3* (**B**).

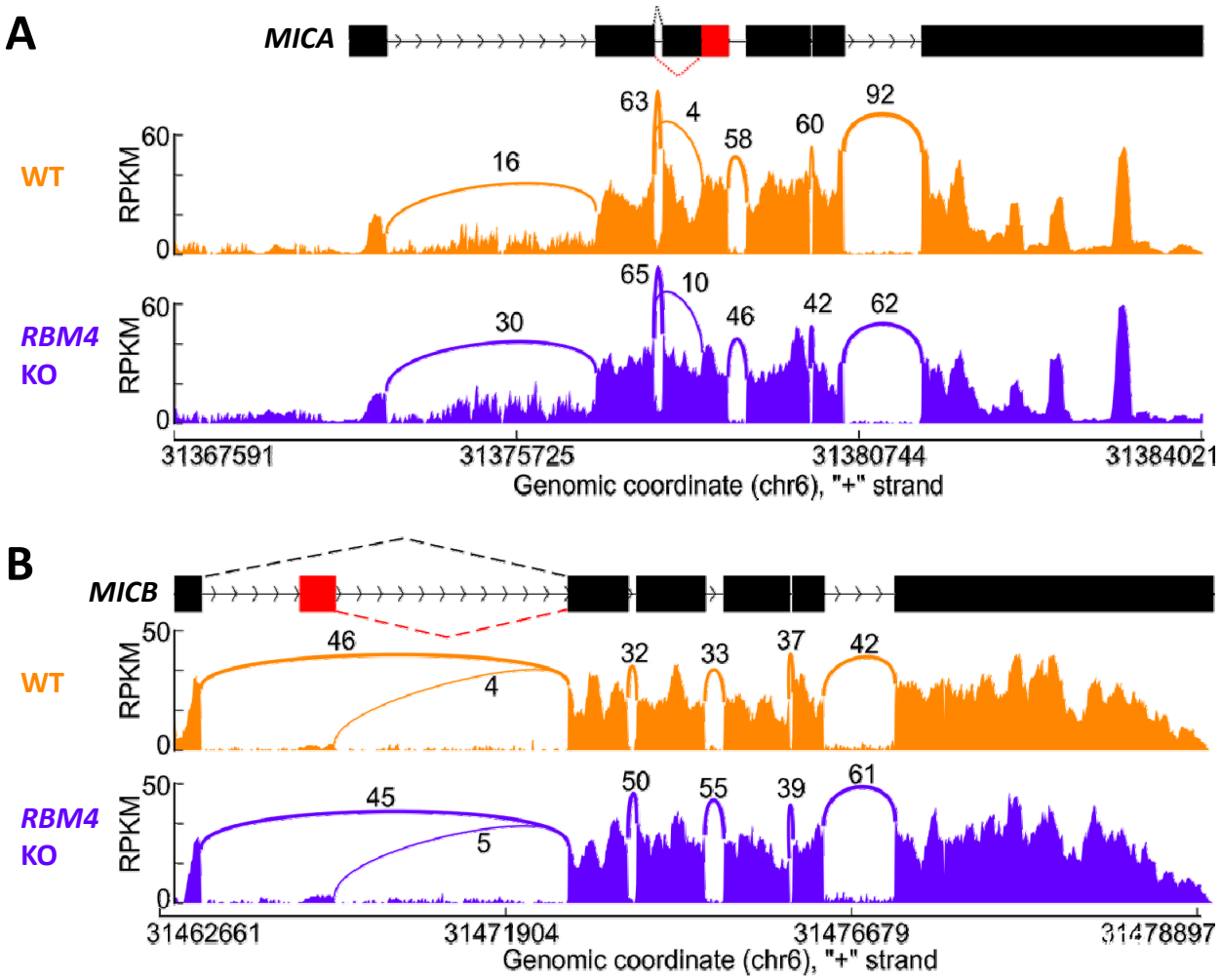

Figure 5-3: The splicing of mRNAs encoding *MICA* and *MICB* is unchanged in *RBM4* KO HAP1 cells

A,B. RNA was isolated from WT and *RBM4* KO HAP1 cells and analyzed by RNA-Seq. MISO was used to generate Sashimi plots of reads mapping to *MICA* (**A**) and *MICB* (**B**).

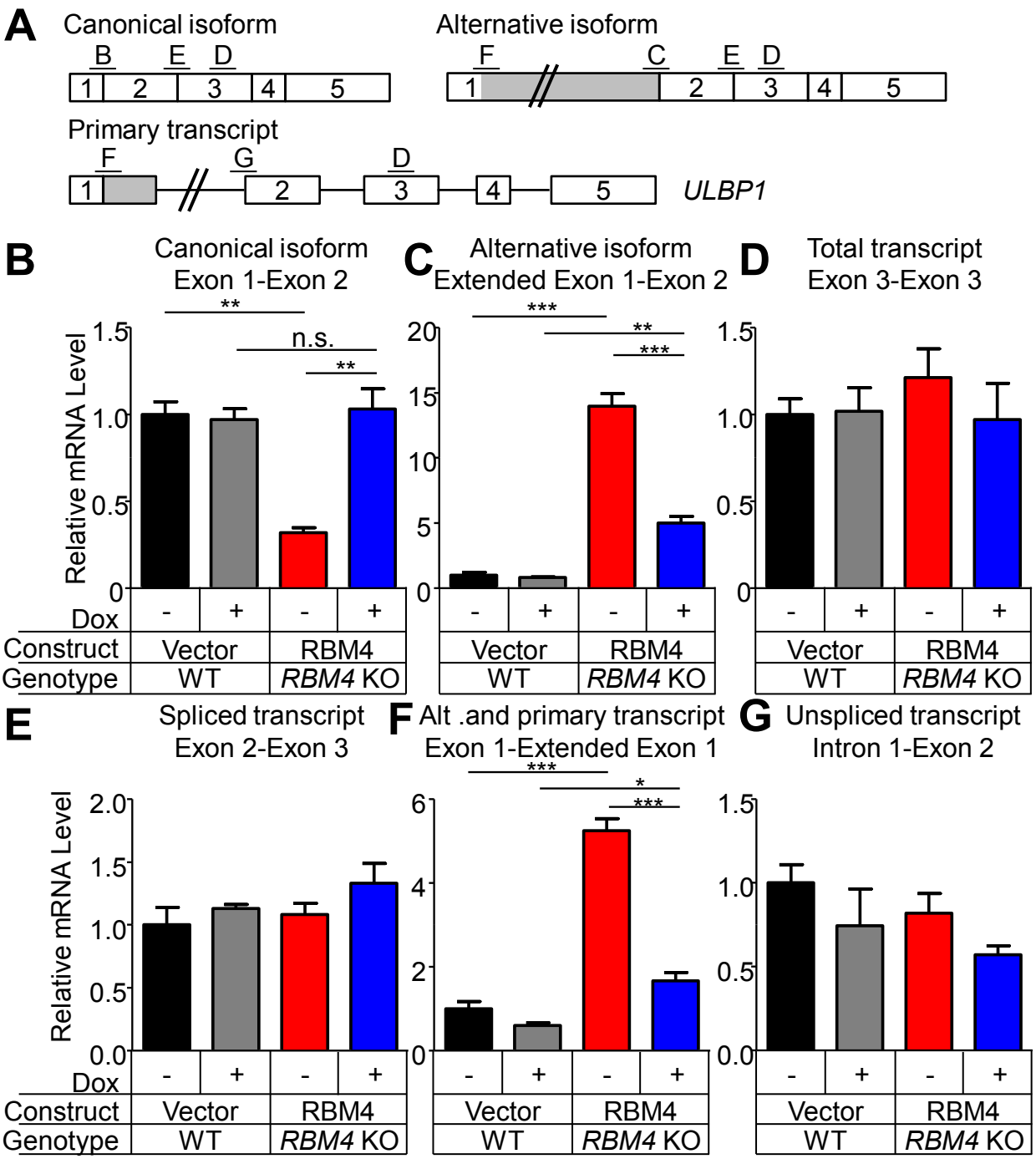

Figure 5-4: RT-qPCR analysis confirms RBM4 suppresses alternative splicing of *ULBP1* mRNA

A. Diagram of the canonical and alternatively spliced isoforms of the *ULBP1* mRNA and primary transcript. The PCR amplicons used in Panels B-G are noted. **B-G.** RT-qPCR analysis of *ULBP1* transcript levels in WT and *RBM4* KO HAP1 cells. Cells were transduced with a doxycycline-inducible RBM4 vector or control vector, and treated with 100 ng/mL Dox for 24 hours. The data were analyzed by 1-way ANOVA with Bonferroni's Multiple Comparisons Test and are representative of 3 independent experiments. **P*<0.05, ***P*<0.01, ****P*<0.001, n.s.: not significant. No differences were significant in Panels D, E, and G.

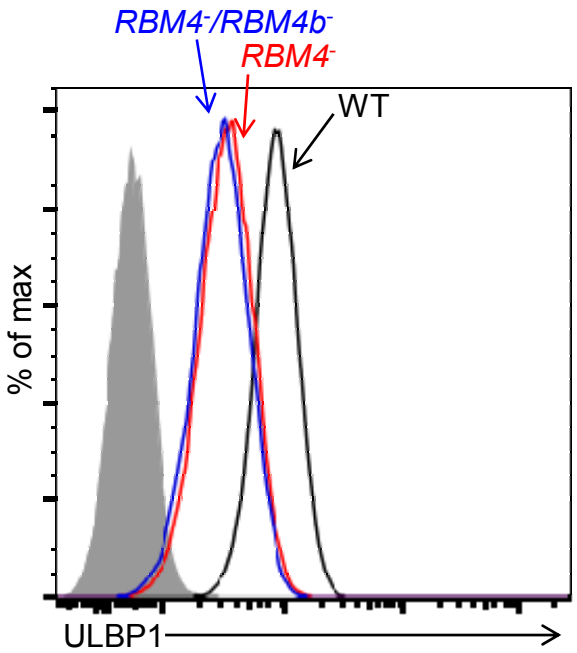

Figure 5-5: ULBP1 expression is identical on *RBM4* KO and *RBM4*/*RBM4*b double-KO HAP1 cells

ULBP1 expression on WT, RBM4 KO, and RBM4/RBM4b double-KO HAP1 cells was analyzed by flow cytometry. Data in this figure are representative of at least three independent experiments.

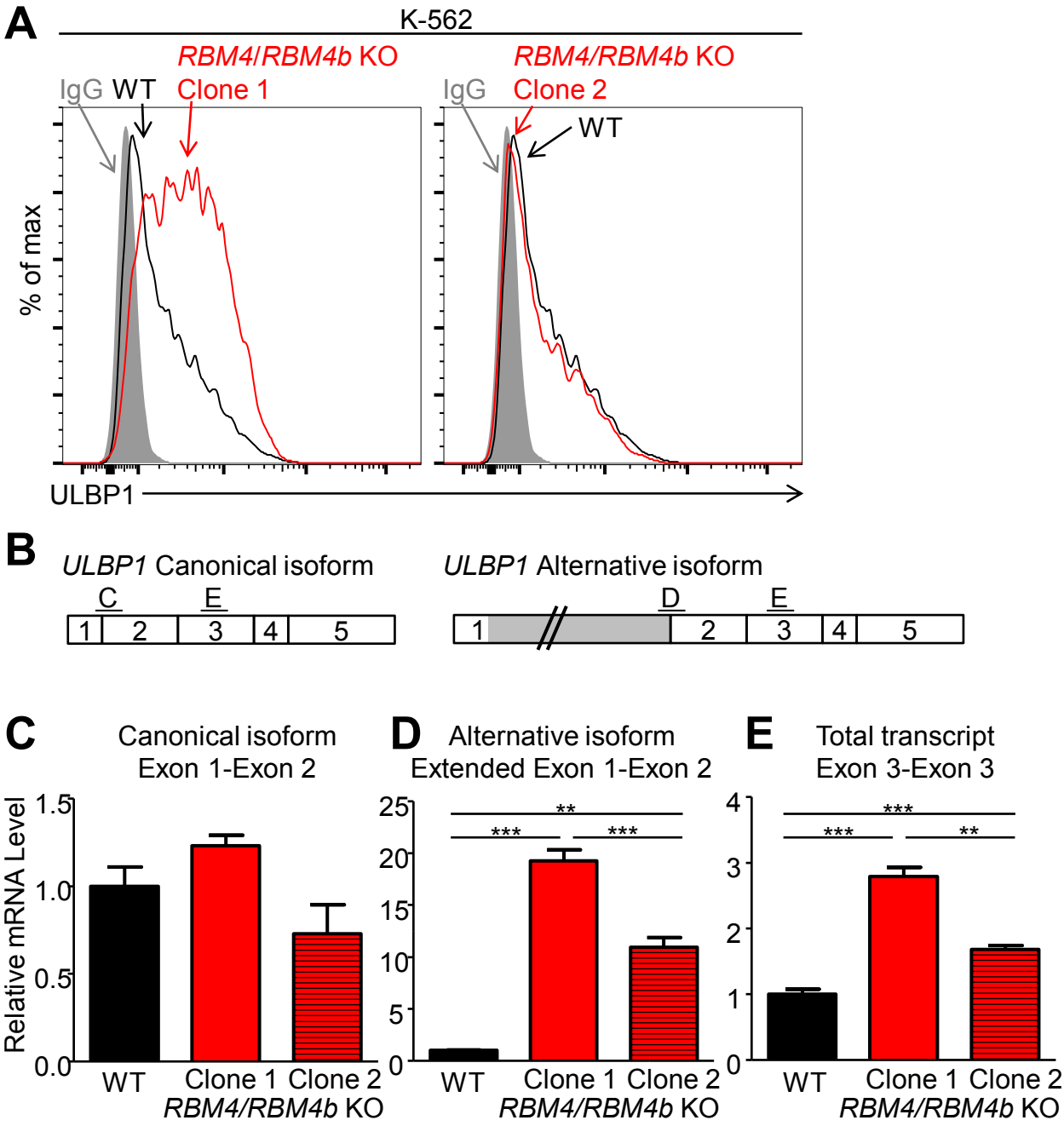

Figure 5-6: Effect of *RBM4*/*RBM4b* deletion in K-562 cells

A. Diagram of the canonical and alternatively spliced isoforms of the *ULBP1* mRNA. The PCR amplicons used in Panels C-E are noted. **C-E.** RT-qPCR analysis of *ULBP1* transcript levels in WT and *RBM4* KO HAP1 cells. Cells were transduced with a doxycycline-inducible RBM4 vector or control vector, and treated with 100 ng/mL Dox for 24 hours. The data were analyzed by 1-way ANOVA with Bonferroni's Multiple Comparisons Test and are representative of 3 independent experiments. **P*<0.05, ***P*<0.01, ****P*<0.001. No differences in Panel C were significant.

Discussion

We identified RBM4 as a second factor responsible for steady-state ULBP1 expression in HAP1 cells. RBM4-deficient HAP1 cells exhibited a 2-3 fold reduction in cell surface ULBP1 and corresponding spliced *ULBP1* mRNA. Interestingly, RBM4 suppresses a novel alternative splicing event in the *ULBP1* transcript. In the absence of RBM4, total *ULBP1* mRNA levels were unchanged, but the alternatively spliced isoform was upregulated while the canonically spliced isoform was downregulated. The alternative isoform of *ULBP1* mRNA contains a premature stop codon early in the protein coding sequence and is unlikely to produce a functional protein. RBM4 has also been implicated in other forms of gene regulation, including translation and miRNA-mediated gene silencing (Lin and Tarn 2009, Uniacke, Holterman et al. 2012). Although RBM4 primarily affects *ULBP1* splicing in HAP1 cells, it is possible it influences ULBP1 translation or gene expression in other cells.

A recent study found that RBM4 regulates the alternative splicing of numerous cancer-related genes. Most interesting, in light of our findings, was the finding based on RNA-Seq analysis that RBM4 expression promoted a tumor-suppressive splicing profile (Wang, Chen et al. 2014). This action occurred in part through the alternative splicing of the *BCL2-L1* gene (*Bcl-x*), wherein RBM4 promoted alternative splicing that generated transcripts encoding the pro-apoptotic isoform Bcl-xS, at the expense of the anti-apoptotic isoform Bcl-xL. Our data suggest that RBM4 further promotes cell death by favoring the canonical splicing of *ULBP1* mRNA, marking cells for elimination by the immune system. Decreased RBM4 expression has been observed in various cancers compared to paired healthy tissues, including lung, breast, and pancreatic cancers. Furthermore, lower RBM4 expression correlated with decreased patient survival (Wang, Chen et al. 2014). We speculate that tumor cells are under selective pressure to downregulate RBM4 expression, as this would allow tumors to evade cell-intrinsic and cell-extrinsic tumor suppressor mechanisms by alternative splicing of *Bcl-x* and *ULBP1*, respectively.

Although we have shown that RBM4 is important for supporting ULBP1 expression, it remains unclear whether the splicing functions of RBM4 are subject to stress-regulation or other forms of regulation. RBM4 is present in normal cells (Markus and Morris 2009) and favors functional expression of ULBP1. However, because ULBP1 gene expression is low or absent in normal cells, RBM4 expression is moot with respect to ULBP1 expression under these conditions. Interestingly, treatment with the oxidative stress agent arsenite, or activation of the $MKK_{3/6}$-p38 MAPK pathway, causes RBM4 phosphorylation and relocalization from the nucleus to the cytoplasm (Lin, Hsu et al. 2007), and it has been reported that this enables RBM4 to interact with mature mRNAs and influence translation (Lin and Tarn 2009, Uniacke, Holterman et al. 2012). By depleting RBM4 from the nucleus, however, it might also result in reduced canonical splicing of *ULBP1* transcripts. These considerations suggest the theoretical possibility that RBM4-directed splicing is regulated by stress pathways, but at present there is no direct evidence for this conclusion, nor do we understand why oxidative stress would be coupled to reduced functional expression of ULBP1.

RBM4 can regulate gene expression in numerous ways in addition to the regulation of alternative splicing (Markus and Morris 2009). RBM4 binds to miRNA:Ago2 complexes and is required for maximal silencing of some miRNA:Ago2 target transcripts (Hock, Weinmann et al. 2007, Lin and Tarn 2009). RBM4 cooperates with HIF2α to promote translation of select mRNAs during hypoxia (Uniacke, Holterman et al. 2012). The overall effect of RBM4 on the expression of a given gene may vary among different cell types. In HAP1 cells, loss of RBM4

appears to alter only the splicing of *ULBP1*, increasing levels of the alternative *ULBP1* isoform at the expense of the canonical, productive isoform. Although RBM4-deficiency in K-562 cells resulted in a similar relative shift in splicing isoforms, the amounts of total *ULBP1* transcripts were increased, and expression of the canonical isoform and cell surface protein were unchanged, or even increased. This suggests RBM4 expression exerts both positive and negative effects on ULBP1 expression in these cells.

A possible, though purely speculative, explanation for the difference between HAP1 and K-562 cells is regulation by miRNAs. If RBM4 guides the RISC to degrade *ULBP1* mRNA in K-562 cells, loss of RBM4 could increase total *ULBP1* mRNA levels. A sufficiently large increase in total *ULBP1* mRNA could yield a net increase in the productive *ULBP1* isoform, even if the RNA splicing pattern was skewed towards the non-productive alternative isoform. This mode of regulation might be absent from HAP1 cells, if, for example, the relevant miRNA is not expressed in those cells.

Our discovery of an alternatively spliced isoform of *ULBP1* mRNA has important consequences for future analysis of ULBP1 expression. Certain stress pathways may increase *ULBP1* transcription, but protein expression would not increase if the transcript is predominantly spliced as the alternative, non-functional isoform. The most informative assays for measuring *ULBP1* mRNA expression must be able to distinguish between the canonical and alternative isoforms. A study of airway epithelial cells showed a roughly 10-fold induction of total *ULBP1* mRNA in response to oxidative stress with hydrogen peroxide treatment, but ULBP1 expression at the cell surface was unchanged (Borchers, Harris et al. 2006). Our data offer a possible explanation for this discrepancy—oxidative stress can deplete RBM4 from the nucleus, which we predict would reduce the splicing of the productive *ULBP1* isoform.

Chapter 4
Generation of *Raet1* knockout mice

Introduction

Mice lacking one or more of the NKG2D ligands have long been desired as a tool by our lab and others for several reasons. Although not directly related to the main themes of this thesis, this chapter provides an account of my successful effort to use the CRISPR/Cas9 methodology to generate mice lacking two key NKG2D ligands, RAE-1ε and RAE-1δ. This chapter also summarizes the application of these mice to test a hypothesis concerning cellular regulation imparted by RAE-1 expression on host cells within tumors.

The issues that could be addressed with NKG2D ligand knockout mice include the following:

- Knockout mice are needed to definitively test the functions of NKG2D ligands.

- A proposed reason for the multitude of NKG2D ligands is the ability to regulate each one differently in response to various stress-induced signals or other signals. Or, the proteins themselves may function somewhat differently in terms of binding to NKG2D or even binding to some other partner. For example, is MULT1 specialized to protect mice against certain kinds of cancer and infections, while RAE-1 protects against others?

- Relatedly, in contexts where multiple NKG2D ligands are expressed, what is the relative contribution of each? NKG2D-deficiency causes early onset of lymphoma in the Eμ-Myc model, and tumors can express both RAE-1 and MULT1. Does one ligand contribute more than the other to the protective effect of NKG2D?

- During the course of my time in the lab, postdoctoral fellow Weiwen Deng developed correlative evidence that RAE-1 expression on myeloid cells may inhibit anti-tumor responses by NK cells (Deng, Gowen et al. 2015). Mice lacking RAE-1 would allow this proposition to be tested.

- A published report suggested that RAE-1 expression promotes cell proliferation in the subventricular zone of the brain, and the proposed function was NKG2D-independent (Popa, Cedile et al. 2011). Although RAE-1 expression was demonstrated, the evidence that it plays an important role in neuronal proliferation was not directly demonstrated. RAE-1-deficient mice would allow for definitive experiments.

- Staining of NKG2D ligands can be difficult, especially in ex vivo samples of cells such as macrophages or primary tumor cells. Mice or cells from them that lack expression of the NKG2D ligands serve as a definitive negative control for such analyses.

Despite the obvious utility of NKG2D ligand knockout mice, there were excellent reasons why such mice had not already been made by traditional gene targeting methods. C57BL/6 (B6) mice have five known NKG2D ligands. If the ligands have overlapping function, the phenotype of any single ligand knockout might be subtle or difficult to interpret. All of the NKG2D ligand genes in mice are linked on chromosome 10, so using the conventional approach to breed double-knockout mice with mutations in two ligand genes from single-knockout mice would require isolation of extremely rare recombinant mice in which a crossover occurred

between neighboring NKG2D ligand genes. Specifically, the genes *Raet1e*, *H60b*, and *Raet1d* (encoding RAE-1ε, H60b, and RAE-1δ, respectively), are located in a ~200 kb cluster. Because of the rarity of crossovers over such a short genetic interval, a RAE-1δ/RAE-1ε double-knockout mouse would almost certainly have required two rounds of gene targeting, and the failure rate for twice targeted embryonic stem cells is generally very high, because the cells differentiate when subjected to extensive handling. The homology between NKG2D ligand genes, especially *Raet1d* and *Raet1e*, would further complicate traditional gene targeting. For all of these reasons, the costs and difficulties of making NKG2D ligand knockout mice were deemed excessively high in light of the unknown payoff.

Generation of mutant mice, genotyping, and propagation of founders

The CRISPR/Cas9 system has revolutionized gene targeting. Injection of zygotes with Cas9 mRNA and guide RNAs against the gene(s) of interest can lead to highly efficient mutagenesis of multiple genes (Wang, Yang et al. 2013). Small insertions and deletions at Cas9 target sites produce mice with loss-of-function mutations in the target gene(s). DNA breaks also stimulate homology-directed repair, allowing loxP sites or reporter constructs to be "knocked in" if a repair template is co-injected (Yang, Wang et al. 2013). Furthermore, when two double-stranded breaks are introduced on the same chromosome, the entire intervening sequence can be deleted (Cong, Ran et al. 2013, Fujii, Kawasaki et al. 2013).

We took advantage of the CRISPR/Cas9 system to generate *Raet1* mutant mice. Owing to the homology between *Raet1d* and *Raet1e*, we were able to use a single sgRNA that targets a sequence common to the second coding exon of both genes. The genomic target sequence with protospacer-adjacent motif (PAM, underlined) was 5'-TAGGTGCAACTTGACCATCAAGG-3'. *Cas9* mRNA and the *Raet1* sgRNA were transcribed in vitro and injected into single-cell embryos as described (Wang, Yang et al. 2013). We believed that the targeted embryos were of pure B6 origin. Unfortunately, we later discovered the mice were on a predominantly B6 background, but with varying degrees of contamination from another strain, possibly CD1, due to a breeding mix-up in the transgenic facility. Injected embryos were implanted into pseudopregnant foster mothers, and at least 19 pups were born. At least three mice died in the first few days after birth, but this is not uncommon in our mouse colony. Sixteen mice survived to the time of weaning.

A note on goal-oriented genotyping

The goal of this project was to obtain useful *Raet1* knockout mice. The goal was *not* a comprehensive investigation of all mutations caused by CRISPR/Cas9 gene targeting. For this reason, complete genotyping of all mice was not performed. For example, PCR genotyping of two mice yielded no product for *Raet1e*. PCR products were obtained for *Raet1d* from these samples, ruling out the possibility that the genomic DNA prep was bad. It is possible that large insertions or deletions were present in the *Raet1e*, but not *Raet1d* cut sites in these mice, preventing amplification of the *Raet1e* locus under the PCR conditions used. The mutations present in these two mice were not investigated further because I had already identified mutant mice that would be of greater utility. Useful mice were bred, and all other founder mice were terminated. Tail issue from all founder mice was taken from all mice upon euthanasia and stored

at -20 °C in case the genetic events that occurred in the terminated strains become of interest in the future.

Mosaicism has been described in Cas9-targeted mice, suggesting that the DNA cleavage event often occurs after cleavage of the fertilized egg, in one of the daughter cells that contribute only a fraction of cells to the resulting embryo. Indeed mosaicism was detected in at least some of the *Raet1* mutant mice. The extent of mosaicism was not investigated. Where tested, almost all of the mutations found in the toe tissue of F_0 mutants were transmitted to F_1 offspring, but only a few of the F_0 mice were actually bred. Genotyping of F_1 mice was aimed at identifying mice with specific mutations that we hoped to propagate.

Genotyping results

Figure 6-1 shows a map of the *Raet1* locus with primer binding sites and genotyping workflow. Genotyping was performed with genomic DNA extracted from toe samples of 1 week-old pups. PCR was performed to amplify ~400 bp regions surrounding the Cas9 target sites in *Raet1d* and *Raet1e*. PCR with primers H and I was performed to amplify fusions of *Raet1d* and *Raet1e* that resulted from deletion of the intervening 190 kb. PCR products were directly sequenced or ligated into the vector pGEM-T Easy, followed by sequencing of plasmid clones.

Table 6-1 summarizes the mutations found in F_0 mice. Out of 16 mice born, 14 carried mutations. We were surprised to find that almost all mutations were biallelic and contained mutations in both *Raet1e* and *Raet1d*. Of the 14 mice carrying any mutation, a WT copy of *Raet1e* or *Raet1d* was only found in one mouse. Mice with mutant *Raet1e* but WT *Raet1d*, or vice versa, were not found. Eight of the 14 mice carried at least one allele where the sequence between the two Cas9 target sites had been deleted, effectively knocking out *Raet1d*, *Raet1e*, and *H60b*.

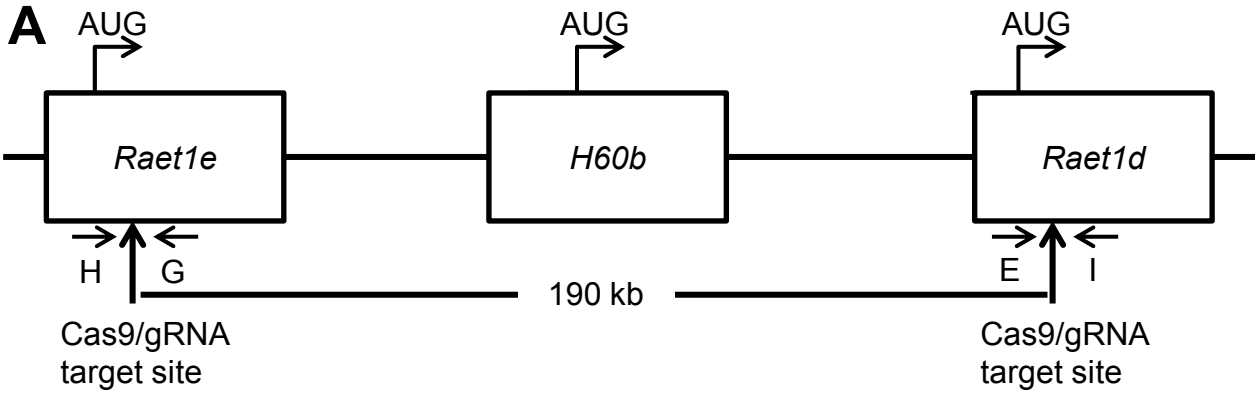

B

Primer pair	Detects
H+G	*Raet1e*
E+I	*Raet1d*
H+I	190 kb deletion

C

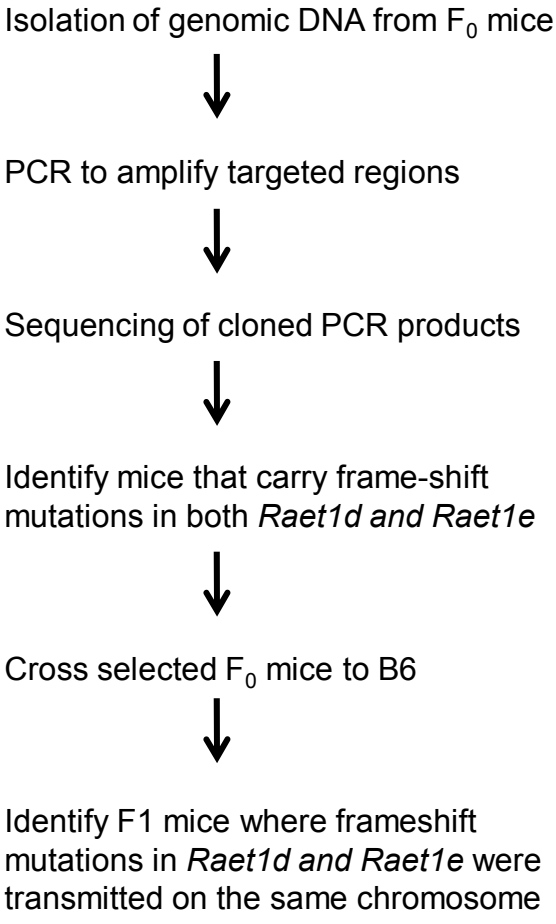

Figure 6-1: Identification of *Raet1* mutant mice
A. Simplified diagram of the *Raet1e-H60b-Raet1d* locus. Translation initiation sites, Cas9/gRNA target sites, and genotyping PCR primers are indicated. For simplicity, the complex exon structure of the genes is not depicted. The diagram is not drawn to scale. **B.** Targets of genotyping PCR primers. **C.** Outline of genotyping and breeding workflow.

Mouse number	*Raet1d* Alleles	*Raet1e* Alleles	Deletion of intervening sequence
1	-3	-4	2 deletion alleles present
2	-11 Net -28 (-33,+5)	-3 Net -11 (-16,+5)	No PCR product
*3	+2 -1	-10	-10 -18
4	WT	WT	Deletion present with multiple point mutations
5	-3 -15	Net +3 (+4,-1) -65	No PCR product
*6	-3 Net -47 (-54,+7)	-1 -3	No PCR product
7	-4 Not sequenced	-7	No PCR product
8	WT	WT	No PCR product
9	WT	WT	No PCR product
*10	+1 -4 -19	-1	Deletion present with multiple point mutations
11	Net -7 (-9,+2)	No PCR product	-17
12	-1	-3 -1	No PCR product
12	-9	-19	No PCR product
14	-12	Net -4 (-6,+2)	-12
15	-3 -29	-9	-3
16	-17	No PCR product	-12

Table 6-1: *Raet1* mutations found in CRISPR/Cas9-targeted mice
Raet1 alleles identified in F_0 mice. Numbers indicate the number of bases inserted or deleted. In the case of large deletions between the Cas9 cut sites, numbers indicate the number of additional bases deleted beyond the cut sites. Additional alleles were present that were not amplified by the PCR conditions used. Asterisks indicate mice used as founders.

Propagation of founder lines

The offspring of three founder mice were chosen for propagation. One line carried a 1 bp insertion in *Raet1d* and a 1 bp deletion in *Raet1e*. The frameshift mutations early in the coding sequences of both genes created effective *Raet1d*/*Raet1e* double-knockout mice. These mice were later discontinued due to the difficulty of genotyping mice with such small mutations. The second line carried a 1 bp insertion in *Raet1e* and a 47 bp net deletion in *Raet1d* (the result of a 54 bp deletion and 7 bp insertion). This line is the "*Raet1*$^{-/-}$" line established for continued use. The 47 bp net deletion in *Raet1d* is much easier to genotype, and the close linkage between *Raet1d* and *Raet1e* precludes the need for routine genotyping of the 1 bp insertion in *Raet1e*. In the third line, the segment of 190 kb between the two Cas9 cut sites (plus an additional 10 bp) was deleted. Preliminary experiments showed these mice to be phenotypically similar to the simple *Raet1*$^{-/-}$ mice. Although these mice also lacked *H60b*, they were discontinued due to concerns about other potential genes or regulatory elements that might also be present in the deleted region. Several non-coding RNAs of unknown function are annotated within the deleted region.

All homozygous *Raet1* mutant mice were grossly phenotypically normal. No obvious defects in development were present. Pups from heterozygous crosses appear to be born at the expected Mendelian ratio, although a small bias against homozygous mutants could have escaped our notice.

Back-crossing

Any strain of mouse can be targeted using CRISPR/Cas9 mutagenesis. Traditional gene targeting, in contrast, is limited to the 129 and B6 mouse strains. Because the efficiency of gene targeting and germline transmission of targeted ES cells is higher in the 129 strain, many knockout mice were generated in 129 ES cells and the knockout allele was later backcrossed onto the B6 genetic background. By making targeted mutations in B6 embryos, laborious and time-consuming back-crossing can be avoided. Generating pure B6 gene targeted mice is inefficient, however. Using CRISPR/Cas9 we can generate mutant mice with high efficiency in B6 mice or other strains as well. Furthermore, off-target mutation rates in Cas9-targeted mice are reportedly low, reducing the need to back-cross to remove off-target mutations.

Although back-crossing might not strictly have been necessary, we began a few generations of back-crossing of the *Raet1*$^{-/-}$ mice out of an abundance of caution. Unfortunately, SNP analysis of tissue from F_0 mice showed 4 clusters of genetic contamination from a non-B6 strain (probably CD-1, based on knowledge of the strains being used in the facility). The contamination was the result of interbreeding of mouse strains several generations prior to the targeting of single-cell embryos. Luckily only a few generations of back-crossing were required to breed out the contamination, and our colony of *Raet1*$^{-/-}$ mice now appears to have a completely B6 background.

Discussion

As mentioned above, post-doctoral fellow Weiwen Deng recently developed correlative evidence that RAE-1 expression on myeloid cells may inhibit anti-tumor responses by NK cells. Staining analyses suggested that the myeloid cells express both RAE-1ε and RAE-1δ. Dr. Deng used the double mutant *Raet1d*$^{-/-}$ *Raet1e*$^{-/-}$ mice to test this model (Deng, Gowen et al. 2015). She found that compared to WT mice, NK cells from *Raet1d*$^{-/-}$ *Raet1e*$^{-/-}$ mice had higher expression of NKG2D and were more responsive to stimulation through NKG2D and other activating receptors. She independently observed that a soluble form of the NKG2D ligand MULT1 promoted tumor rejection by NK cells. Her data suggest that the anti-tumor effect of soluble MULT1 is at least in part due to the ability of soluble MULT1 to block interactions between NKG2D on NK cells and RAE-1 on other cells.

Raet1d$^{-/-}$ *Raet1e*$^{-/-}$mice will continue to be valuable research tools for the Raulet lab. Current graduate student Thornton Thompson is studying the expression of RAE-1 on tumor cells and on peritoneal and tumor-associated macrophages and monocytes. He is using *Raet1d*$^{-/-}$ *Raet1e*$^{-/-}$ mice to test the functional consequences of RAE-1 expression by these cells. In the coming months, fertilized eggs from *Raet1d*$^{-/-}$ *Raet1e*$^{-/-}$ mice will be targeted with the CRISPR/Cas9 system to generated mice lacking all known NKG2D ligands.

Chapter 7
Conclusion

The drivers of ULBP1 expression we have identified are likely to cooperate with previously described stress pathways that regulate ULBP1. Other transcription factors that bind the *ULBP1* gene and drive gene expression include Sp1, Sp3, and the tumor suppressor p53 (though p53 does not bind in the promoter of the gene (Lopez-Soto, Quinones-Lombrana et al. 2006, Textor, Fiegler et al. 2011). It is possible that one or more of these factors are responsible for basal transcription of *ULBP1* we observed in *ATF4* KO cells. Additional stress pathways including heat shock, proliferation, and the DNA damage response drive expression of other NKG2D ligands, and the combined expression level of all the NKG2D ligands on a given cell will contribute to its ability to activate NK cells (Gasser, Orsulic et al. 2005, Venkataraman, Suciu et al. 2007, Jung, Hsiung et al. 2012).

The layers of ULBP1 regulation we have described could allow NKG2D ligand expression to be fine-tuned to reflect the "threat level" of the cell. Maximal ULBP1 expression requires transcription of the *ULBP1* gene, splicing of the functional mRNA isoform, and translation and trafficking of the protein to the cell surface. ATF4 could upregulate *ULBP1* transcription, but other factors may amplify the extent of ULBP1 transcription, and maximal cell surface expression would also require RBM4 to direct splicing of the functional isoform. HSPA13 may regulate the protein post-translationally. Ubiquitous RBM4 expression is "safe" for normal, healthy cells, since functional *ULBP1* cannot be spliced unless the gene is transcribed in the first place.

Additional layers of regulation are imparted by the existence of multiple NKG2D ligands. The different ligands may play specialized roles in specific cell types or in response to certain forms of cell stress. In support of this hypothesis, postdoctoral fellow Weiwen Deng showed that a soluble form of MULT promotes NK cell activation and tumor elimination (Deng, Gowen et al. 2015). Soluble MULT1 blocked suppressive interactions between NKG2D and RAE-1 expressed by tumor-associated myeloid cells. Using *Raet1* KO mice that I generated, Deng showed that RAE-1 molecules play a role in immunosuppression in the tumor environment. This result highlights the concept that different NKG2D ligands play distinct roles. In the future, mice will be generated that lack other NKG2D ligands (e.g. MULT1 or H60c), or that lack NKG2D ligands altogether.

The mouse tumor cell lines B16 and RMA-S are frequently used in our lab and others. These cell lines are useful for many reasons, one of which is their complete lack of NKG2D ligand expression. This makes B16 and RMA-S somewhat unique among tumor cell lines, which frequently express one or more NKG2D ligands. The CRISPR/Cas9 system gives us the ability to knock out multiple NKG2D ligands in almost any cell line, expanding the catalog of tumor models that can be used in experiments where NKG2D ligand expression is undesirable.

The results of our screen highlight diverse mechanisms for the control of NKG2D ligand expression. To the best of our knowledge, none of the hits we investigated are related to previously known drivers of ULBP1 or other NKG2D ligands. The effects found were primarily specific to ULBP1, as expression levels of MICA, MICB, ULBP2, and ULBP3 expression were maintained in all of our mutants. Screens for drivers of other NKG2D ligands will be the subject of future work, and the advent of CRISPR/Cas9-based screens allow for the screening of many additional cell lines (Gilbert, Horlbeck et al. 2014, Shalem, Sanjana et al. 2014, Wang, Wei et al. 2014). The advent of these powerful screens and ultra-efficient gene targeting methodologies will greatly accelerate progress in all areas of biology.

References

Ameri, K., C. E. Lewis, M. Raida, H. Sowter, T. Hai and A. L. Harris (2004). "Anoxic induction of ATF-4 through HIF-1-independent pathways of protein stabilization in human cancer cells." Blood **103**(5): 1876-1882. doi: 10.1182/blood-2003-06-1859.

Andersson, B. S., M. Beran, S. Pathak, A. Goodacre, B. Barlogie and K. B. McCredie (1987). "Ph-positive chronic myeloid leukemia with near-haploid conversion in vivo and establishment of a continuously growing cell line with similar cytogenetic pattern." Cancer Genet Cytogenet **24**(2): 335-343. doi:

Andresen, L., S. L. Skovbakke, G. Persson, M. Hagemann-Jensen, K. A. Hansen, H. Jensen and S. Skov (2012). "2-deoxy D-glucose prevents cell surface expression of NKG2D ligands through inhibition of N-linked glycosylation." J Immunol **188**(4): 1847-1855. doi: 10.4049/jimmunol.1004085.

Appenzeller-Herzog, C. and M. N. Hall (2012). "Bidirectional crosstalk between endoplasmic reticulum stress and mTOR signaling." Trends Cell Biol **22**(5): 274-282. doi: 10.1016/j.tcb.2012.02.006.

Ardolino, M., A. Zingoni, C. Cerboni, F. Cecere, A. Soriani, M. L. Iannitto and A. Santoni (2011). "DNAM-1 ligand expression on Ag-stimulated T lymphocytes is mediated by ROS-dependent activation of DNA-damage response: relevance for NK-T cell interaction." Blood **117**(18): 4778-4786. doi: 10.1182/blood-2010-08-300954.

Ashkar, A. A., S. Reid, E. F. Verdu, K. Zhang and B. K. Coombes (2009). "Interleukin-15 and NK1.1+ cells provide innate protection against acute Salmonella enterica serovar Typhimurium infection in the gut and in systemic tissues." Infect Immun **77**(1): 214-222. doi: 10.1128/IAI.01066-08.

Bae, J. S., N. Y. Koo, E. Namkoong, A. J. Davies, S. K. Choi, Y. Shin, M. Jin, S. M. Hwang, K. Mikoshiba and K. Park (2013). "Chaperone stress 70 protein (STCH) binds and regulates two acid/base transporters NBCe1-B and NHE1." J Biol Chem **288**(9): 6295-6305. doi: 10.1074/jbc.M112.392001.

Bartkova, J., Z. Horejsi, K. Koed, A. Kramer, F. Tort, K. Zieger, P. Guldberg, M. Sehested, J. M. Nesland, C. Lukas, T. Orntoft, J. Lukas and J. Bartek (2005). "DNA damage response as a candidate anti-cancer barrier in early human tumorigenesis." Nature **434**(7035): 864-870. doi: 10.1038/nature03482.

Bi, M., C. Naczki, M. Koritzinsky, D. Fels, J. Blais, N. Hu, H. Harding, I. Novoa, M. Varia, J. Raleigh, D. Scheuner, R. J. Kaufman, J. Bell, D. Ron, B. G. Wouters and C. Koumenis (2005). "ER stress-regulated translation increases tolerance to extreme hypoxia and promotes tumor growth." EMBO J **24**(19): 3470-3481. doi: 10.1038/sj.emboj.7600777.

Blais, J. D., V. Filipenko, M. Bi, H. P. Harding, D. Ron, C. Koumenis, B. G. Wouters and J. C. Bell (2004). "Activating transcription factor 4 is translationally regulated by hypoxic stress." Mol Cell Biol **24**(17): 7469-7482. doi: 10.1128/MCB.24.17.7469-7482.2004.

Borchers, M. T., N. L. Harris, S. C. Wesselkamper, M. Vitucci and D. Cosman (2006). "NKG2D ligands are expressed on stressed human airway epithelial cells." Am J Physiol Lung Cell Mol Physiol **291**(2): L222-231. doi: 10.1152/ajplung.00327.2005.

Butler, J. E., M. B. Moore, S. R. Presnell, H. W. Chan, N. J. Chalupny and C. T. Lutz (2009). "Proteasome regulation of ULBP1 transcription." J Immunol **182**(10): 6600-6609. doi: 10.4049/jimmunol.0801214.

Cabibbo, A., M. Pagani, M. Fabbri, M. Rocchi, M. R. Farmery, N. J. Bulleid and R. Sitia (2000). "ERO1-L, a human protein that favors disulfide bond formation in the endoplasmic reticulum." J Biol Chem **275**(7): 4827-4833. doi:

Carette, J. E., C. P. Guimaraes, M. Varadarajan, A. S. Park, I. Wuethrich, A. Godarova, M. Kotecki, B. H. Cochran, E. Spooner, H. L. Ploegh and T. R. Brummelkamp (2009). "Haploid genetic screens in human cells identify host factors used by pathogens." Science **326**(5957): 1231-1235. doi: 10.1126/science.1178955.

Carette, J. E., C. P. Guimaraes, I. Wuethrich, V. A. Blomen, M. Varadarajan, C. Sun, G. Bell, B. Yuan, M. K. Muellner, S. M. Nijman, H. L. Ploegh and T. R. Brummelkamp (2011). "Global gene disruption in human cells to assign genes to phenotypes by deep sequencing." Nat Biotechnol **29**(6): 542-546. doi: 10.1038/nbt.1857.

Carette, J. E., M. Raaben, A. C. Wong, A. S. Herbert, G. Obernosterer, N. Mulherkar, A. I. Kuehne, P. J. Kranzusch, A. M. Griffin, G. Ruthel, P. Dal Cin, J. M. Dye, S. P. Whelan, K. Chandran and T. R. Brummelkamp (2011). "Ebola virus entry requires the cholesterol transporter Niemann-Pick C1." Nature **477**(7364): 340-343. doi: 10.1038/nature10348.

Carreau, A., B. El Hafny-Rahbi, A. Matejuk, C. Grillon and C. Kieda (2011). "Why is the partial oxygen pressure of human tissues a crucial parameter? Small molecules and hypoxia." J Cell Mol Med **15**(6): 1239-1253. doi: 10.1111/j.1582-4934.2011.01258.x.

Chen, H., Y. X. Pan, E. E. Dudenhausen and M. S. Kilberg (2004). "Amino acid deprivation induces the transcription rate of the human asparagine synthetase gene through a timed program of expression and promoter binding of nutrient-responsive basic region/leucine zipper transcription factors as well as localized histone acetylation." J Biol Chem **279**(49): 50829-50839. doi: 10.1074/jbc.M409173200.

Chung, S., Z. Zhou, K. A. Huddleston, D. A. Harrison, R. Reed, T. A. Coleman and B. C. Rymond (2002). "Crooked neck is a component of the human spliceosome and implicated in the splicing process." Biochim Biophys Acta **1576**(3): 287-297. doi:

Cimprich, K. A. and D. Cortez (2008). "ATR: an essential regulator of genome integrity." Nat Rev Mol Cell Biol **9**(8): 616-627. doi: 10.1038/nrm2450.

Cong, L., F. A. Ran, D. Cox, S. Lin, R. Barretto, N. Habib, P. D. Hsu, X. Wu, W. Jiang, L. A. Marraffini and F. Zhang (2013). "Multiplex genome engineering using CRISPR/Cas systems." Science **339**(6121): 819-823. doi: 10.1126/science.1231143.

Croxford, J. L., M. L. Tang, M. F. Pan, C. W. Huang, N. Kamran, C. M. Phua, W. J. Chng, S. B. Ng, D. H. Raulet and S. Gasser (2013). "ATM-dependent spontaneous regression of early Emu-myc-induced murine B-cell leukemia depends on natural killer and T cells." Blood **121**(13): 2512-2521. doi: 10.1182/blood-2012-08-449025.

Deng, W., B. G. Gowen, L. Zhang, L. Wang, S. Lau, A. Iannello, J. Xu, T. L. Rovis, N. Xiong and D. H. Raulet (2015). "A shed NKG2D ligand that promotes natural killer cell activation and tumor rejection." Science. doi: 10.1126/science.1258867.

Diefenbach, A., E. R. Jensen, A. M. Jamieson and D. H. Raulet (2001). "Rae1 and H60 ligands of the NKG2D receptor stimulate tumour immunity." Nature **413**(6852): 165-171. doi: 10.1038/35093109.

Diefenbach, A., E. Tomasello, M. Lucas, A. M. Jamieson, J. K. Hsia, E. Vivier and D. H. Raulet (2002). "Selective associations with signaling proteins determine stimulatory versus costimulatory activity of NKG2D." Nat Immunol **3**(12): 1142-1149. doi: 10.1038/ni858.

Dong, J., H. Qiu, M. Garcia-Barrio, J. Anderson and A. G. Hinnebusch (2000). "Uncharged tRNA activates GCN2 by displacing the protein kinase moiety from a bipartite tRNA-binding domain." Mol Cell **6**(2): 269-279. doi:

Fang, H., S. Panzner, C. Mullins, E. Hartmann and N. Green (1996). "The homologue of mammalian SPC12 is important for efficient signal peptidase activity in Saccharomyces cerevisiae." J Biol Chem **271**(28): 16460-16465. doi:

Fernandez, P. M., S. O. Tabbara, L. K. Jacobs, F. C. Manning, T. N. Tsangaris, A. M. Schwartz, K. A. Kennedy and S. R. Patierno (2000). "Overexpression of the glucose-regulated stress gene GRP78 in malignant but not benign human breast lesions." Breast Cancer Res Treat **59**(1): 15-26. doi:

Fujii, W., K. Kawasaki, K. Sugiura and K. Naito (2013). "Efficient generation of large-scale genome-modified mice using gRNA and CAS9 endonuclease." Nucleic Acids Res **41**(20): e187. doi: 10.1093/nar/gkt772.

Fujimoto, T., M. Onda, H. Nagai, T. Nagahata, K. Ogawa and M. Emi (2003). "Upregulation and overexpression of human X-box binding protein 1 (hXBP-1) gene in primary breast cancers." Breast Cancer **10**(4): 301-306. doi:

Gasser, S., S. Orsulic, E. J. Brown and D. H. Raulet (2005). "The DNA damage pathway regulates innate immune system ligands of the NKG2D receptor." Nature **436**(7054): 1186-1190. doi: 10.1038/nature03884.

Gasser, S. and D. H. Raulet (2006). "Activation and self-tolerance of natural killer cells." Immunol Rev **214**: 130-142. doi: 10.1111/j.1600-065X.2006.00460.x.

Gilbert, L. A., M. A. Horlbeck, B. Adamson, J. E. Villalta, Y. Chen, E. H. Whitehead, C. Guimaraes, B. Panning, H. L. Ploegh, M. C. Bassik, L. S. Qi, M. Kampmann and J. S. Weissman (2014). "Genome-Scale CRISPR-Mediated Control of Gene Repression and Activation." Cell **159**(3): 647-661. doi: 10.1016/j.cell.2014.09.029.

Gorgoulis, V. G., L. V. Vassiliou, P. Karakaidos, P. Zacharatos, A. Kotsinas, T. Liloglou, M. Venere, R. A. Ditullio, Jr., N. G. Kastrinakis, B. Levy, D. Kletsas, A. Yoneta, M. Herlyn, C. Kittas and T. D. Halazonetis (2005). "Activation of the DNA damage checkpoint and genomic instability in human precancerous lesions." Nature **434**(7035): 907-913. doi: 10.1038/nature03485.

Guerra, N., Y. X. Tan, N. T. Joncker, A. Choy, F. Gallardo, N. Xiong, S. Knoblaugh, D. Cado, N. M. Greenberg and D. H. Raulet (2008). "NKG2D-deficient mice are defective in tumor surveillance in models of spontaneous malignancy." Immunity **28**(4): 571-580. doi: 10.1016/j.immuni.2008.02.016.

Han, J., S. H. Back, J. Hur, Y. H. Lin, R. Gildersleeve, J. Shan, C. L. Yuan, D. Krokowski, S. Wang, M. Hatzoglou, M. S. Kilberg, M. A. Sartor and R. J. Kaufman (2013). "ER-stress-induced transcriptional regulation increases protein synthesis leading to cell death." Nat Cell Biol **15**(5): 481-490. doi: 10.1038/ncb2738.

Hansen, B. S., M. H. Vaughan and L. Wang (1972). "Reversible inhibition by histidinol of protein synthesis in human cells at the activation of histidine." J Biol Chem **247**(12): 3854-3857. doi:

Harding, H. P., I. Novoa, Y. Zhang, H. Zeng, R. Wek, M. Schapira and D. Ron (2000). "Regulated translation initiation controls stress-induced gene expression in mammalian cells." Mol Cell **6**(5): 1099-1108. doi:

Harding, H. P., Y. Zhang, H. Zeng, I. Novoa, P. D. Lu, M. Calfon, N. Sadri, C. Yun, B. Popko, R. Paules, D. F. Stojdl, J. C. Bell, T. Hettmann, J. M. Leiden and D. Ron (2003). "An

integrated stress response regulates amino acid metabolism and resistance to oxidative stress." Mol Cell **11**(3): 619-633. doi:
Heinemann, A., F. Zhao, S. Pechlivanis, J. Eberle, A. Steinle, S. Diederichs, D. Schadendorf and A. Paschen (2012). "Tumor suppressive microRNAs miR-34a/c control cancer cell expression of ULBP2, a stress-induced ligand of the natural killer cell receptor NKG2D." Cancer Res **72**(2): 460-471. doi: 10.1158/0008-5472.CAN-11-1977.
Heinz, S., C. Benner, N. Spann, E. Bertolino, Y. C. Lin, P. Laslo, J. X. Cheng, C. Murre, H. Singh and C. K. Glass (2010). "Simple combinations of lineage-determining transcription factors prime cis-regulatory elements required for macrophage and B cell identities." Mol Cell **38**(4): 576-589. doi: 10.1016/j.molcel.2010.05.004.
Helenius, A. and M. Aebi (2004). "Roles of N-linked glycans in the endoplasmic reticulum." Annu Rev Biochem **73**: 1019-1049. doi: 10.1146/annurev.biochem.73.011303.073752.
Herberman, R. B., M. E. Nunn, H. T. Holden and D. H. Lavrin (1975). "Natural cytotoxic reactivity of mouse lymphoid cells against syngeneic and allogeneic tumors. II. Characterization of effector cells." Int J Cancer **16**(2): 230-239. doi:
Hetz, C. (2012). "The unfolded protein response: controlling cell fate decisions under ER stress and beyond." Nat Rev Mol Cell Biol **13**(2): 89-102. doi: 10.1038/nrm3270.
Hock, J., L. Weinmann, C. Ender, S. Rudel, E. Kremmer, M. Raabe, H. Urlaub and G. Meister (2007). "Proteomic and functional analysis of Argonaute-containing mRNA-protein complexes in human cells." EMBO Rep **8**(11): 1052-1060. doi: 10.1038/sj.embor.7401088.
Hsiung, M. Y. B. (2008). Regulation of genes encoding murine Rae1 natural killer cell activating ligands Ph. D. in Molecular and Cell Biology, University of California, Berkeley.
Iannello, A., T. W. Thompson, M. Ardolino, S. W. Lowe and D. H. Raulet (2013). "p53-dependent chemokine production by senescent tumor cells supports NKG2D-dependent tumor elimination by natural killer cells." J Exp Med **210**(10): 2057-2069. doi: 10.1084/jem.20130783.
Jain, R. K. (2005). "Normalization of tumor vasculature: an emerging concept in antiangiogenic therapy." Science **307**(5706): 58-62. doi: 10.1126/science.1104819.
Jamieson, A. M., A. Diefenbach, C. W. McMahon, N. Xiong, J. R. Carlyle and D. H. Raulet (2002). "The role of the NKG2D immunoreceptor in immune cell activation and natural killing." Immunity **17**(1): 19-29. doi:
Jheng, J. R., J. Y. Ho and J. T. Horng (2014). "ER stress, autophagy, and RNA viruses." Front Microbiol **5**: 388. doi: 10.3389/fmicb.2014.00388.
Jost, S. and M. Altfeld (2013). "Control of human viral infections by natural killer cells." Annu Rev Immunol **31**: 163-194. doi: 10.1146/annurev-immunol-032712-100001.
Jung, H., B. Hsiung, K. Pestal, E. Procyk and D. H. Raulet (2012). "RAE-1 ligands for the NKG2D receptor are regulated by E2F transcription factors, which control cell cycle entry." J Exp Med **209**(13): 2409-2422. doi: 10.1084/jem.20120565.
Karre, K., H. G. Ljunggren, G. Piontek and R. Kiessling (1986). "Selective rejection of H-2-deficient lymphoma variants suggests alternative immune defence strategy." Nature **319**(6055): 675-678. doi: 10.1038/319675a0.
Katz, Y., E. T. Wang, E. M. Airoldi and C. B. Burge (2010). "Analysis and design of RNA sequencing experiments for identifying isoform regulation." Nat Methods **7**(12): 1009-1015. doi: 10.1038/nmeth.1528.

Kiessling, R., E. Klein and H. Wigzell (1975). ""Natural" killer cells in the mouse. I. Cytotoxic cells with specificity for mouse Moloney leukemia cells. Specificity and distribution according to genotype." Eur J Immunol **5**(2): 112-117. doi: 10.1002/eji.1830050208.

Kim, D., G. Pertea, C. Trapnell, H. Pimentel, R. Kelley and S. L. Salzberg (2013). "TopHat2: accurate alignment of transcriptomes in the presence of insertions, deletions and gene fusions." Genome Biol **14**(4): R36. doi: 10.1186/gb-2013-14-4-r36.

Kim, H., A. Bhattacharya and L. Qi (2015). "Endoplasmic reticulum quality control in cancer: Friend or foe." Semin Cancer Biol. doi: 10.1016/j.semcancer.2015.02.003.

Koditz, J., J. Nesper, M. Wottawa, D. P. Stiehl, G. Camenisch, C. Franke, J. Myllyharju, R. H. Wenger and D. M. Katschinski (2007). "Oxygen-dependent ATF-4 stability is mediated by the PHD3 oxygen sensor." Blood **110**(10): 3610-3617. doi: 10.1182/blood-2007-06-094441.

Koumenis, C., C. Naczki, M. Koritzinsky, S. Rastani, A. Diehl, N. Sonenberg, A. Koromilas and B. G. Wouters (2002). "Regulation of protein synthesis by hypoxia via activation of the endoplasmic reticulum kinase PERK and phosphorylation of the translation initiation factor eIF2alpha." Mol Cell Biol **22**(21): 7405-7416. doi:

Lai, M. C., H. W. Kuo, W. C. Chang and W. Y. Tarn (2003). "A novel splicing regulator shares a nuclear import pathway with SR proteins." EMBO J **22**(6): 1359-1369. doi: 10.1093/emboj/cdg126.

Lange, P. S., J. C. Chavez, J. T. Pinto, G. Coppola, C. W. Sun, T. M. Townes, D. H. Geschwind and R. R. Ratan (2008). "ATF4 is an oxidative stress-inducible, prodeath transcription factor in neurons in vitro and in vivo." J Exp Med **205**(5): 1227-1242. doi: 10.1084/jem.20071460.

Lanier, L. L., J. H. Phillips, J. Hackett, Jr., M. Tutt and V. Kumar (1986). "Natural killer cells: definition of a cell type rather than a function." J Immunol **137**(9): 2735-2739. doi:

Li, H., T. Lakshmikanth, C. Garofalo, M. Enge, C. Spinnler, A. Anichini, L. Szekely, K. Karre, E. Carbone and G. Selivanova (2011). "Pharmacological activation of p53 triggers anticancer innate immune response through induction of ULBP2." Cell Cycle **10**(19): 3346-3358. doi: 10.4161/cc.10.19.17630.

Liao, Y., T. S. Fung, M. Huang, S. G. Fang, Y. Zhong and D. X. Liu (2013). "Upregulation of CHOP/GADD153 during coronavirus infectious bronchitis virus infection modulates apoptosis by restricting activation of the extracellular signal-regulated kinase pathway." J Virol **87**(14): 8124-8134. doi: 10.1128/JVI.00626-13.

Lin, J. C., M. Hsu and W. Y. Tarn (2007). "Cell stress modulates the function of splicing regulatory protein RBM4 in translation control." Proc Natl Acad Sci U S A **104**(7): 2235-2240. doi: 10.1073/pnas.0611015104.

Lin, J. C. and W. Y. Tarn (2009). "RNA-binding motif protein 4 translocates to cytoplasmic granules and suppresses translation via argonaute2 during muscle cell differentiation." J Biol Chem **284**(50): 34658-34665. doi: 10.1074/jbc.M109.032946.

Lodoen, M., K. Ogasawara, J. A. Hamerman, H. Arase, J. P. Houchins, E. S. Mocarski and L. L. Lanier (2003). "NKG2D-mediated natural killer cell protection against cytomegalovirus is impaired by viral gp40 modulation of retinoic acid early inducible 1 gene molecules." J Exp Med **197**(10): 1245-1253. doi: 10.1084/jem.20021973.

Lopez-Soto, A., A. Quinones-Lombrana, R. Lopez-Arbesu, C. Lopez-Larrea and S. Gonzalez (2006). "Transcriptional regulation of ULBP1, a human ligand of the NKG2D receptor." J Biol Chem **281**(41): 30419-30430. doi: 10.1074/jbc.M604868200.

Lord, C. J. and A. Ashworth (2012). "The DNA damage response and cancer therapy." Nature **481**(7381): 287-294. doi: 10.1038/nature10760.

Lu, P. D., H. P. Harding and D. Ron (2004). "Translation reinitiation at alternative open reading frames regulates gene expression in an integrated stress response." J Cell Biol **167**(1): 27-33. doi: 10.1083/jcb.200408003.

Luo, S., P. Baumeister, S. Yang, S. F. Abcouwer and A. S. Lee (2003). "Induction of Grp78/BiP by translational block: activation of the Grp78 promoter by ATF4 through and upstream ATF/CRE site independent of the endoplasmic reticulum stress elements." J Biol Chem **278**(39): 37375-37385. doi: 10.1074/jbc.M303619200.

Ma, Y. and L. M. Hendershot (2004). "The role of the unfolded protein response in tumour development: friend or foe?" Nat Rev Cancer **4**(12): 966-977. doi: 10.1038/nrc1505.

Mali, P., L. Yang, K. M. Esvelt, J. Aach, M. Guell, J. E. DiCarlo, J. E. Norville and G. M. Church (2013). "RNA-guided human genome engineering via Cas9." Science **339**(6121): 823-826. doi: 10.1126/science.1232033.

Marcus, A., B. G. Gowen, T. W. Thompson, A. Iannello, M. Ardolino, W. Deng, L. Wang, N. Shifrin and D. H. Raulet (2014). "Recognition of tumors by the innate immune system and natural killer cells." Advances in immunology **122**: 91-128. doi: 10.1016/B978-0-12-800267-4.00003-1.

Markus, M. A. and B. J. Morris (2009). "RBM4: a multifunctional RNA-binding protein." The international journal of biochemistry & cell biology **41**(4): 740-743. doi: 10.1016/j.biocel.2008.05.027.

Markus, M. A. and B. J. Morris (2009). "RBM4: a multifunctional RNA-binding protein." Int J Biochem Cell Biol **41**(4): 740-743. doi: 10.1016/j.biocel.2008.05.027.

Matts, R. L., J. R. Schatz, R. Hurst and R. Kagen (1991). "Toxic heavy metal ions activate the heme-regulated eukaryotic initiation factor-2 alpha kinase by inhibiting the capacity of hemin-supplemented reticulocyte lysates to reduce disulfide bonds." J Biol Chem **266**(19): 12695-12702. doi:

McEwen, E., N. Kedersha, B. Song, D. Scheuner, N. Gilks, A. Han, J. J. Chen, P. Anderson and R. J. Kaufman (2005). "Heme-regulated inhibitor kinase-mediated phosphorylation of eukaryotic translation initiation factor 2 inhibits translation, induces stress granule formation, and mediates survival upon arsenite exposure." J Biol Chem **280**(17): 16925-16933. doi: 10.1074/jbc.M412882200.

Mohr, I. and N. Sonenberg (2012). "Host translation at the nexus of infection and immunity." Cell Host Microbe **12**(4): 470-483. doi: 10.1016/j.chom.2012.09.006.

Mucaj, V., J. E. Shay and M. C. Simon (2012). "Effects of hypoxia and HIFs on cancer metabolism." Int J Hematol **95**(5): 464-470. doi: 10.1007/s12185-012-1070-5.

Mullins, C., H. A. Meyer, E. Hartmann, N. Green and H. Fang (1996). "Structurally related Spc1p and Spc2p of yeast signal peptidase complex are functionally distinct." J Biol Chem **271**(46): 29094-29099. doi:

Munshi, N. C., T. Hideshima, D. Carrasco, M. Shammas, D. Auclair, F. Davies, N. Mitsiades, C. Mitsiades, R. S. Kim, C. Li, S. V. Rajkumar, R. Fonseca, L. Bergsagel, D. Chauhan and K. C. Anderson (2004). "Identification of genes modulated in multiple myeloma using genetically identical twin samples." Blood **103**(5): 1799-1806. doi: 10.1182/blood-2003-02-0402.

Nice, T. J. (2009). Post-Translational Regulation of the NKG2D Ligand Mult1 in Response to Cell Stress. Berkeley, CA,**:** 99 leaves.

Nice, T. J., L. Coscoy and D. H. Raulet (2009). "Posttranslational regulation of the NKG2D ligand Mult1 in response to cell stress." J Exp Med **206**(2): 287-298. doi: 10.1084/jem.20081335.

Nice, T. J., W. Deng, L. Coscoy and D. H. Raulet (2010). "Stress-regulated targeting of the NKG2D ligand Mult1 by a membrane-associated RING-CH family E3 ligase." J Immunol **185**(9): 5369-5376. doi: 10.4049/jimmunol.1000247.

Oslowski, C. M. and F. Urano (2011). "Measuring ER stress and the unfolded protein response using mammalian tissue culture system." Methods Enzymol **490**: 71-92. doi: 10.1016/B978-0-12-385114-7.00004-0.

Otterson, G. A., G. C. Flynn, R. A. Kratzke, A. Coxon, P. G. Johnston and F. J. Kaye (1994). "Stch encodes the 'ATPase core' of a microsomal stress 70 protein." EMBO J **13**(5): 1216-1225. doi:

Ozcan, U., L. Ozcan, E. Yilmaz, K. Duvel, M. Sahin, B. D. Manning and G. S. Hotamisligil (2008). "Loss of the tuberous sclerosis complex tumor suppressors triggers the unfolded protein response to regulate insulin signaling and apoptosis." Mol Cell **29**(5): 541-551. doi: 10.1016/j.molcel.2007.12.023.

Pan, Y. X., H. Chen, M. M. Thiaville and M. S. Kilberg (2007). "Activation of the ATF3 gene through a co-ordinated amino acid-sensing response programme that controls transcriptional regulation of responsive genes following amino acid limitation." Biochem J **401**(1): 299-307. doi: 10.1042/BJ20061261.

Pende, D., P. Rivera, S. Marcenaro, C. C. Chang, R. Biassoni, R. Conte, M. Kubin, D. Cosman, S. Ferrone, L. Moretta and A. Moretta (2002). "Major histocompatibility complex class I-related chain A and UL16-binding protein expression on tumor cell lines of different histotypes: analysis of tumor susceptibility to NKG2D-dependent natural killer cell cytotoxicity." Cancer Res **62**(21): 6178-6186. doi:

Pfuhl, T., A. Mamiani, M. Durr, S. Welter, J. Stieber, J. Ankara, M. Liss, T. Dobner, A. Schmitt, P. Falkai, E. Kremmer, V. Jung, S. Barth and F. A. Grasser (2008). "The LARK/RBM4a protein is highly expressed in cerebellum as compared to cerebrum." Neurosci Lett **444**(1): 11-15. doi: 10.1016/j.neulet.2008.08.017.

Popa, N., O. Cedile, X. Pollet-Villard, C. Bagnis, P. Durbec and J. Boucraut (2011). "RAE-1 is expressed in the adult subventricular zone and controls cell proliferation of neurospheres." Glia **59**(1): 35-44. doi: 10.1002/glia.21074.

Quinlan, A. R. and I. M. Hall (2010). "BEDTools: a flexible suite of utilities for comparing genomic features." Bioinformatics **26**(6): 841-842. doi: 10.1093/bioinformatics/btq033.

Raulet, D. H. (2003). "Roles of the NKG2D immunoreceptor and its ligands." Nat Rev Immunol **3**(10): 781-790. doi: 10.1038/nri1199.

Raulet, D. H., S. Gasser, B. G. Gowen, W. Deng and H. Jung (2013). "Regulation of ligands for the NKG2D activating receptor." Annual review of immunology **31**: 413-441. doi: 10.1146/annurev-immunol-032712-095951.

Reimold, A. M., N. N. Iwakoshi, J. Manis, P. Vallabhajosyula, E. Szomolanyi-Tsuda, E. M. Gravallese, D. Friend, M. J. Grusby, F. Alt and L. H. Glimcher (2001). "Plasma cell differentiation requires the transcription factor XBP-1." Nature **412**(6844): 300-307. doi: 10.1038/35085509.

Reimold, A. M., P. D. Ponath, Y. S. Li, R. R. Hardy, C. S. David, J. L. Strominger and L. H. Glimcher (1996). "Transcription factor B cell lineage-specific activator protein regulates the gene for human X-box binding protein 1." J Exp Med **183**(2): 393-401. doi:

Robinson, J. T., H. Thorvaldsdottir, W. Winckler, M. Guttman, E. S. Lander, G. Getz and J. P. Mesirov (2011). "Integrative genomics viewer." Nat Biotechnol **29**(1): 24-26. doi: 10.1038/nbt.1754.

Ron, D. and P. Walter (2007). "Signal integration in the endoplasmic reticulum unfolded protein response." Nat Rev Mol Cell Biol **8**(7): 519-529. doi: 10.1038/nrm2199.

Roybal, C. N., L. A. Hunsaker, O. Barbash, D. L. Vander Jagt and S. F. Abcouwer (2005). "The oxidative stressor arsenite activates vascular endothelial growth factor mRNA transcription by an ATF4-dependent mechanism." J Biol Chem **280**(21): 20331-20339. doi: 10.1074/jbc.M411275200.

Rutkowski, D. T. and R. J. Kaufman (2003). "All roads lead to ATF4." Dev Cell **4**(4): 442-444. doi:

Schneider, C. L. and A. W. Hudson (2011). "The human herpesvirus-7 (HHV-7) U21 immunoevasin subverts NK-mediated cytoxicity through modulation of MICA and MICB." PLoS Pathog **7**(11): e1002362. doi: 10.1371/journal.ppat.1002362.

Schroder, M. and R. J. Kaufman (2005). "The mammalian unfolded protein response." Annu Rev Biochem **74**: 739-789. doi: 10.1146/annurev.biochem.73.011303.074134.

Shaffer, A. L., M. Shapiro-Shelef, N. N. Iwakoshi, A. H. Lee, S. B. Qian, H. Zhao, X. Yu, L. Yang, B. K. Tan, A. Rosenwald, E. M. Hurt, E. Petroulakis, N. Sonenberg, J. W. Yewdell, K. Calame, L. H. Glimcher and L. M. Staudt (2004). "XBP1, downstream of Blimp-1, expands the secretory apparatus and other organelles, and increases protein synthesis in plasma cell differentiation." Immunity **21**(1): 81-93. doi: 10.1016/j.immuni.2004.06.010.

Shalem, O., N. E. Sanjana, E. Hartenian, X. Shi, D. A. Scott, T. S. Mikkelsen, D. Heckl, B. L. Ebert, D. E. Root, J. G. Doench and F. Zhang (2014). "Genome-scale CRISPR-Cas9 knockout screening in human cells." Science **343**(6166): 84-87. doi: 10.1126/science.1247005.

Shifrin, N., D. H. Raulet and M. Ardolino (2014). "NK cell self tolerance, responsiveness and missing self recognition." Semin Immunol **26**(2): 138-144. doi: 10.1016/j.smim.2014.02.007.

Shiloh, Y. and Y. Ziv (2013). "The ATM protein kinase: regulating the cellular response to genotoxic stress, and more." Nat Rev Mol Cell Biol **14**(4): 197-210. doi:

Shuda, M., N. Kondoh, N. Imazeki, K. Tanaka, T. Okada, K. Mori, A. Hada, M. Arai, T. Wakatsuki, O. Matsubara, N. Yamamoto and M. Yamamoto (2003). "Activation of the ATF6, XBP1 and grp78 genes in human hepatocellular carcinoma: a possible involvement of the ER stress pathway in hepatocarcinogenesis." J Hepatol **38**(5): 605-614. doi:

Sonenberg, N. and A. G. Hinnebusch (2009). "Regulation of translation initiation in eukaryotes: mechanisms and biological targets." Cell **136**(4): 731-745. doi: 10.1016/j.cell.2009.01.042.

Soriani, A., A. Zingoni, C. Cerboni, M. L. Iannitto, M. R. Ricciardi, V. Di Gialleonardo, M. Cippitelli, C. Fionda, M. T. Petrucci, A. Guarini, R. Foa and A. Santoni (2009). "ATM-ATR-dependent up-regulation of DNAM-1 and NKG2D ligands on multiple myeloma cells by therapeutic agents results in enhanced NK-cell susceptibility and is associated with a senescent phenotype." Blood **113**(15): 3503-3511. doi: 10.1182/blood-2008-08-173914.

Suragani, R. N., R. S. Zachariah, J. G. Velazquez, S. Liu, C. W. Sun, T. M. Townes and J. J. Chen (2012). "Heme-regulated eIF2alpha kinase activated Atf4 signaling pathway in oxidative stress and erythropoiesis." Blood **119**(22): 5276-5284. doi: 10.1182/blood-2011-10-388132.

Sutherland, C. L., N. J. Chalupny, K. Schooley, T. VandenBos, M. Kubin and D. Cosman (2002). "UL16-binding proteins, novel MHC class I-related proteins, bind to NKG2D and activate multiple signaling pathways in primary NK cells." J Immunol **168**(2): 671-679. doi:

Suzuki, R., M. Matsuda, K. Watashi, H. Aizaki, Y. Matsuura, T. Wakita and T. Suzuki (2013). "Signal peptidase complex subunit 1 participates in the assembly of hepatitis C virus through an interaction with E2 and NS2." PLoS Pathog **9**(8): e1003589. doi: 10.1371/journal.ppat.1003589.

Tabas, I. and D. Ron (2011). "Integrating the mechanisms of apoptosis induced by endoplasmic reticulum stress." Nat Cell Biol **13**(3): 184-190. doi: 10.1038/ncb0311-184.

Takada, A., S. Yoshida, M. Kajikawa, Y. Miyatake, U. Tomaru, M. Sakai, H. Chiba, K. Maenaka, D. Kohda, K. Fugo and M. Kasahara (2008). "Two novel NKG2D ligands of the mouse H60 family with differential expression patterns and binding affinities to NKG2D." J Immunol **180**(3): 1678-1685. doi:

Textor, S., N. Fiegler, A. Arnold, A. Porgador, T. G. Hofmann and A. Cerwenka (2011). "Human NK cells are alerted to induction of p53 in cancer cells by upregulation of the NKG2D ligands ULBP1 and ULBP2." Cancer Res **71**(18): 5998-6009. doi: 10.1158/0008-5472.CAN-10-3211.

Thiaville, M. M., E. E. Dudenhausen, C. Zhong, Y. X. Pan and M. S. Kilberg (2008). "Deprivation of protein or amino acid induces C/EBPbeta synthesis and binding to amino acid response elements, but its action is not an absolute requirement for enhanced transcription." Biochem J **410**(3): 473-484. doi: 10.1042/BJ20071252.

Tomasec, P., V. M. Braud, C. Rickards, M. B. Powell, B. P. McSharry, S. Gadola, V. Cerundolo, L. K. Borysiewicz, A. J. McMichael and G. W. Wilkinson (2000). "Surface expression of HLA-E, an inhibitor of natural killer cells, enhanced by human cytomegalovirus gpUL40." Science **287**(5455): 1031. doi:

Ulbrecht, M., S. Martinozzi, M. Grzeschik, H. Hengel, J. W. Ellwart, M. Pla and E. H. Weiss (2000). "Cutting edge: the human cytomegalovirus UL40 gene product contains a ligand for HLA-E and prevents NK cell-mediated lysis." J Immunol **164**(10): 5019-5022. doi:

Uniacke, J., C. E. Holterman, G. Lachance, A. Franovic, M. D. Jacob, M. R. Fabian, J. Payette, M. Holcik, A. Pause and S. Lee (2012). "An oxygen-regulated switch in the protein synthesis machinery." Nature **486**(7401): 126-129. doi: 10.1038/nature11055.

Vandesompele, J., K. De Preter, F. Pattyn, B. Poppe, N. Van Roy, A. De Paepe and F. Speleman (2002). "Accurate normalization of real-time quantitative RT-PCR data by geometric averaging of multiple internal control genes." Genome Biol **3**(7): RESEARCH0034. doi:

Vattem, K. M. and R. C. Wek (2004). "Reinitiation involving upstream ORFs regulates ATF4 mRNA translation in mammalian cells." Proc Natl Acad Sci U S A **101**(31): 11269-11274. doi: 10.1073/pnas.0400541101.

Venkataraman, G. M., D. Suciu, V. Groh, J. M. Boss and T. Spies (2007). "Promoter region architecture and transcriptional regulation of the genes for the MHC class I-related chain A and B ligands of NKG2D." J Immunol **178**(2): 961-969. doi:

Vivier, E., D. H. Raulet, A. Moretta, M. A. Caligiuri, L. Zitvogel, L. L. Lanier, W. M. Yokoyama and S. Ugolini (2011). "Innate or adaptive immunity? The example of natural killer cells." Science **331**(6013): 44-49. doi: 10.1126/science.1198687.

Vivier, E., E. Tomasello, M. Baratin, T. Walzer and S. Ugolini (2008). "Functions of natural killer cells." Nat Immunol **9**(5): 503-510. doi: 10.1038/ni1582.

Wang, H., H. Yang, C. S. Shivalila, M. M. Dawlaty, A. W. Cheng, F. Zhang and R. Jaenisch (2013). "One-step generation of mice carrying mutations in multiple genes by CRISPR/Cas-mediated genome engineering." Cell **153**(4): 910-918. doi: 10.1016/j.cell.2013.04.025.

Wang, T., J. J. Wei, D. M. Sabatini and E. S. Lander (2014). "Genetic screens in human cells using the CRISPR-Cas9 system." Science **343**(6166): 80-84. doi: 10.1126/science.1246981.

Wang, Y., D. Chen, H. Qian, Y. S. Tsai, S. Shao, Q. Liu, D. Dominguez and Z. Wang (2014). "The splicing factor RBM4 controls apoptosis, proliferation, and migration to suppress tumor progression." Cancer Cell **26**(3): 374-389. doi: 10.1016/j.ccr.2014.07.010.

Wouters, B. G. and M. Koritzinsky (2008). "Hypoxia signalling through mTOR and the unfolded protein response in cancer." Nat Rev Cancer **8**(11): 851-864. doi: 10.1038/nrc2501.

Xuan, B., Z. Qian, E. Torigoi and D. Yu (2009). "Human cytomegalovirus protein pUL38 induces ATF4 expression, inhibits persistent JNK phosphorylation, and suppresses endoplasmic reticulum stress-induced cell death." J Virol **83**(8): 3463-3474. doi: 10.1128/JVI.02307-08.

Yang, H., H. Wang, C. S. Shivalila, A. W. Cheng, L. Shi and R. Jaenisch (2013). "One-step generation of mice carrying reporter and conditional alleles by CRISPR/Cas-mediated genome engineering." Cell **154**(6): 1370-1379. doi: 10.1016/j.cell.2013.08.022.

Zhang, T., A. Barber and C. L. Sentman (2006). "Generation of antitumor responses by genetic modification of primary human T cells with a chimeric NKG2D receptor." Cancer Res **66**(11): 5927-5933. doi: 10.1158/0008-5472.CAN-06-0130.

Zoncu, R., A. Efeyan and D. M. Sabatini (2011). "mTOR: from growth signal integration to cancer, diabetes and ageing." Nat Rev Mol Cell Biol **12**(1): 21-35. doi: 10.1038/nrm3025.